Optimal Control of Voltage and Reactive Power Sources in Power Systems with Presence of Renewable Energy

Der Fakultät für Ingenieurwissenschaften
Abteilung Elektrotechnik und Informationstechnik
der Universität Duisburg-Essen

zur Erlangung des akademischen Grades

Doktors der Ingenieurwissenshaften

genehmigte Dissertation

von

Van-Hoan Pham
aus
Can Tho, Vietnam

Gutachter: Prof. Dr.-Ing. habil. István Erlich
Gutachter: Prof. Dr.-Ing. Kai Strunz
Tag der mündlichen Prüfung: 23.06.2015

Abstract

Renewable energy resources such as solar and wind are being connected to power systems worldwide in large numbers. As a result of the intermittent nature of these sources, in addition to the steadily increasing overall load demand, the electricity systems currently are faced with many challenges in security and operational reliability. With modern advanced grid-integration techniques, these energy resources are enabled to become reactive power sources, which offer themselves as cheap means for control. They are therefore being included with the other reactive power sources such as shunt reactor, tap- changer, etc., as crucial measures in new controllers to avoid serious problems occurring in the power system. Within this context, the primary objective of this thesis is the utilization of mathematical advances, recent developments in optimization algorithms, statistical simulation and analysis methods, to evaluate the performance of existing control approaches as well as to propose new controller schemes for optimal control of voltage and reactive power sources in power system.

Besides the challenges named above, the control task in power systems has to contend with inaccurate model and not up-to-date system topology information. A new measurement based approach recently developed is currently attracting the attention of researchers. This concept is introduced in this thesis and is modified for use in optimal control of voltage and reactive power sources in power system.

The final focus of the thesis is a mechanism to obtain a mutual compromise amongst the many actors in power system to achieve a certain globally optimum goal (e.g., voltage control, etc.). For this purpose a multi-agents based techniques are found to be suitable, and are presented in this thesis. In fact, voltage control problems typically involve different grids and operators to effectively deal with the coordination of the control actions among the neighboring power systems. Operators' unwillingness to reveal local system data is, however, a big barrier which can only be solved through a harmonious cooperation mechanism amongst themselves.

Kurzfassung

Erneuerbare Energiequellen wie die Sonnen- und Windenergie werden weltweit in großen Stückzahlen an Energieversorgungsnetzen angeschlossen. Als Ergebnis der intermittierenden Natur dieser Quellen - neben dem stetig steigenden Bedarf an Energie – stehen die Stromnetze derzeit vielen Herausforderungen bezüglich Sicherheit und Versorgungszuverlässigkeit gegenüber. Mit modernen Anschlusstechniken können diese neuen Energiequellen als Blindleistungsquellen und somit als wirtschaftlich günstige Mittel für die Regelung des Netzes herangezogen werden. Sie können im Zusammenspiel mit den anderen Blindleistungsquellen bzw. Spannungsregelern, wie z. B. Querdrossel, Stufenschalter, usw., in Maßnahmen eingebunden werden, die mit Hilfe neuer Regler ernsthafte Probleme in Stromnetzen zu vermeiden bezwecken. In diesem Zusammenhang ist das primäre Ziel dieser Arbeit unter Verwendung von mathematischen Fortschritten, den neusten Entwicklungen in Optimierungsalgorithmen sowie statistische Simulation- und Analysemethoden, die Leistung der bestehenden Kontrollansätzen zu bewerten und neue Regelstrukturen zur optimalen Spannungs- und Blindleistungsregelung in Stromnetzen zu entwerfen.

Neben den oben genannten Herausforderungen muss die Netzregelungsaufgabe mit ungenauen Modellen und oft nicht aktualisierte System-Topologie Daten konfrontiert. Ein vor kurzem entwickelter neuer messungsbasierter Ansatz wird von Forschern derzeit zur Überwindung dieses Problems als nützlich angesehen. Dieses Konzept ist in der vorliegenden Arbeit vorgestellt und ist für den Einsatz in eine optimale Spannungs- und Blindleistungsregelung in Energienetzen eingeführt.

Der letzte Schwerpunkt der Arbeit befasst sich mit einem Mechanismus, um einen gegenseitigen Kompromiss zwischen den vielen Akteuren in dezentralen Energiesystemen zu erreichen, damit ein bestimmtes global optimales Ziel (z. B. Spannungsprofil, o.ä.) erreicht werden kann. Hierzu eignen sich die multiagentenbasierten Techniken und werden in dieser Arbeit angewendet. In der Tat erfordert das Spannungsregelungsproblem in Netzen mit mehreren Betreibern eine effektive Koordination zwischen den Kontrollmaßnahmen benachbarter Netzbetreiber. Mangelnde Bereitschaft lokaler Systemdaten zu benachbarten Systembetreibern offen zu legen ist jedoch ein großes Hindernis, das nur durch eine kooperative Zusammenarbeit gelöst werden kann.

Acknowledgement

I would first like to thank and acknowledge Prof. István Erlich for his consistent guidance and support. His perpetual energy and enthusiasm for my work motivated me throughout the course of this work. I appreciate all his contributions of time, ideas, and funding to make my Ph.D. experience productive and stimulating.

I am very thankful to German Academic Exchange Service (DAAD), for financial support during nearly four years of my Ph.D. course.

Also greatly appreciated is the excellent work environment created by my colleagues. All of you have been a source of friendships as well as good advice and collaboration.

I gratefully acknowledge the members of my Ph.D. committee for their time and valuable feedback on a preliminary version of this thesis.

My Vietnamese friends in Dortmund, Münster and Duisburg have made living in Germany enjoyable for me and for my family. Thanks a lot for the wonderful brotherhood and friendship. Thanks for easily helping me and my family when we needed.

Last but not least, my deepest love and gratitude to my wife Tran Thi Thanh Khuong and our daughter Pham Khanh Chi. Thanks for my wife for her continuous support in the most difficult times during the period of the study. I would like to express my ultimate gratitude to my parents and my parents in law for their endless prays and their outstanding support.

Table of Contents

List of Figure

List of Table

Chapter 1
Introduction

1.1 Motivation

From developing to developed countries, integration of renewable energy sources (RES) has been attracting bounteous concerns of researchers and authorities on technical, economic and environmental aspects. This trend is proper solution for lack of fuel fossil energy sources and building eco-friendly power system targeted by many countries. Accommodation of RES penetration has given rise to many challenges. A typical one among them is to handle the intermittent nature of RES leading to violation of operation constraints due to the fact that power systems in most countries were designed based on 'fit and forget' approach in which all technical concerns were solved only at the planning stage. As a result besides money-consuming choice of system reinforcement, the term of 'smart grid' was introduced in order to underscore necessity of solutions at operation stage that are demonstrated in this thesis being cost-effective and efficient to deal with challenges raised by integration of RES through five following topics.

Topic 1: With the increasing integration of wind power plants (WPPs), grid utilities require extended reactive power supply capability, not only during voltage dips, but also in steady state operation. This can be seen from grid codes of several countries where the steady state reactive power requirements are defined alternatively in terms of the power factor, the amount of reactive power supplied or the voltage at the point of common coupling (PCC). Typically, the available reactive power sources within the WPP are wind generators, conventional compensation elements, or some version of FACTS devices. Hence, finding coordinated reactive power control strategies to address the optimal reactive power dispatch (ORPD) problem are increasingly crucial to researchers.

Topic 2: Renewable energy sources are of great relevance for achieving predominantly environment-friendly electric power supply. Thus, thousands of wind generators (WGs) are going operational every year worldwide and this trend seems to be accelerating. Remarkably, most of these generators, especially in Europe, are integrated into existing distribution

systems, which has led to renewed emphasis on the study of several planning and operational implications. The issue of voltage and reactive power control in distribution systems with large-scale integration of wind power has been widely investigated by using a deterministic framework, which is based on a single (e.g. worst case) scenario or a reduced set of representative scenarios. This framework has been considered for design and testing of both individual and coordinated control schemes. Several research efforts have recently been conducted from stochastic analysis point of view. Their results underscore the potential need of further research for new solutions to meet the operational security challenges related to increasing uncertainties brought about by widespread integration of distributed generation and higher demand side response, both with different control functionalities.

Topic 3: Intermittent renewable energy resources (RES) like solar and wind will be connected largely to European distribution networks due to the recent new targets for RES penetration in the European Union (globally 20% of energy consumption covered by RES by 2020). This entails several challenges to system reliability and security, especially in short term operation time frame, where a high degree of variability of power supply from RES may occur. Therefore, developing new control architectures to be used in future new configuration of distribution networks is crucial to achieve optimal, flexible, and efficient operation with minimum risk of security threats. To this aim, several approaches have adopted *optimal power flow based strategies* in the proposed control architectures with centralized controllers. Alternatively, other adaptive control approaches based on integration of *sensitivities theory* into centralized controllers has drawn much attention in recent years: These approaches are suitable for online application of controllers. On the other hand, to deal with global challenges in whole power systems, there have been many debates in recent years on a shift in preference from passive control schemes to '*active network management*' (smart grid) which not only adjusts networks for LF, but also minimizes the effect on adjacent networks. Another permanently existing challenge for developing new control architectures is to provide optimal control actions based on few available measurements of several buses. A controller being able to solve these challenges is expected.

Topic 4: Voltage control and ORPD play an important role in guaranteeing not only secure power flow but also to optimize operational states of the system that achieve the largest possible benefit from an economical perspective. This issue has become more important in

recent years due to the increased number of market participants, the continuous growth of power demands as well as the large-scale integration of renewable resources. There are large numbers of publications dealing with the solution of the ORPD problem by using *model-based* approach through power flow calculations. Basically, the model-based approach refers to the state estimation, that system states are estimated through both available measurements and the system model. These approaches are often faced with a drawback such as strong dependence of the performance of the algorithm on accuracy of the system model. In the 2011 San Diego blackout, for example, the fact that the system model was not up-to-date resulted in inaccurate state estimation, and operators were not aware that certain lines were overloaded or close to being overloaded. Therefore, it is necessary to develop a new method to overcome inaccuracy of the system model.

Topic 5: Voltage stability assessment is one of the major concerns in power system planning and secure operation as power grids span over several regions and sometimes even countries. A direct link between the voltage and the reactive power makes it possible to control the voltage to desired values by the control of reactive power. The operator of the power system is responsible to control the transmission system voltage which means enough reactive power available to handle voltage violation conditions. To achieve certain global control objectives (e.g. N-1 secure operation, reactive power planning, minimization of losses etc.) it is necessary to coordinate control actions among the regional operators. Cooperation of regional operators in solving ORPD problems on large systems is beneficial despite of many challenges. One major challenge is the fact that each regional operator is typically not enthusiastic to expose the local system data.

1.2 Objectives

The overall objective of this thesis is to study and propose an effective counter-measure for the ORPD and voltage problems. The specific objectives of the research described hereafter are summarized as followings.

- Proposal for a novel control scheme based on a heuristic optimization algorithm, that is able to adapt with existing centralized controllers of wind farms.
- A probabilistic evaluation of the effectiveness of different approaches that could be used in WGs for voltage and reactive power control during normal (i.e. steady state or

quasi-steady state) conditions in distribution networks by taking into account possible uncertainties.

- Proposal for a new architecture of centralized controller for the *active network management* which is able to optimally drive the online network operation with only few available measurements at several selected buses subjected to operation security constraints (i.e., voltage violation).
- Establishment of the mathematical formulation in context of addressing ORPD problems by using a measurement-based approach, and the theoretical and numerical demonstration of the approach's performance for overcoming challenges of inaccurate model and unknown topology changes in power systems.
- Proposal for a control scheme that cooperates among the regional operators in solving ORPD and voltage problems while avoiding exposing local system data pertaining to regional infrastructure.

1.3 Organization of Thesis

Chapter 2 introduces a heuristic optimization-based controller for online optimal control of reactive power sources in wind power plants, which can be implemented as an extension to the existing WPP control structures. Grid code of WPP integration in several countries is discussed in details. Performance of the controllers is discussed and demonstrated.

Chapter 3 presents probabilistic procedure to evaluate the effects of voltage and reactive control methods for local and coordinated control schemes applied to wind generators in distribution networks. Uncertainties related to variation of load demand, wind speed and outage of WGs are effectively characterized. An approach employing a Monte Carlo based framework is introduced to ascertain the benefits and drawbacks of each scheme with respect to the resulting statistical attributes of voltage profiles, tap activity of on-load tap changers (OLTC) and total active power losses.

Chapter 4 proposes a new scheme of centralized controller, which belongs to the class of using sensitivities approach, in distribution networks to meet requirements and objectives of both the TSO and DNO. Principles of model predictive control and its adaption into the control scheme are presented. Simulation results reveal that the proposed controller is able to accommodate largely increasing integration of distributed generators into distribution

networks with limited number of measurements on hand, and it can significantly relieve computational burden.

Chapter 5 introduces an application of a measurement based approach on solving the optimal reactive power dispatch problem. Aspects concerned of using the approach to estimate sensitivities are reviewed and discussed in terms of voltage and reactive sources control. Simulation results and concluding remarks are presented to demonstrate feasibility and promising potential of the approach for future studies.

Chapter 6 presents multi-agent control scheme to coordinate the control actions among the various grids while preserving sensitive local system data that regional operators are often not willing to disclose. Furthermore, impacts of control parameters on performance of introduced control scheme are thoroughly analyzed in order to depict its own facing challenges in the context of practical implementation.

Finally, the thesis is concluded in Chapter 7.

Chapter 2
Online optimal control of reactive sources in wind power plants

Online measurements of all buses are available in several kinds of micro-grids or wind power plants, and this enables centralized controllers. In wind power plants there are various reactive power sources that possess either continuous behavior, such as wind generators, or discrete one, such as shunt reactors, tap changers of transformers; therefore, operation coordination among them in an optimal manner to achieve a certain target, such as losses minimization, is big challenge since it falls into the category of mixed-integer nonlinear optimization problems. Moreover, for connection to power systems, wind power plants are demanded to provide reactive power amount according to voltage at connection point that has been stated in grid code at several countries. To deal with above mentioned challenges, this chapter proposes a heuristic optimization based and centralized controller that is to incorporate reactive power optimization into a global WPP's control loop so that it can be used online to determine the optimal distribution of reactive power, which is needed to meet grid code requirements, among the available Var sources. The optimization problem is handled using an optimization algorithm belonging to the class of heuristic optimization algorithms that has been successfully demonstrated to be effective on solving the mixed-integer nonlinear optimization problems.

2.1 Introduction

Wind power has firmly positioned itself as one of the most important renewable energy source over the past two decades. As of this writing, the share of wind power in relation to the overall installed capacity has increased significantly due to the policy incentives adopted by several countries to support renewable energy development, and this trend is in all likelihood set to continue. In some countries, the share of wind in relation to the overall installed capacity is already approaching the 50% mark [1].

With the increasing integration of wind power plants (WPPs), grid utilities require extended reactive power supply capability, not only during voltage dips, but also in steady state operation. According to the grid codes [2], the steady state reactive power requirements are defined alternatively in terms of the power factor, the amount of reactive power supplied or the voltage at the point of common coupling (PCC). Typically, the available reactive power sources within the WPP are wind generators, conventional compensation elements or some version of FACTS devices. Besides, the control systems, which modern wind generators employ, are characterized by fast response time and thus open up additional unconventional options to provide extra reactive power support [3]. Hence, coordinated reactive power control strategies have been suggested based on the operational chart of variable speed wind generators [1], [4]. The optimal utilization of reactive sources in WPPs has also been addressed in recent literature, in which the optimal reactive power dispatch problem (ORPDP) was formulated as minimum power loss or minimum voltage deviation as targets [5]-[6]. In [3] and [7], a predictive control approach, where the ORPDP also accounts for minimization of the cost of operation associated with the number of on-load tap changes (OLTC), is suggested.

Mathematically the ORPDP falls into the category of mixed-integer nonlinear optimization problems. Classical gradient-based optimization algorithms may fail to solve such problems due to the difficulties in handling non-convex and discontinuous problems as well as discrete variables. Moreover, the accuracy of the solution is quite sensitive to the initial points [5]. In recent years, an ever-increasing research effort has been dedicated to the solution of the ORPDP based on the application of a variety of heuristic optimization algorithms such as genetic algorithm [6], particle swarm optimization [3], differential evolution [8], evolutionary programming [9], ant colony optimization [10], and bacterial foraging optimization [11]. These techniques have indeed demonstrated effectiveness in overcoming the disadvantages of classical algorithms. Particularly, particle swarm optimization and differential evolution have received great attention from researchers due to their searching power. Nevertheless, some pitfalls for the use of these techniques should be considered in order to avoid premature convergence and local stagnation since their searching capability is highly dependent on appropriate parameter settings as evidenced in several applications [10]-[13].

The main objective of this chapter is to introduce a new scheme of the heuristic optimization based controller for online optimal control of reactive power sources in WPPs, which can be implemented as an extension to the existing WPP control structures. Centralization of the controller is showed at the point of that all measurements are collected, processed, and then control actions are given by a controller only. Online measurements at all buses are requisite, since optimal power flow calculation is adopted in such controller. Common controllers include a PI (proportional integral) control unit for offsetting the difference between grid code reactive power requirement and the reactive power currently supplied at the point of common coupling (PCC). The output of the PI block constitutes the reactive power that needs to be supplied on top of the current setting which should be distributed between the available Var sources in an optimal manner. Based on measurements and tracking the current settings of each wind turbine, transformer and compensation elements, the optimization, for any given operating point, will result in optimal distribution of reactive power between each of the sources currently in service leading to minimum losses while at the same time satisfying mandatory reactive power supply.

The remainder of this chapter is organized as follows. Section 2.2 gives an overview of the proposed control strategy, discussing the main implementation issues. In Section 2.3, a test case is developed and evaluated. Finally, conclusions and outlook for future work are presented in Section 2.4.

2.2 Proposed control strategy

The implementation aspects of the proposed strategy for online reactive power control in WPPs are summarized in Fig. 2.1. Considering the availability of a data acquisition system to provide measurements related to actual status of all wind generators (WGs), transformers, and compensation devices within the WPP, the adopted control approach continuously fulfills the grid code requirement at PCC (e.g. Q_{ref}) by means of a slow response controller which allows the optimum management of the available WPP's Var sources during normal (i.e. steady-state or quasi steady-state) conditions. Although such kind of control is coupled to local fast control scheme at every Var source, it has a slow response to small operational changes (i.e. time frame of 10 s to a few minutes) and does not provide any fast reaction during large disturbances in order to avoid undesirable interactions.

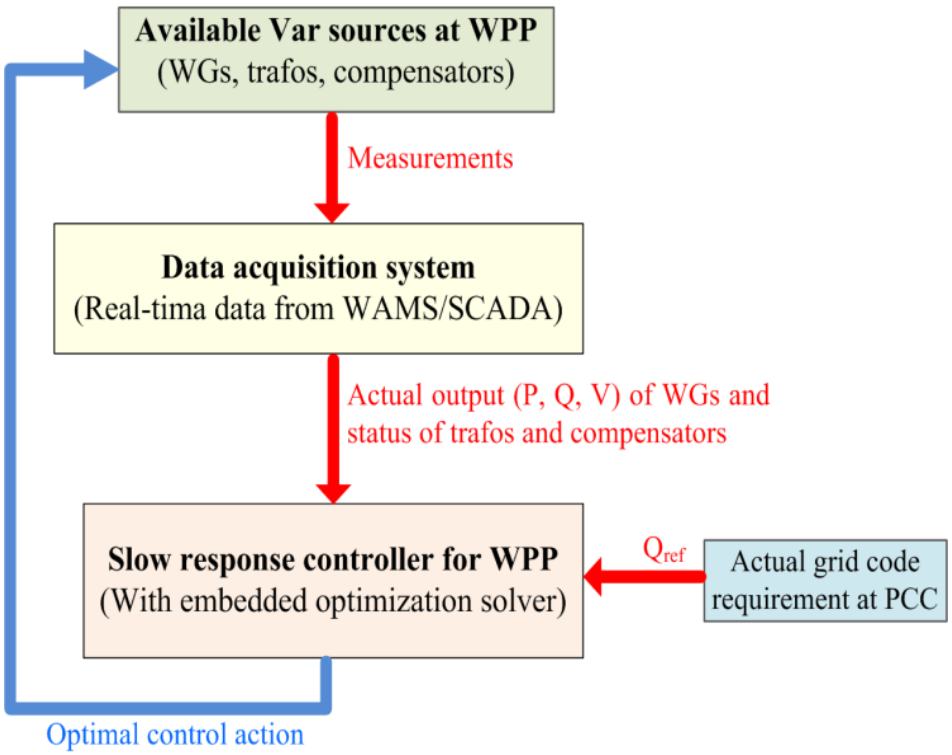

Fig. 2.1 Implementation procedure for slow reactive power control at WPPs

It is emphasized that the proposed controller is exclusively conceived (from WPP operation point of view) for continuous fulfillment (in an optimal manner) of grid code requirement at PCC and not for system-wide reactive power control purposes. So analysis with large scale system modeling beyond the PCC is not needed to illustrate the implementation and the test results provided in this chapter.

2.2.1 Wind power plant benchmark layout

The implementation of the proposed control strategy is illustrated henceforward by considering the WPP layout shown in Fig. 2.2. It should however be pointed out that due to its versatility and simplicity, this control strategy can be straightforwardly adapted to other configurations. The layout resembles the commonly used topology for offshore WPP, which is normally connected to the main grid using long cables with step-up transformers at both ends. Due to large charging currents of cables, line reactors are connected at one or both ends of the cables. In the example presented in this chapter a switched reactor is connected to the grid side bus bar. Although not considered in this chapter, FACTS devices are sometimes

included to provide fast and continuous Var control. Also for very long cables it is common to connect permanently connected shunt reactors directly to both ends of the cable which are switched always together with the cable.

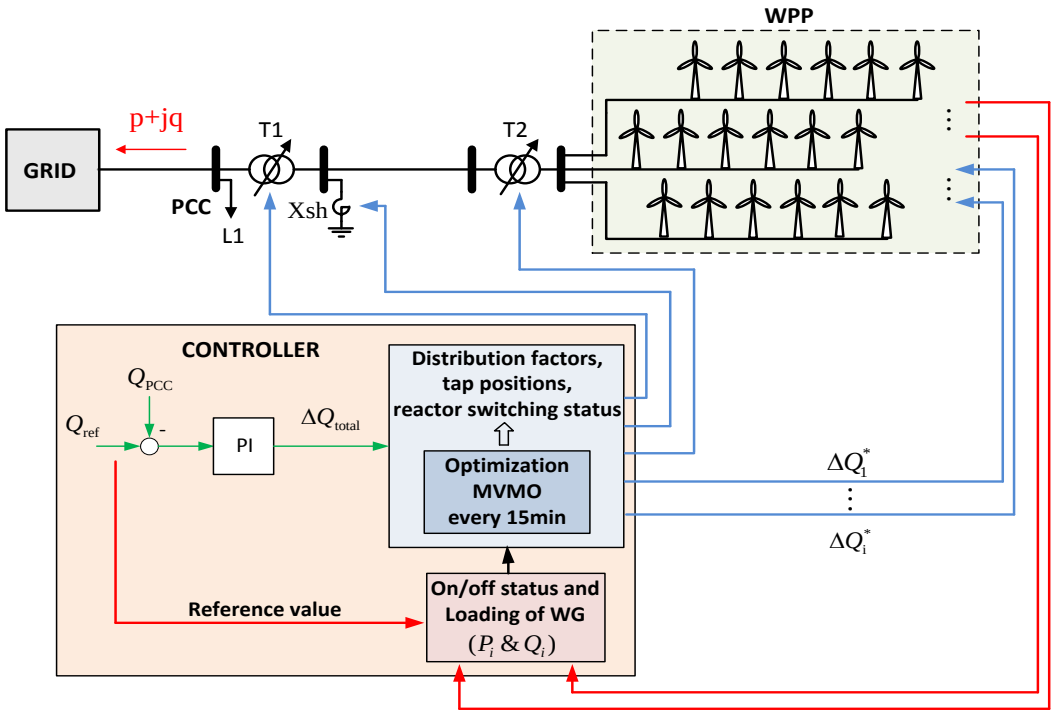

Fig. 2.2 WPP control schema including online optimization

2.2.2 Implementation of the controller

At the WPP level, a certain degree of coordination is necessary between different devices within the WPP facility to provide proper control reactions with respect to the PCC. Thus, the task of the WPP controller is to control the reference inputs (i.e. set points) of the individual wind generators and possible additional active or passive reactive power compensation equipment, so that control requirements at the PCC are met. The transmission system operators (TSOs) commonly define such requirements in their grid codes for the respective voltage levels. Grid codes may depend, to some extent, on the specific conditions of the TSO and therefore, they can differ from company to company even within the same country [16]. A typical requirement during normal operating conditions, which was build based on data in [17], is illustrated in Fig. 2.3.

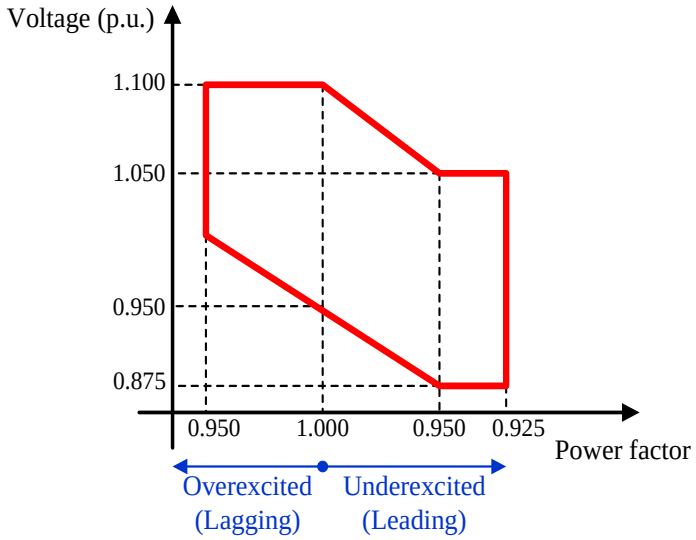

Fig. 2.3 Example for grid code requirement at PCC: Minimum requirements for reactive power compensation of a generation plant with unrestricted active power output

The WPP must be able to operate at any point within the area in the diagram. Besides, the requirements can alternatively be formulated in terms of power factor or reactive power reference at the PCC, with the latter being used in this chapter. Thus, the subsequent analysis considers that the WPP should always attempt to supply the required reactive power at the PCC (Q_{ref}).

From Fig. 2.2, note that the proposed WPP controller includes a PI control block, which is used to continuously adapt the generated reactive power to the reference at the PCC. It is worth to recall that the controller is characterized by a slow reaction (e.g. within a time frame of around 10 seconds to few minutes) to adapt the overall WPP response to changing steady-state requirements (cf. Subsection II.B). Therefore, for design purposes, the proportional gain of the PI block can be considered relatively small and the integral time constant can be set within 10 - 20 s. The output signal of the PI unit constitutes the additional reactive power needed to meet the requirement at the PCC, which is distributed to the individual WPP Var sources based on an optimization module that assigns the optimal set point to each source with the ultimate goal of operating the WPP with minimum losses while fulfilling the reactive power requirements at the PCC

2.2.3 WPP Var control considerations

The proposed controller, as depicted in Fig. 2.2, is intended for reactive power control by considering load flow and topology changes. The control task is to be performed only during normal (i.e. steady-state or quasi steady-state) conditions. Thus, it requires a slow response to adapt the overall WPP response (i.e. by optimally adjusting the long-term reactive power reference inputs for all available controllable Var sources) to changing steady-state requirements. A time frame of 10 seconds to few minutes is commonly sufficient [15]. Hence, the controller does not provide fast response during grid faults in order to avoid triggering of oscillations and unnecessary control actions. Such a fast control, which is beyond the scope of this chapter, can only be implemented at the level of individual wind generators and should react to fast voltage changes within 20-30 ms without altering the longer-term settings of the slow controller. It is also worth mentioning that, in case of a voltage drop, there should be a predominance of fast control on individual generator whereas slow control at overall plant level should be prioritized under steady state conditions.

2.2.4 Optimization module

The optimization module is used for efficient operation of the WPP as per grid reactive power requirements. It optimizes power flow in such a way that the total losses of the wind energy system are minimized. The resulting set points are provided to the Var sources. Some sources, which can play a role in minimizing system losses, if operated optimally, can be varied continuously (e.g. wind generator reactive power output) while others allow variation only stepwise (e.g. transformer tap position). Thus the task which has to be solved represents a mixed-integer optimization problem. The set points of wind generators are normally controlled by the WPP controller by allocating the required reactive power (output of the WPP controller) equally to each generator. In contrast, the optimization suggested in this chapter can modify the reference settings by deviating from the uniform Var distribution when necessary. The resulting Var references are sent via communication link to the wind turbines.

In current WPP operating practice, the transformers tap positions are controlled by separate and independent voltage controllers. However, according to the approach here the control of tap positions is part of the optimization. Assuming that the actual operational status of each wind generator (i.e. on/off status, current output power) as well as the current tap

settings of transformer and compensation elements are available, the optimization problem can mathematically be formulated as follows:

Minimize

$$\mathrm{OF} = \sqrt{p^2 + q^2} \tag{2.1}$$

Subject to

$$\mathbf{p}(\mathbf{v}, \boldsymbol{\theta}, \mathbf{n}) - \mathbf{p}_{\mathrm{g}} + \mathbf{p}_{\mathrm{d}} = 0 \tag{2.2}$$

$$\mathbf{q}(\mathbf{v}, \boldsymbol{\theta}, \mathbf{n}) - \mathbf{q}_{\mathrm{g}} + \mathbf{q}_{\mathrm{d}} = 0 \tag{2.3}$$

$$\mathbf{v}_{\min} \le \mathbf{v} \le \mathbf{v}_{\max} \tag{2.4}$$

$$\mathbf{i} \le \mathbf{i}^{\lim} \tag{2.5}$$

$$\mathbf{s} \le \mathbf{s}^{\lim} \tag{2.6}$$

$$\mathbf{q}_{\mathrm{WT}}^{\min} \le \mathbf{q}_{\mathrm{WT}} \le \mathbf{q}_{\mathrm{WT}}^{\max} \tag{2.7}$$

$$\mathbf{tap}_{\min} \le \mathbf{tap} \le \mathbf{tap}_{\max} \tag{2.8}$$

$$0 \le \gamma_{\mathrm{X_{sh}}} \le 1 \tag{2.9}$$

The bus voltage magnitude vector and its corresponding limits are denoted by $\mathbf{v}$, $\mathbf{v_{min}}$ and $\mathbf{v_{max}}$, whereas $\mathbf{i}$ and $\mathbf{s}$ are the current and apparent power flow vectors in the branches with limits defined by $\mathbf{i}^{\lim}$ and $\mathbf{s}^{\lim}$, respectively. $\mathbf{p}_{\mathrm{g}}$ and $\mathbf{q}_{\mathrm{g}}$ are the nodal active and reactive power generation vectors whereas $\mathbf{p}_{\mathrm{d}}$ and $\mathbf{q_d}$ are the nodal active and reactive power demand vectors. $\mathbf{p}(.)$ and $\mathbf{q}(.)$ stand for nodal active and reactive power injection vectors

Recalling Fig. 2.2, the objective function, as defined in (5.22), entails indirectly the minimization of total losses of the wind energy system while satisfying the reactive power requirement at PCC, since the terms p and q in the equation equal the difference between the injection from the WPP and the fictitious consumption associated to the load L1, which represents a dummy load whose real part corresponds with the nominal WPP active power and the imaginary component with Q_{ref}, respectively. Constraints (2.2) and (2.3) account for nodal balance, whereas the constraint set (2.7) – (2.9) is composed of bounds on the decision variables, which include:

- The vectors of Var limits ($\mathbf{q}_{\mathrm{WT}}^{\min}$ and $\mathbf{q}_{\mathrm{WT}}^{\max}$) for the wind generators, which can be obtained from the active/reactive power capability curves supplied by the manufacturers.
- The vectors of transformer discrete tap change limits ($\mathbf{tap}_{\min}$ and $\mathbf{tap}_{\max}$).
- On/off switching status $\gamma_{\mathrm{X_{sh}}}$ of the reactor $\mathrm{X_{sh}}$.

Again, it is worth emphasizing that the significance of the minimum attainable value of the objective function, as defined in (5.22), is twofold:

i) Operation of the WPP with minimum losses

ii) Meeting the required reactive power at the PCC

Simultaneously the internal voltage profiles (e.g. at wind generator terminals) will be kept within acceptable ranges.

The reactive power contribution of each wind generator is determined by

$$\Delta Q_{\mathrm{i}} = \frac{\Delta Q_{\mathrm{total}}}{\mathrm{n}} \cdot d_{\mathrm{i}} \tag{2.10}$$

where n is the number of wind turbines, d_{i} is the distribution factor assigned to the i-th wind generator and $\Delta Q_{\mathrm{total}}$ is the output of the WPP controller. The control strategy, as suggested in this chapter, can be also interpreted as an implicit optimal adjustment of the distribution factors (i.e. allocation) to changing operating conditions. Nevertheless, the optimization module can also operate in an alternative mode which optimally coordinates the settings of transformer and compensation elements only while allowing uniform reactive power distribution among wind generators. This may be favorable if the different utilization of wind turbines for Var generation will not result in significant reduction of losses.

During continuous operating regime of the WPP, the aforesaid measurements are supplied to the optimization module, which delivers the optimal decisions, obtained from the solution to the optimization problem as described above, as control signals to the various Var sources at each time step for the given operating point. This kind of optimization can be repeated in certain time intervals, e.g. every 5-15 minutes. The determination of the solution to the optimization problem is handled through the optimization module embedded with a heuristic optimization algorithm that will be described below.

2.2.5 A heuristic optimization algorithm

MVMO is a population-based stochastic optimization algorithm that has been recently developed and shown to have a remarkably better performance, compared to other basic and enhanced evolutionary algorithms, especially in terms of convergence behavior [18]. The basic theoretical background of MVMO has been published in [14].

2.3 Test results

The proposed online optimal control strategy is tested on a WPP whose layout is as shown in Fig. 2.2. It consists of 18 generators each rated at 5 MW and is connected to the 220-kV-power grid through two 100 MVA transformers and one 110 kV submarine cable $(0.062 + j0.11\ \Omega/\mathrm{km})$ of about 30 km length. Both transformers are equipped with OLTC. The PCC is considered at the 220-kV-side of the transformer T1 (220±19%/110 kV with 33 taps). The transformer T2 is rated at 110±13.0%/31.5 kV with 13 taps. The distances from each generator to the main collector of the WPP are uneven. The voltage at the wind turbine terminals is to be maintained between 0.92 and 0.97 kV (i.e. 920 – 970 V) where the nominal value is 0.95 kV (i.e. 950 V). For all other nodes ±5% range around the nominal voltage is prescribed. The excessive charging current of the submarine cable is compensated by connecting a shunt reactor on one side of the cable. The reactor is rated at 500 Ω and is adjusted with on/off control.

The exemplary wind profile shown in Fig. 2.4 is used for the simulation. To highlight the relevance of the online reactive power control problem, the grid code requirements corresponding to the actual operating condition are defined as stepwise changes of the reactive power reference at PCC as shown in Fig. 2.5.

Three cases are considered for comparison purposes:

Case 1: Optimal adjustment of all Var sources to meet the actual reactive power requirement at PCC including both OLTC settings, shunt reactor on/off commands and individual reactive power of each wind turbine (i.e. different distribution factors for each wind turbines). The controller calculates the optimal settings every 15 minutes.

Case 2: Optimal adjustment of the shunt reactor, both OLTC and a uniform wind turbine reactive power to be generated by all wind generators.

Case 3: The optimization is not implemented. The PCC controller output distributed equally to all operating wind turbines. The OLTCs are controlling the bus bar voltage at 110 kV and 33 kV level respectively. This case represents the common operating mode of wind farms currently implemented. The reactor is switched at the predefined time taken from Case 1 and 2.

Fig. 2.6 to Fig. 2.9 describe the dispatch curves of the WPP Var sources under the above-mentioned different cases. The advantages of using the proposed controller are demonstrated in Fig. 2.10 to Fig. 2.13.

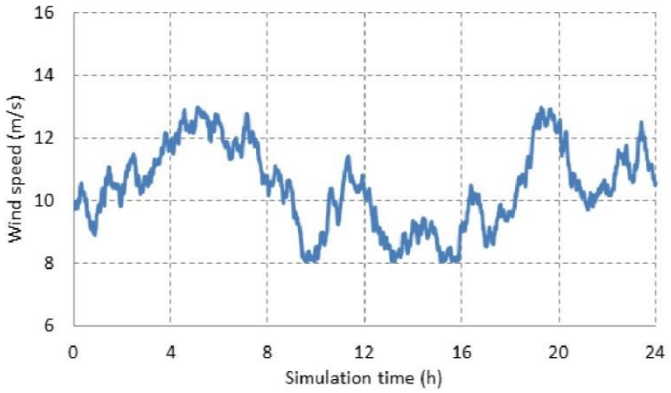

Fig. 2.4 Wind power variation

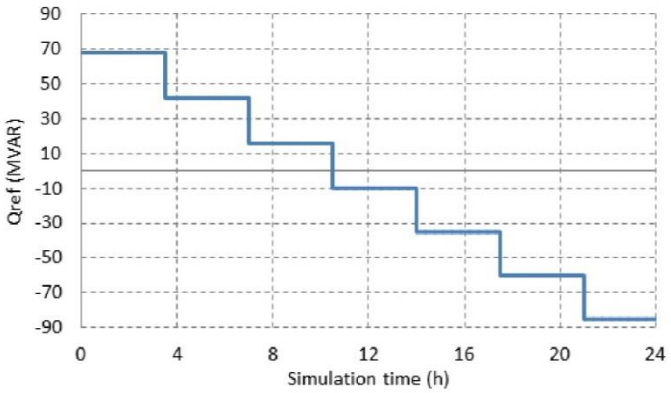

Fig. 2.5 Reactive power requirement at the PCC

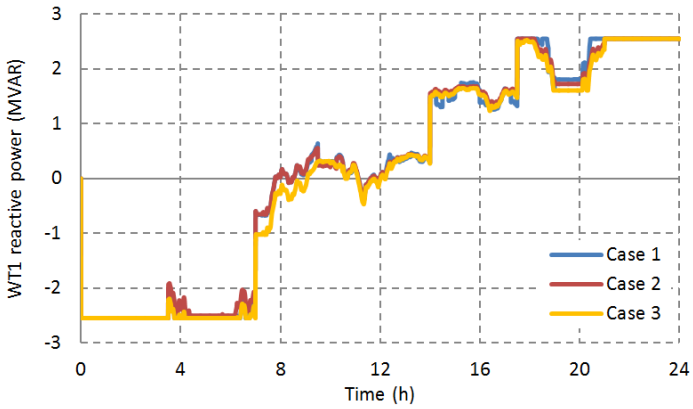

Fig. 2.6 Reactive power output of wind generator 1

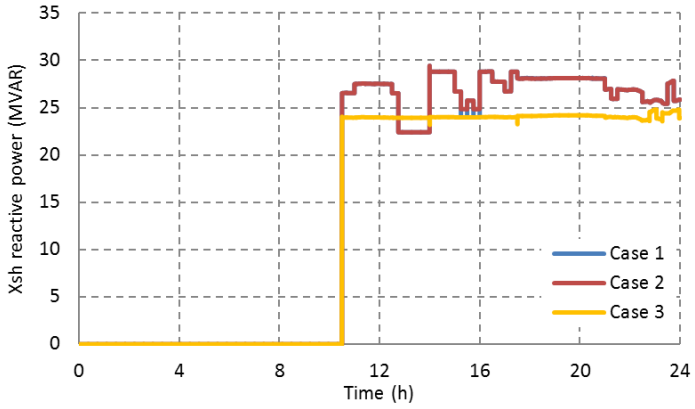

Fig. 2.7 Reactive power of the reactor

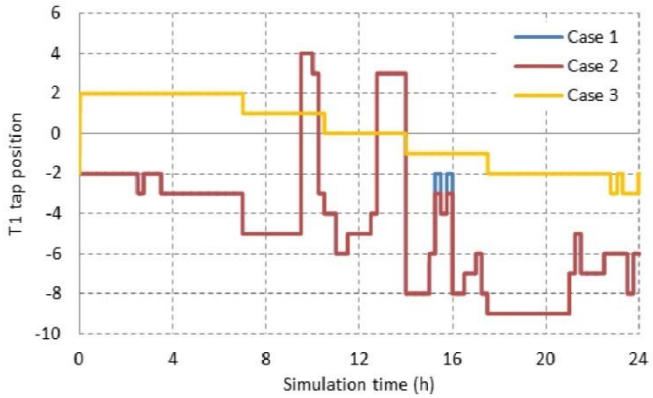

Fig. 2.8 OLTC tap positions – T1

From Fig. 2.6, it can be seen that the generator reactive power output curves corresponding to Cases 1 and 2 are very close at each time interval. This is reasonable since the adopted WPP layout did not involve large asymmetrical distances between generators, which was reflected in comparable distribution factors in both cases. The wind farm is almost capable to meet the Var requirements except in the extreme situations shown at both ends of the curves in Fig. 2.12. By contrast, in Case 3 the optimization tool is not used. The required reactive power from the PI controller is distributed equally to the wind turbines and the OLTCs are controlling the respective bus bar voltages. Due to the PI characteristic of the WPP controller the Var requirements are met in similar manner as in Case 1 and 2 (Fig. 2.12) as long as the wind turbines maximum reactive power capability is not reached. However, the voltage level controlled by the OLTCs is not optimal in Case 3. As can be seen from Fig. 2.13 the terminal voltage of the wind turbines exceeds the prescribed range of 0.92-0.97 kV considerably. Lower voltages will result in higher losses, which is the case in the second half

of the day in the simulated scenario. This will also lead to smaller total power being supplied at the PCC as shown in Fig. 2.11. It seems from Fig. 2.10 that for positive reactive power demand (left hand side) the losses are smaller in Case 3. However, this is due to the high voltage value, which is higher than the allowed 0.97 kV. Small temporary violations of the voltage limits can also happen in Cases 1 and 2 owing to the fact that the optimization is carried out every 15 minutes and in the meantime the wind power fed-in may change.

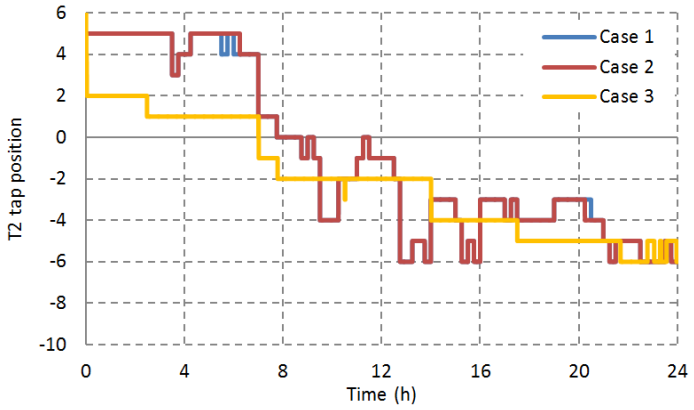

Fig. 2.9 OLTC tap positions – T2

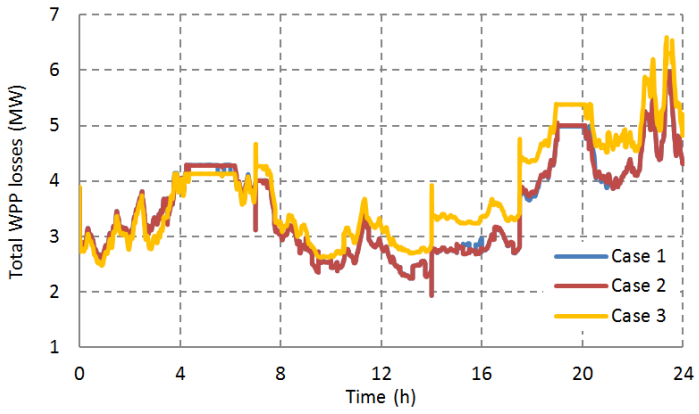

Fig. 2.10 Total active power losses of wind farm

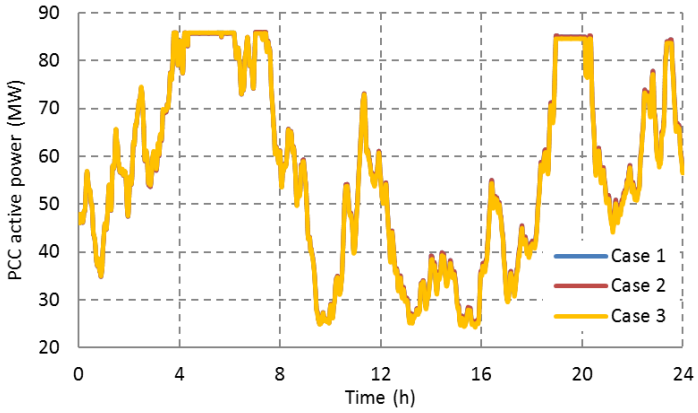

Fig. 2.11 Active power at PCC

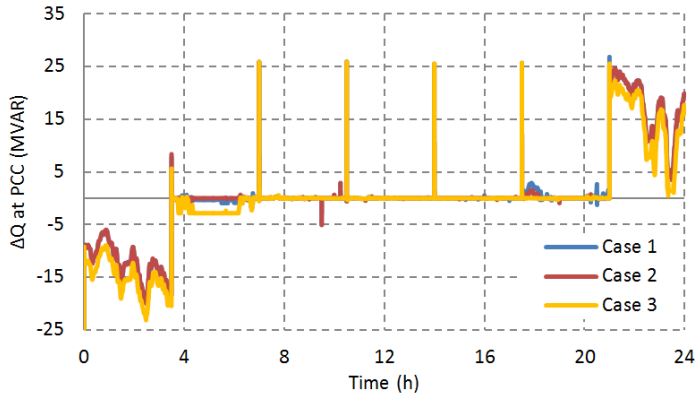

Fig. 2.12 Difference between demanded and supplied reactive power at PCC

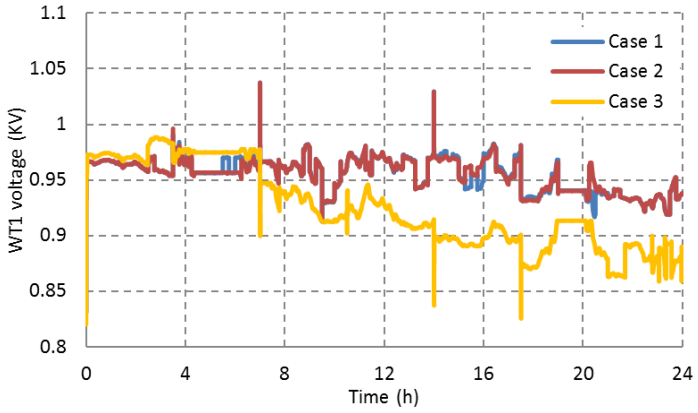

Fig. 2.13 Terminal voltage of wind generator 1

From Fig. 2.7, note that the reactor is switched on at the same point in time for all cases due to the actual compensation need from this point. The step variation of its reactive power is attributable to OLTC changes. Fig. 2.8 and Fig. 2.9 show the total number of tap

movements in the daily operation of the WPP for T1 and T2, respectively. Remarkably, more movements would be necessary in cases 1 and 2 to meet grid code requirements corresponding to the actual measurements from the WPP.

2.4 Summary

In this chapter, a novel control strategy has been suggested and successfully applied for online optimal control of wind power plant reactive sources. It can be implemented as an extension to the existing WPP control structures. Based on measurements from the plant indicating the actual settings of its Var sources and the actual active power generated by the wind turbines the optimal utilization of Var sources and OLTC positions are determined. The results of optimal wind turbine Var settings are incorporated into the existing WPP controller by distribution factors. The suggested approach guarantees not only optimal WPP operation but is also robust. As backup option uniform distribution factors can be used that corresponds with the current status of implementations without the extension by the optimizer. Depending on the WPP design uniform distribution of Var generation to the wind turbines may be sufficient. Results demonstrate that the incorporation of the controller at overall plant level entails optimal operation with smaller energy losses than the direct local control of Var sources as well as continuous fulfillment of operational requirements. However, the simulation results have shown that the required number of transformer tap changes will also increase when the suggested optimal controller approach is used.

Future research work is being directed towards inclusion of predictive control issues where actions are taken on the basis of a wind speed forecast in order to avoid unnecessary short term OLTC tap changes.

Chapter 3
Probabilistic evaluation of voltage and reactive power control methods of wind generators

The coordinated control scheme in the heuristic optimization based controller, introduced in chapter 2 contains the distinct advantages, and it could be an option of distribution network operators (DNOs) besides the other options such as local control schemes. As a contribution to DNOs, this chapter aims at presenting a comprehensive approach to evaluate the effects of local and coordinated control schemes applied to wind generators (WGs) in distribution networks in terms of voltage and reactive power control methods. This is very necessary because the increasing trend of wind power integration in distribution networks may leads to violation of operation constraints, such as voltage violation, due to power flow changing. A full study on the effects of voltage and reactive power control methods would help DNOs not only to answer whether operation constraints are satisfied, but also to be able to quantify operation benefits of each possible control scheme. The study in this chapter is performed based on a probabilistic framework instead of deterministic due to the fact that due to the deterministic framework often based on a single (e.g. worst case) scenario or a reduced set of representative scenarios, it is not able to provide an adequate consideration of all possible uncertainties.

3.1 Introduction

Renewable energy sources are of great relevance to achieving predominantly environment-friendly electric power supply. Thus, thousands of wind generators (WGs) are going operational every year worldwide and this trend seems to be accelerating [19]. Remarkably, most of these generators, especially in Europe, are integrated into existing distribution systems, which has led to renewed emphasis on the study of several planning and operational implications.

The issue of voltage and reactive power control in distribution systems with large scale integration of wind power has been widely investigated by using a deterministic framework, which bases on a single (e.g. worst case) scenario or a reduced set of representative scenarios. This framework has been considered for design and testing of both individual and coordinated control schemes. While design of individual control systems has been quite common in practice, the development of coordinated schemes is receiving more attention due to the availability of more sophisticated technologies for data acquisition and communication as well as more powerful computational resources. So far, based on classical or heuristic optimization, some centralized control strategies have been devised for optimal coordination of available voltage control devices [20]-[23]. Also, multiagent system-based dispatch strategies of distributed generators have been proposed to provide enhanced joint voltage support [24], [25].

Several research efforts have recently been conducted from stochastic analysis point of view. Probabilistic [26]-[31] and fuzzy load flow based approaches [32] have surveyed variations in voltage profiles considering uncertainties associated to load, wind speed forecasts, and component failure rates, to name a few. In [31], enhanced system overall voltage performance under wide range of (variable) operating conditions is pursued through operational decisions aiming at minimizing either marginal active power loss or marginal total active power demand while satisfying constraints on boundary bus voltage magnitudes. Moreover, an approach for combined local and remote voltage and reactive power control, with minimum power loss as a target, was proposed in [32] by considering short-term load and wind power forecasts. Results of the aforesaid contributions underscore the potential need of further research for new solutions to meet the operational security challenges related to increasing uncertainties brought about by widespread integration of distributed generation and higher demand side response, both with different control functionalities.

In view of this, the work presented in this chapter concerns a probabilistic evaluation of the effectiveness of different approaches that could be used in WGs for voltage and reactive power control during normal (i.e. steady-state or quasi steady-state) conditions in distribution networks. Although such kind of control is coupled to fast control scheme at individual WG, it has a slow response to small operational changes (i.e. time frame of 10 s to few minutes) and does not provide any fast reaction during large disturbances in order to avoid undesirable

adverse implications. The goal is thus to enhance the system controllability by introducing a corrective action that adjusts the long-term reactive power set-point at WGs such that improved voltage profile is achieved. Considering a test distribution network and uncertainties associated to load and wind generation variability, four different control philosophies are analyzed and compared by using a Monte Carlo (MC)-based framework. Three of these strategies constitute uncoordinated local control whereas the last one employs a coordinated centralized control scheme, performed as an optimization task. Performance comparisons, in terms of voltage profile variability and collateral implications on operational losses and costs, are provided.

The chapter is organized as follows: Section 3.2 reviews some issues on reactive power hierarchical control scheme for WGs and the studied control strategies. The methodological evaluation procedure is given in Section 3.3, discussing all relevant implementation aspects. Section 3.4 illustrates and discusses the results obtained in a 20 kV radial distribution network. Finally, conclusions and outline for future research are summarized in Section 3.5.

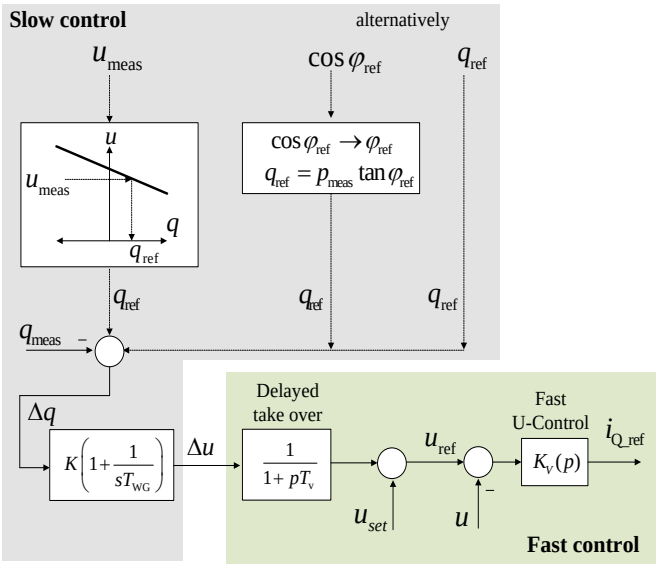

Fig. 3.1 Hierarchical Var control scheme of wind generators

3.2 Reactive power control considerations

The existence of a hierarchical control framework for voltage and reactive power control at WGs, such as the one illustrated in Fig. 3.1, is assumed for the research purposes of this

work. Broadly speaking, it comprises two control functionalities with different control targets and responses, which should not mutually interfere.

The slow control functionality is expected to react only during normal (i.e. steady-state or quasi steady-state) conditions, because its working principle is characterized by a slow response (e.g. 10 seconds to few minutes) to adapt the WG response to changing steady-state requirements. Hence, it does not provide any fast reaction during grid faults in order to avoid triggering of oscillations and unnecessary control actions. By contrast, the fast control functionality should react quickly to fast voltage changes within 20-30 ms without altering the longer-term settings of the slow controller. The work presented in this chapter focuses on slow control functionality, which could be implemented in different ways as shown in the upper part of Fig. 3.1. An investigation on interactions between both functionalities and potential implications is beyond the scope of the chapter and will be presented in a future publication.

As mentioned previously, the slow control functionality has the task of adjusting the reference inputs (i.e. set-points $-q_{ref}$ in Fig. 3.1) for all available Var controllers at WGs in order to meet steady-state voltage/reactive power operational requirements. This task can be performed by considering either standalone (i.e. local) or collectively managed (i.e. coordinated) control philosophy. Thus, the purpose of this research work is to ascertain the effectiveness of different steady-state Var control methods for WG. The first three methods described in the following represent local control strategy whereas the last method can be characterized as a coordinated one.

3.2.1 Local slow control approaches

In this case, the reference inputs of the controllers are derived from local quantities like the generated active power or WG terminal voltage. Grid codes may depend, to some extent, on specific conditions of the distribution network operators (DNOs) and therefore, they can differ from company to company even within the same country. Thus, any of the following methods could be selected to provide particular supplementary voltage and reactive power control capability for WGs.

3.2.1.1. Constant power factor (PF) control method

According to some settled technical guidelines, distribution-connected WGs are often required to operate at a fixed PF, an issue that may imply limited reactive power support [33]. A typical requirement is usually unity PF [34], but, in some European countries like Denmark and Germany, it could be a value between 0.95 *inductive* and 0.95 *capacitive* [35]. The terms *inductive* or *capacitive* PF refers to absorption or injection of reactive power by the WG, respectively. Thus, the analysis that will be provided in Section IV for this control method considers three different fixed PF requirements: a) 0.95 (capacitive), b) Unity, and c) 0.95 (inductive). The scheme for this control method is shown in Fig. 3.2. Note that the reactive power reference input $Q_{\text{ref\_WG}}$ is a function of the angle φ_{ref} corresponding to the underlying PF requirement and the steady-state WG active power output. The reactive power is usually controlled by a PI controller and therefore, the actual supplied reactive power will always correspond with the reference value provided that no limitations are reached.

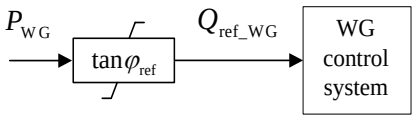

Fig. 3.2 Constant power factor control

3.2.1.2. Voltage droop control method

A reactive power versus voltage (QV) characteristic has been also implemented as an advanced form of WG voltage and reactive power control, as it is required, for instance, in the UK grid code [36] as well as in [37]. Comparing to constant PF control, the scheme shown in Fig. 3.3 defines $Q_{\text{ref\_WG}}$ as a function of the steady-state WG terminal voltage V_{WG} and a pre-specified voltage tolerance characteristic (e.g. around the rated voltage), which has been set in this chapter within ±5% considering a WG reactive power rating of ±0.33 p.u. Again, like in constant power factor control, it is assumed that the reference reactive power is really injected by the WG.

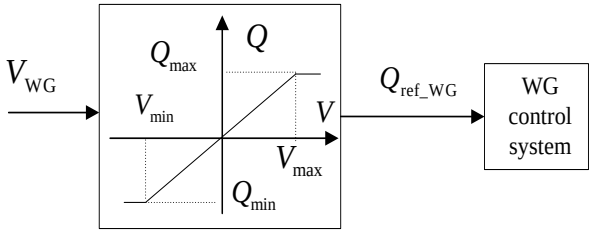

Fig. 3.3 Voltage droop control

3.2.1.3. Direct voltage control method

This kind of control is intended to continuously fulfill a target voltage set-point by injecting the required field currents [38]-[39] as long as technical limitations are not exceeded. The corresponding voltage controller shows PI characteristic (see Fig. 3.4). Usually, the voltage reference input V_{ref_WG} is normally set at 1.0 p.u. Despite the fact that the control deviation in steady state is normally zero, there are several operational concerns, especially, regarding adverse interactions with other voltage controllers in the network resulting in unacceptable voltage excursions and higher losses. However, these issues were not considered in this study.

Consider that the only difference between voltage droop control and direct voltage control is the corresponding controller which is in the first case a proportional one and shows PI characteristic when direct voltage control is implemented.

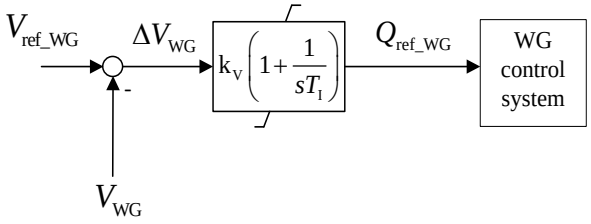

Fig. 3.4 Direct voltage control approach

3.2.1.4. Coordinated control method

The framework for coordinated reactive power control is graphically described in Fig. 3.5, which could be conceived as a central control unit. It receives commands from the DNO and measurements describing the actual load flow profile and status of the controllable Var

sources in order to perform an optimization task. The solution of the optimization, for any given operating point, results in optimal distribution of reactive power between each of the sources currently in service leading to minimum losses while satisfying steady-state operational requirements. Such an optimization task, which constitutes a nonlinear mixed-integer problem with discontinuous multimodal and non-convex landscape, is handled in this chapter through enhanced version of mean-variance mapping optimization algorithm (MVMO), presented in [40], with the theoretical background originally published in [41].

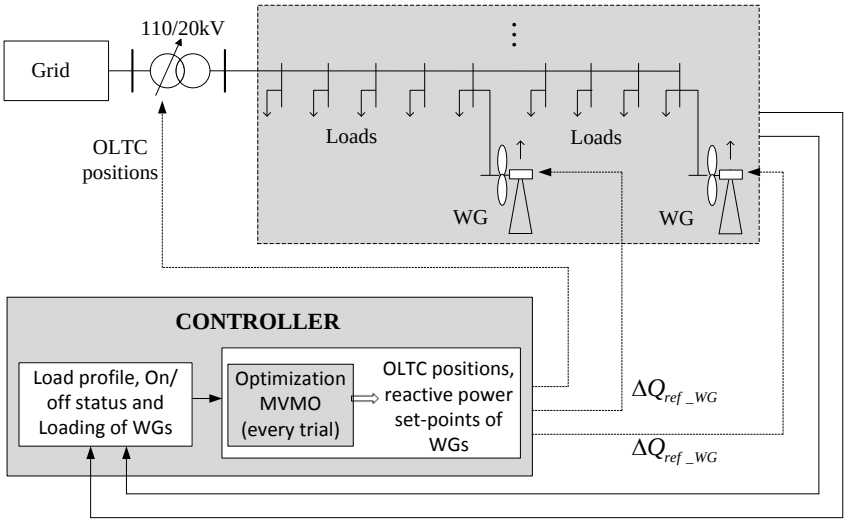

Fig. 3.5 Overview of steady-state coordinated reactive power control

Mathematically, the optimal steady-state coordination of controllable Var sources is formulated as follows:

Minimize

$$OF = P_{\text{loss}} = \sum_{k=1}^{N_l} P_k \tag{3.1}$$

Subject to

- Voltage at all buses:

$$V_i^{\min} \le V_i \le V_i^{\max} \tag{3.2}$$

- Reactive power of WGs:

$$Q_{\text{WG}i}^{\min} \le Q_{\text{WG}i} \le Q_{\text{WG}i}^{\max} \tag{3.3}$$

- OLTC positions:

$$tap_{\mathrm{OLTC}}^{\min} \le tap \le tap_{\mathrm{OLTC}}^{\max} \tag{3.4}$$

where P_{loss} is the total active power losses, P_k is the active power loss in branch k and N_l is the total number of branches:

$$P_{k=(i,j)} = G_{ij}\left(V_i^2 + V_j^2 - 2V_iV_j\cos\delta_{ij}\right) \tag{3.5}$$

G_{ij} is the conductance and δ_{ij} is the difference in the voltage angle between i-th bus and j-th bus, respectively. The subscripts min and max denote minimum and maximum limits, respectively. It is assumed that no requirements with respect to reactive power exchange with the grid is defined, otherwise the required value must be considered as additional constraint in the optimization.

It is worth clarifying that the above simple formulation does not aim at simultaneous minimization of the on-load tap changer (OLTC) operations. This issue will be analyzed in a future work which deals with predictive control issues where actions are taken on the basis of time correlated forecasts of demand and wind power in order to avoid unnecessary short-term OLTC tap changes. Moreover, in comparison with other methods, the coordinated control method is a method strongly based on the availability of the communication system. A drawback of this method is the dependence of the control performance on additional issues, such as, time delay of data transmission, reliability of communication devices, etc. which are, however, not investigated in this chapter.

3.3 Methodological procedure

The goal of the survey presented in this chapter is to gather insight on how each of the four methods for WG's slow Var control described in the previous section impacts the steady-state performance of a distribution network. To this aim, the MC-based procedure depicted in Fig. 3.6 is proposed for evaluation of system performance under a wide range of operating conditions. Preliminarily, the component models (e.g. WG, lines, OLTC, loads) required for steady-state analysis of the studied distribution network and the probabilistic models of system input variables (e.g. probability distribution functions –PDFs- associated to nodal demand and WGs variations) are defined. Then, the procedure starts by drawing random samples of continuous (i.e. nodal demands and wind speed) and discrete (i.e. WG outage occurrence) input variables according to their respective PDF models. Each trial input vector defines an operating state for which the long-term reference inputs (i.e. steady-state set-

points) should be determined for every controllable Var source based either on local or on optimal coordinated targets. Relevant data concerning variation of voltage profiles, operation of OLTC and active power losses are stored at every MC trial until a predefined criterion for statistical convergence is met. Finally, comparisons between control methods can be carried out based on the resulting statistical attributes.

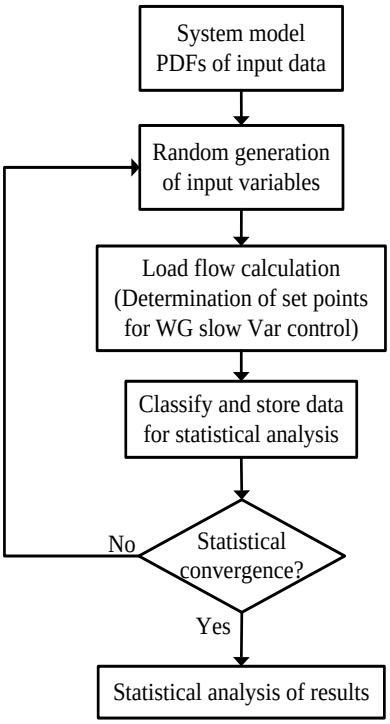

Fig. 3.6 Overview of the proposed approach

3.3.1 Random generation of input variables

Two types of input uncertainties are considered: i) Load demand variation, and ii) WG output. Values for these input variables are generated at every MC trial via simple random sampling scheme from their respective PDF models, which are discussed in the following subsections.

3.3.2 PDF of nodal demand

In the short-term operational planning horizon (e.g. 3 to 5 years), the probabilistic modeling of the variations of distribution system's nodal load demands bases on several aspects related to daily consumption patterns and seasonal effects. Recent studies have focused on this issue by using multivariate normal PDF (MVN-PDF) model and the so-called

load profile indexes (LPIs), derived from load demand surveys across distribution feeders for different classes of consumers (e.g. residential, commercial, and industrial) [42]-[43].

The probabilistic evaluation performed in this work constitutes a non-chronological Monte Carlo type simulation process, for which it is enough to represent correlated nodal demand variations by means of MVN-PDF model [44]. Based on collection of historical information of nodal demand, the MVN-PDF can be approximated through a Gaussian mixture model (GMM), which constitutes a parametric PDF represented as a weighted sum of Gaussian probabilistic densities [44], [45]:

$$p(\boldsymbol{x}|\boldsymbol{\lambda}) = \sum_{i=1}^{M} \omega_i g(\boldsymbol{x}|\boldsymbol{\mu}_i, \boldsymbol{\Sigma}_i) \tag{3.6}$$

where $\boldsymbol{x}$ denotes D-dimensional continuous-valued data vector (i.e. measurements). $\boldsymbol{\lambda}$ is chosen from the set of parameters $\left\{\boldsymbol{\lambda} : \boldsymbol{\lambda} = \{\omega_i, \boldsymbol{\mu}_i, \boldsymbol{\Sigma}_i\}_{i=1}^{M}\right\}$, M is the number of mixture components, ω_i ω_i denotes mixture weight, and $g(x|\mu_i, \Sigma_i)$ $g(\boldsymbol{x}|\boldsymbol{\mu}_i, \boldsymbol{\Sigma}_i)$ stands for component Gaussian densities. Each component density is a D-variate Gaussian function of the form

$$g(\boldsymbol{x}|\boldsymbol{\mu}_i, \boldsymbol{\Sigma}_i) = \frac{1}{(2\pi)^{\frac{D}{2}} |\boldsymbol{\Sigma}_i|^{\frac{1}{2}}} \exp\left(-\frac{1}{2}(\boldsymbol{x} - \boldsymbol{\mu}_i)' \boldsymbol{\Sigma}_i^{2} (\boldsymbol{x} - \boldsymbol{\mu}_i)\right) \tag{3.7}$$

with mean vector $\boldsymbol{\mu}_i$ and covariance matrix $\boldsymbol{\Sigma}_i$. The mixture weights satisfy the constraint that the sum of all the weights must equal one. This condition is necessary because a PDF must be nonnegative and the integral of a PDF over the sample space of the random quantity it represents must add up to unity.

The procedure introduced in [44] is used in this chapter to perform identification of the GMM parameters as well as mixture reduction and merging

3.3.3 PDF of variations of WG production

The variable output behavior of WGs can be modeled statistically by considering two type of uncertainties, one related to the on/off of service status and another one related to wind speed variability.

In this work, the operational status of every WG is assumed as an independent event and described by means of two-state discrete PDF, where the probability of outage (P_F) and the

probability of operation ($\mathbf{P}_O$) are defined in terms of the expected time in operation state (E_{TO}) and the expected time in idle state (E_{TF}).

$$P_F = \frac{E_{TF}}{E_{TF} + E_{TO}}, \quad P_O = \frac{E_{TO}}{E_{TF} + E_{TO}} \tag{3.8}$$

The GMM model is also used in this work to model stochastic wind speed variations, because the advantage of GMM is that different types of empirical PDFs, which do not fit any known single PDF (e.g. normal, Weibull), can be (fairly) represented as a convex combination of several normal distributions.

3.3.4 Determination of set points for slow Var control

A power flow calculation is carried out for each set of sampled WG (status and output power) and load (active and reactive power) variations, in order to determine the corresponding system operating state. As mentioned in Section 2.1 for local slow control methods, the reference input of each controller being studied is derived from local quantities like the generated active power (Constant PF control) or WG terminal voltage (Voltage droop control and Direct voltage control). Those quantities are outcomes of power flow calculation. For the coordinated control method, the reference inputs are directly determined by solving the optimization problem defined by (3.1) – (3.4). For studied control method and for every sampled operating state, the information gathered from power flow analysis allows structuring a statistical database to be used in subsequent system's steady-state performance comparisons in terms of voltage profile variation, OLTC tap changes and active power losses. The information is stored until a statistical convergence criterion is met.

3.3.5 Statistical convergence

A stopping rule is usually used as the statistical convergence criterion in MC based procedures. The purpose of a stopping rule is to provide a compromise between the accuracy needed and the computational effort which is sufficient to achieve some specified confidence level of the estimated statistics. A procedure which performs such an assessment is termed Sequential Estimation [46]. This rule is applied in the proposed approach based on sequential calculation of the relative error ε_r:

$$\varepsilon_r = \frac{\left[\Phi^{-1}(1-\delta/2)\right] \times \sqrt{\sigma'(P_{loss})_N / N}}{E(P_{loss})_N} \tag{3.9}$$

where Φ^{-1} is the inverse function of the normal distribution with mean zero and standard deviation one, 1-δ/2 is the specified coverage probability (0<δ<1), N is the actual sample size, and $E(P_{loss})_N$ and $\sigma'(P_{loss})_N$ are the mean and the variance of the system total active power losses P_{loss} computed in N sampled operating states, respectively. This rule is applied in the proposed MC-based procedure, and it basically consists of computing the relative error in every MC simulation and comparing it with a target relative error (i.e. 0.01). The MC procedure stops when ε_r is less than the target relative error.

3.3.6 Analysis of results

The effects of the steady-state control methods described in the previous section are evaluated and compared by considering MC-based evaluation of the system without operation of the WGs as the baseline case, and the incorporation of the WGs with any of these methods embedded into their control schemes.

Performance comparisons are based on the resulting statistical attributes (e.g. empirical PDF of output variables and blox plots) of system output variables, namely, voltage profile, operation range of OLTC and active power losses.

3.4 Test results and discussion

3.4.1 Test network and experimental conditions

The MC-based approach is tested on a 20 kV radial distribution network with four identical feeders, whose single-line diagram is illustrated in Fig. 3.7. This network has been chosen because its arrangement resembles a typical case in Germany, and the purpose is to evaluate the implications of adding WGs (with any of the previously introduced methods for slow reactive power control) as distributed generators. Such kind of analysis is of interest for distribution system planning and operation. The modeling is done by using parameters taken from a real German distribution network. Distribution cable with parameters R = 0.206 Ω/km, X = 0.177 Ω/km, and C = 235.4 nF/km is used. The distance between two adjacent buses is 1 km, whereas the maximum load demand at every load bus is 1 MW. The distribution network is fed from the 110 kV sub-transmission grid through a 31.5 MVA step-down transformer equipped with OLTC at the primary side.

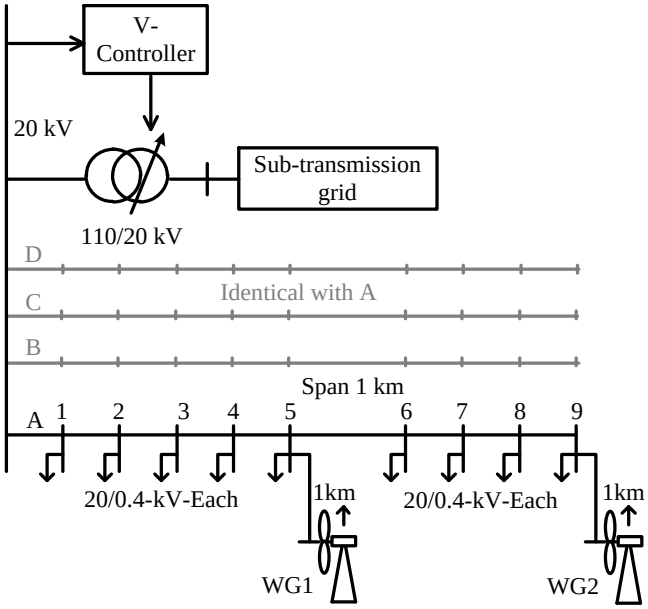

Fig. 3.7 Distribution test system

Two possible additions of WG capacity, as shown in Table 3-1, are evaluated. In the first case, it is considered that 8 MW of wind capacity is installed at buses 5 and 9 of each feeder. The installed capacity doubles for the second case.

Table 3-1 WG capacity

	Scenario A	Scenario B
WG1	4 x 2 MW	8 x 2 MW
WG2	4 x 2 MW	8 x 2 MW

The OLTC operation principle is illustrated in Fig. 3.8. Basically, if the difference between the voltage set-point V_{set} (i.e. 1.01 p.u. corresponding to 20.2 kV) and measured voltage V_{mes} is outside the predefined dead band, the tap-changer will be activated after a given time delay. However, the time delay is omitted in this study, since steady-state operating condition is considered. The OLTC installed on the primary side of the transformer is able to supply ±16% voltage regulation of nominal voltage at secondary side with 27 steps. The dead band is ±75% of voltage deviation arising from one tap-change (i.e. 20.2 ±0.1846 kV). A hysteresis as it is implemented in real OLTC control is not considered in this study.

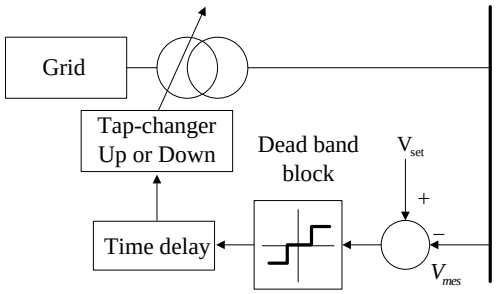

Fig. 3.8 OLTC operation principle

Details of system components, the control methods, MVMO settings, and the PDFs used to demonstrate the proposed methodology are given in the Appendix. Numerical experiments were performed on a Dell 3350 Laptop with an Intel® Core™ i7-2640 central processing unit (CPU), 2.8 GHz processing speed, and 8GB RAM. The modeling, load flow and optimization are using the simulation package PSD [47]. The target relative error for MC is set at 0.01. The number of iterations and the computing time measures associated to MC run performed for each investigated case are given in Table 3-2. Remarkably, different number of iterations is needed for each case to achieve the target relative error, because the system behavior is affected differently by the choice of the control method. Coordinated control entails the highest computational burden due to repetitive execution of optimization task. Besides, for this method, it was found out that, as shown in the exemplary case of Fig. 3.9, the minimization of total losses converges on average after 100 iterations in all sampled scenarios. The computation effort associated to a MC run can be significantly reduced through distributed computing.

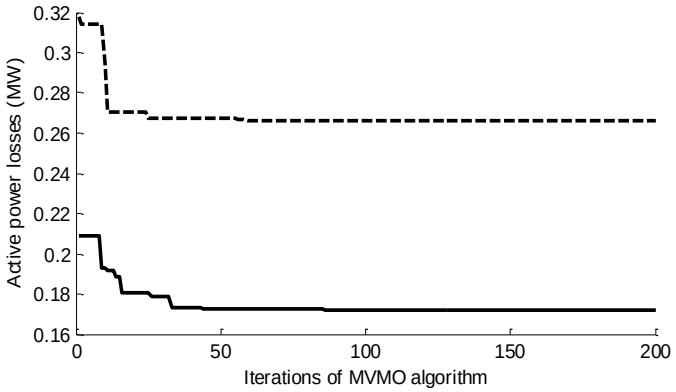

Fig. 3.9 Convergence behavior of active power losses. Dashed and solid line style denote scenario A and B, respectively

Table 3-2 Number of iterations and CPU time involved in MC simulation

Control methods	Number of iterations		Average CPU time (sec)	
	Scenario A	Scenario B	Scenario A	Scenario B
No WGs	29349	29349	3521,9	3521,9
Capacitive PF control	46202	44295	5544,2	5315,4
Unity PF control	21087	39551	2530,4	4746,1
Inductive PF control	35096	38448	4211,5	4613,8
Voltage droop control	41678	19363	2500,7	1161,8
Direct voltage control	36756	38932	4410,7	4671,8
Coordinated control	42767	41482	9408,7	9126,1

3.4.2 Effects on the voltage profile

A MC run results in a large data size due to the number of output variables to be analyzed and the wide range of simulated operating conditions. Thus, the variability of output variables is summarized in different ways in this chapter for ease of understanding. Firstly, the effects of each control method on voltage profile are analyzed by using the box plots depicted in Fig. 3.10 for an intermediate bus (without WG) and the end bus (with WG) of a single feeder. The box plot is a simple graphical representation of groups of numerical data, which allows empirical comparisons between statistical parameters without making any assumption of data's distribution function. Each box shown in the figure provides an intuitive indication of the degree of data concentration between the lower and upper quartiles quartiles (i.e. 25th and 75th percentiles of the data, represented by the lower and upper edges of the box, the size of the box called the Interquartile Range -IQR). The central mark of each box denotes the median, whereas the lines extending vertically from the box (whiskers) indicate the variability (i.e. degree of dispersion and skewness in the data) outside the upper and lower quartiles within a length of 1.5*IQR. Any values not included between the whiskers (outliers) constitute observations that deviate markedly from the rest of the data and indicate the possibility of having a heavy-tailed distribution.

The whiskers and the outliers observed for voltage variations at bus 3 (intermediate bus) and bus 9 (end bus) indicate clearly that the PDF of bus voltages would not follow a single Gaussian distribution, so the GMM model could be also used for output variables. Moreover,

the outliers indicate the occurrence of special operating conditions characterized by high/low load demand and low/high contribution from WGs, for which the control action pushes the bus voltage closer to either upper or lower allowed limit. Comparing with the baseline case, it can be also seen that the presence of WGs with any of the slow voltage control methods will result, in general terms (cf. edges and central mark of the boxes), in an attempt to keep the bus voltages close to the nominal value. Besides, the following peculiarities associated to the statistical information contained in the boxes are highlighted:

- A few differences are noticeable when the constant power factor control method is used with any predefined PF. Despite the closeness of the median to the rated bus voltage, operation of the WGs with constant capacitive PF may involve slightly wider fluctuations as compared to unity or inductive PF modes. The reason is that WGs in this mode inject not only active power but also reactive power into the distribution network.
- In term of local control methods, the best performance is achieved when direct voltage method is chosen, since it supplies the least variability of the voltage magnitude across the feeders. This is reasonable, since any deviation in steady-state is proportionally addressed. The second best performance is obtained when voltage droop control method is used.
- Higher penetration of wind power generation results in better voltage regulation of direct voltage control as well as of the coordinated control due to larger ability in terms of reactive power adjustment by WGs. In contrast, in spite of increased penetration, the use of other local control methods does not directly entail a reduced voltage fluctuation.
- Although small variability is introduced by coordinated control method, it pushes the voltage close to the upper limit (considering ±5% allowed voltage range) as a result of the overall coordinated management, which is minimization of losses.

i) Bus#3

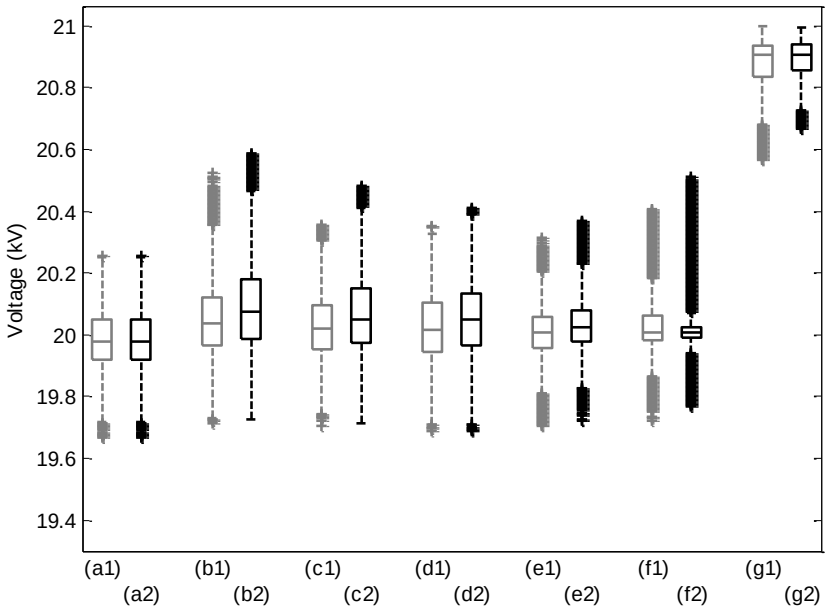

ii) Bus#9

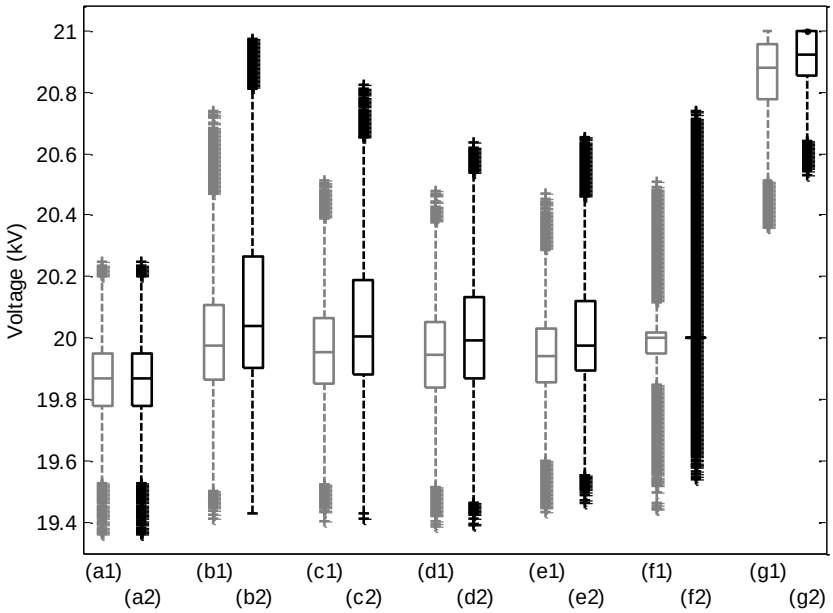

Fig. 3.10 Box plot of the voltage at bus#3 and bus#9, respectively: (a) No WGs, (b) Capacitive PF control, (c) Unit PF control, (d) Inductive PF control, (e) Voltage droop control, (f) Direct voltage control, (g) Coordinated control. Number '1' and '2' stands for Scenario A and B, respectively

3.4.3 Variability at OLTC

A summary of probabilities associated to tap activity in the OLTC is given in Table 3-3. The table cells containing highest and second highest probabilities are highlighted with dark and light gray, respectively. Depending on the sampled operating condition, the OLTC reacts under voltage increase or decrease (denoted by the negative or positive sign of the tap position) at the secondary side. The following remarks are excerpted:

- Note in the table that, for the baseline case as well as for all methods, the OLTC is mostly adjusted to offset voltage drops occurring in the distribution system (i.e. high probabilities for taps with negative sign). These situations arise when the sampled load demand is high while the sampled wind speed is low or a WG is out of service.
- It can be seen that there is a relative high probability of setting the tap at neutral position, especially if direct voltage control is used. Furthermore, the almost negligible probability for tap positions 1 and 2 indicate that the OLTC may be hardly ever adjusted to these positions to reduce voltage rises.
- With increasing penetration of wind power (i.e. higher possibility for reactive power support from WGs), the probabilities of changing the tap to offset voltage drops decrease whereas the probability of setting the tap at neutral position increases.
- The high probabilities associated to the tap positions -1 to -3 indicate that OLTC operation would be frequently required even though local voltage control is available. Besides, the OLTC is mostly set at position -4 when the coordinated control method is used. This issue corresponds with the fact that this method focuses exclusively on minimization ol losses and is in agreement with the remark made in the previous subsection. The joint minimization of losses and OLTC tap changes is therefore recommended.
- If constant PF control method is chosen, it would be preferable to adopt capacitive (leading) PF mode, since it decreases the probability of changing the tap position as compared to unit and inductive PF modes.
- Direct voltage control entails less frequent tap changes and thus constitutes the most attractive option among local control methods. Again, voltage droop control is the second best alternative for local control. Nevertheless, the slope of the VQ could be modified in this method for performance improvement.

Table 3-3 Probability of tap positions

Control method	Scenario	Tap position								
		-6	-5	-4	-3	-2	-1	0	1	2
No WGs	---		$4x10^{-5}$	0.038	0.152	0.534	0.272	0.004		
Capacitive PF control	A			0.016	0.089	0.392	0.399	0.104	$4x10^{-5}$	
	B			0.012	0.070	0.310	0.340	0.220	0.036	0.007
Unit PF control	A			0.023	0.122	0.511	0.333	0.010		
	B			0.019	0.115	0.510	0.350	0.010	$4x10^{-5}$	
Inductive PF control	A		0.001	0.055	0.256	0.501	0.185	0.003		
	B	$3x10^{-4}$	0.019	0.147	0.278	0.408	0.145	0.002		
Voltage droop control	A			0.003	0.098	0.504	0.387	0.008		
	B			$0.6x10^{-4}$	0.088	0.548	0.356	0.008		
Direct voltage control	A			$2.6x10^{-4}$	0.068	0.211	0.460	0.260		
	B		0.0342	0.138	0.064	0.083	0.186	0.540		
Coordinated control	A	0.009	0.117	0.816	0.058					
	B		0.027	0.740	0.160	0.072				
	← Voltage increase									

3.4.4 System losses

Fig. 3.11 shows the mean and variance (lines extending vertically from the means) of active power losses associated to the use of each control method and for both cases of wind power penetration. Note that, for any control method, the increased penetration is reflected in higher mean and variance of system losses. The use of constant PF control method with inductive PF mode would increase significantly the system losses as compared to the other two variants of this method and the other control methods as well. Despite the advantages indicated in previous subsections, direct voltage control method seems less attractive, in terms of effect on system losses, as compared to voltage droop control, especially if the penetration increases. Indeed, since the functionality of voltage control in voltage droop control method is explicitly relieved, which indicates less required amount of reactive power injection/absorption, reactive power transfer in whole network decreases, and hence the losses decrease accordingly. As expected, coordinated control method entails the best performance in terms of system losses.

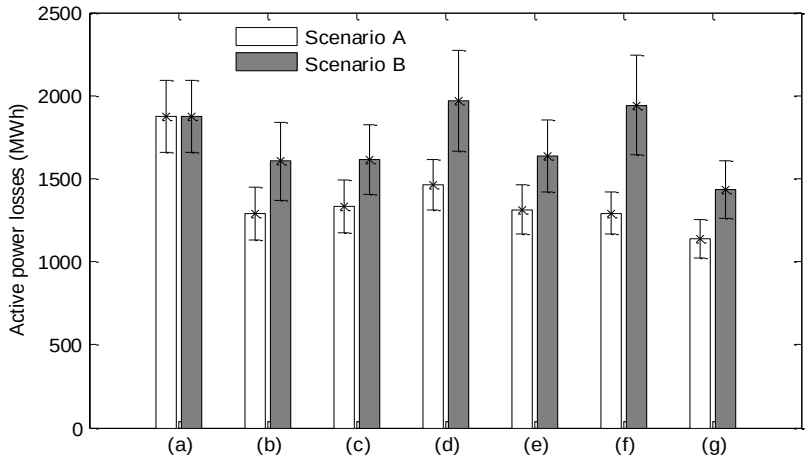

Fig. 3.11 Total active power losses: (a) No WGs, (b) Capacitive PF control, (c) Unit PF control, (d) Inductive PF control, (e) Voltage droop control, (f) Direct voltage control, (g) Coordinated control

3.5 Conclusions

This chapter provides a comparative analysis of different control methods that could be used in WGs connected to distribution systems for voltage and reactive power control during steady-state operating conditions. Based on models describing variation of load demand, wind speed and availability status of WGs, a MC-based procedure was proposed and employed to evaluate the implications of using any of the studied method from a probabilistic point of view.

Numerical tests performed on a radial distribution network, built to resemble the arrangement of a typical case in Germany, have evidenced that direct voltage and voltage droop control methods entail an enhanced system performance among all studied methods for local control. The direct voltage control is slightly superior to voltage droop control to achieve a desirable good voltage profile while involving less probability of changing the OLTC tap position from the neutral position, but it results in higher system losses, especially for high wind power penetration. Nevertheless, if the Volt/Var characteristic of voltage droop control is properly modified, its efficiency could be improved. The information gathered from the probabilistic study will be used to address this issue in a future publication. The coordinated control method entails minimum system losses in all sampled operating conditions, but at the expense of pushing the bus voltages closer to the upper limit and a high

probability of requiring a change of OLTC tap position. This issue can be tackled by pursuing the simultaneous minimization of system losses and OLTC tap changes.

Chapter 4
Voltage and reactive power control based on adaptive step optimization

In existing distribution networks only few measurement devices are equipped at several selected buses; therefore, the heuristic optimization based control scheme in chapter 2 is not applicable due to lack of necessary information leading to impossibility of optimal power flow calculation. A counter-measure to this is utilization of sensitivities, that can be estimated through available limited information in addition to pseudo-measurements created by historic data, to calculate optimal control actions. One of drawbacks of the sensitivities based controllers is inaccuracy of estimated sensitivities resulted from restriction of available information and hence excessive control actions could happens as a response. To this point, this chapter presents a sensitivities based controller for online centralized control scheme in distribution networks, which combines a proportional integral (PI) for control unit in incorporation with a corrective control unit (CCU) which is inspired from Model Predictive Control (MPC), in order to overcome inaccuracy of sensitivities. The proposed controller is designed to accommodate increasing penetration of distributed generation in active distribution networks, to satisfy reactive power requirement of the transmission system operators (TSOs) while maintaining voltages in distribution networks and simultaneously minimize the total active power losses, hence also meet operation requirements of distribution network operators (DNOs). Moreover, computational burden of the proposed controller is almost assigned to the CCU which is only activated in several conditions, thus leading to computational benefits.

4.1 Introduction

Intermittent renewable energy resources (RES) like solar and wind will be connected largely to European distribution networks due to the recent new targets for RES penetration

in the European Union (globally 20% of energy consumption covered by RES by 2020) [49]. This entails several challenges to system reliability and security, especially in short term operation time frame, where a high degree of variability of power supply from RES may occur [50]. Therefore, developing new control architectures for use in future new configuration of distribution networks is crucial to achieve optimal, flexible, and efficient operation with minimum risk of occurrence of security threats.

To this aim, several approaches have adopted *optimal power flow based strategies* in the proposed control architectures with centralized controllers. For instance, the approaches presented in [51]-[56] base on different optimization formulations in order to achieve different operational targets. Moreover, it could be easily seen that minimization of active power losses often appears in objective function of these approaches. While in [51], [52] and [53], losses minimization serves as essential optimization target, other approaches combine it with additional target, such as the annual active generation curtailment cost [54], voltage variation [55], or reducing the amount of reactive power imported from TSOs [56]. Disadvantage of power flow calculation based approaches is high demand of available information that is not the case in existing distribution networks.

Alternatively, other adaptive control approaches base on integration of *sensitivities theory* into centralized controllers has drawn much attention in recent years: These approaches are suitable for online application of controllers. In [57], an approach based on voltage-sensitivity factors to minimize the annual active generation curtailment cost is proposed. Besides, some approaches are also introduced to maintain voltage within its limit in [58], [59] and [60], to mitigate voltage rise and line overloads in [61]. However, there is no discussions on methods against the case of excessive control actions are caused by imprecisely estimated sensitivities.

On the other hand, to deal with global challenges in whole power systems, there have been many debates in recent years on a shift in preference from passive control schemes to '*active network management*' (smart grid) [62] which not only adjust networks for LF, but also minimize the effect on adjacent networks. For instance, the grid codes [63] and the European Network of Transmission System Operators for Electricity [64] define a set of common requirements at the interface between transmission and distribution networks (or wind farms in particularly, discussed in chapter 2). Authors in [52], [65], [66] and [67] propose different

measures to reduce impact of DGs on the transmission system through regulating reactive power exchange at the point of common coupling (PCC).

This chapter proposes a new architecture of centralized controller for the *active network management* which is able to optimally drive the online network operation with available measurements of several selected buses subjected to operation security constraints (i.e., voltage violation). The proposed controller is designed to satisfy reactive power requirement of the transmission system operators (TSOs) while maintaining voltages in distribution networks within an allowable range and simultaneously minimize the total active power losses. Architecture of the controller is formed by incorporation of two following controllers:

● The PI controller with slow response undertakes a task of fulfilling requirements of TSO (i.e. reactive power import/export from distribution networks at the point of common coupling (PCC)) by equally distributing reactive power demand into available Var sources. The controller's limitation is specified based on the compliance simulations for reactive power ranges of transmission connected distribution networks, presented in [64].

● and a controller, based on the principles of Model Predictive Control (MPC) in addition to sensitivities theory to enable its real-time implementation, is adopted to satisfy requirements of DNO such as voltage profile and losses minimization. The controller serving as a corrective control unit (CCU), hence only trigged when necessary, is needed to correct control actions in optimal manner based on measurements at selected busses and offline trained model knowledge

Peculiarity of the proposed controller is achievement of synthesized capabilities as follows:

- Capability of continuous fulfillment of the TSO requirement without computation burden.

- Capability of overcoming model inaccuracies or delays of the control actions to correct voltage profile.

- Capability of achieving optimization objectives, such as losses minimization, of entire network with limited number of available measurements.

- Capability of driving the network operation close to optimal operating point as fast as possible without violation on operation conditions, even model inaccuracies or delays of the control actions subjected

- Capability of alleviating computation burden.

The chapter is organized as follows: Section 4.2 explains the overall operation principle of the proposed controller and Section 4.3 contains description in detailed of the CCU. Test network and algorithm implementation given in Section 4.4. Then simulation results and discussion is presented in Section 4.5 with conclusions given in Section 4.6.

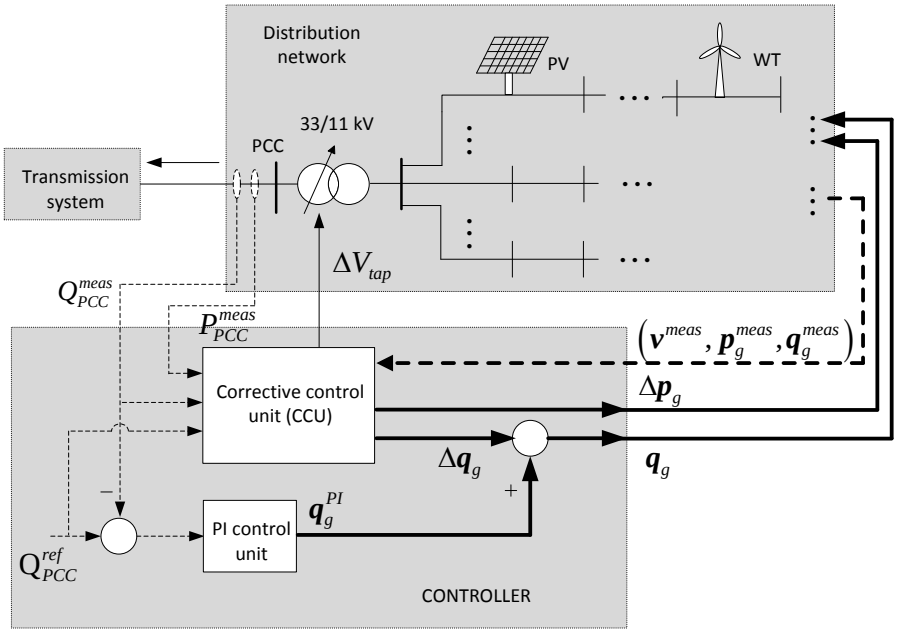

Fig. 4.1 The proposed controller scheme

4.2 Proposed control strategy

The proposed controller's scheme is sketched in Fig. 4.1 with two main control units such as the PI control unit and the CCU inspired by MPC. While the PI control unit carries out fulfilling reactive power demand (Q_{PCC}^{ref}) requested by TSOs (e.g. to meet certain grid code requirements), the CCU operates to correct the control variables for purpose of the losses minimization and voltage correction. The controller presented in this chapter focuses on slow control functionality, which is characterized by a slow response (e.g. 10 seconds to few minutes) to adapt the DG response to changing steady-state requirements. In this study, there are three kinds of control variables:

$$\boldsymbol{u} = \left[\boldsymbol{q}_g, V_{tap}, \boldsymbol{p}_g\right]^T \tag{4.1}$$

with ^{T} denotes array transposition, $\boldsymbol{q}_g$, V_{tap}, $\boldsymbol{p}_g$ are reactive power injection of DGs, voltage set-point of the transformer, and active power injection of DGs, respectively .

The control algorithm can be summarized as follows:

- Firstly, the proposed controller collects necessary measurements such as ($Q_{PCC}^{meas}, \boldsymbol{v}^{meas}, \boldsymbol{p}_g^{meas}, \boldsymbol{q}_g^{meas}$) where Q_{PCC} and $\boldsymbol{v}$ are reactive power exchange at PCC and voltages at selected buses, and subscript ^{meas} stands for measurements
- Then, the controller, performs its calculation to output control actions such as reactive power set-points of DGs ($\boldsymbol{q}_g = \boldsymbol{q}_g^{PI} + \Delta\boldsymbol{q}_g$) where $\boldsymbol{q}_g^{PI}$ is reactive power injection of DGs requested by PI control unit, and change of voltage set-point of the OLTC transformer (ΔV_{tap}), curtailment of active power injection of DGs ($\Delta\boldsymbol{p}_g$) when needed. These control actions will be transmitted into corresponding components in the network to perform local control.
- Except $\boldsymbol{q}_g$ which was calculated in the controller, at local level other set-points as ($V_{tap}, \boldsymbol{p}_g$) are computed as presented in Fig. 4.2 in which V_{tap}^{ref} is based on initial setting of the tap changer and $\boldsymbol{p}_g^{ref}$ is calculated based on actual operating conditions such as wind speed, solar intensity, etc. Note that subscript ^{ref} stands for reference value.

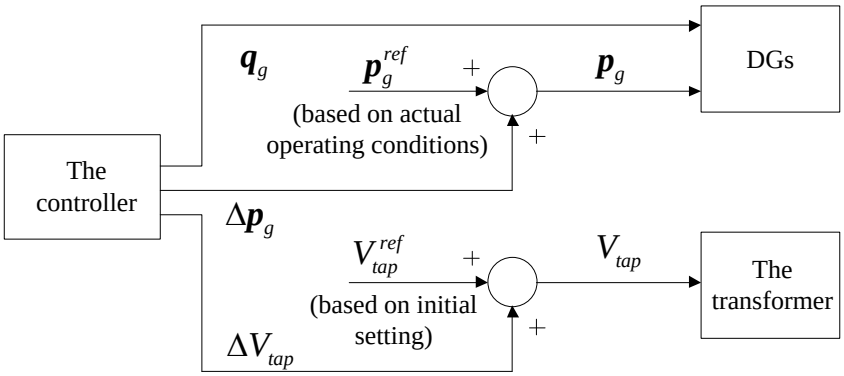

Fig. 4.2 Calculation of set-points at local level

4.3 The corrective control unit

The CCU is infrequently triggered under predefined conditions that will be discussed later, to correct voltage profile and minimize the total losses, as shown in Fig. 4.3. As soon as triggered, the CCU starts collecting available online measurements. Some of them are predefined as input of an artificial neural network (ANN) which is offline trained to output

sensitivities. Process of determining control actions is performed afterwards in inclusion of online measurements and sensitivities provided by the ANN. Next, to avoid inaccurate measurements caused transient phenomenon after control actions implementation, the new measurements for next calculation iteration will be performed after a time delay T_{delay}. N_{step} is a predefined value to limit the number of calculation iterations of the CCU per a triggering.

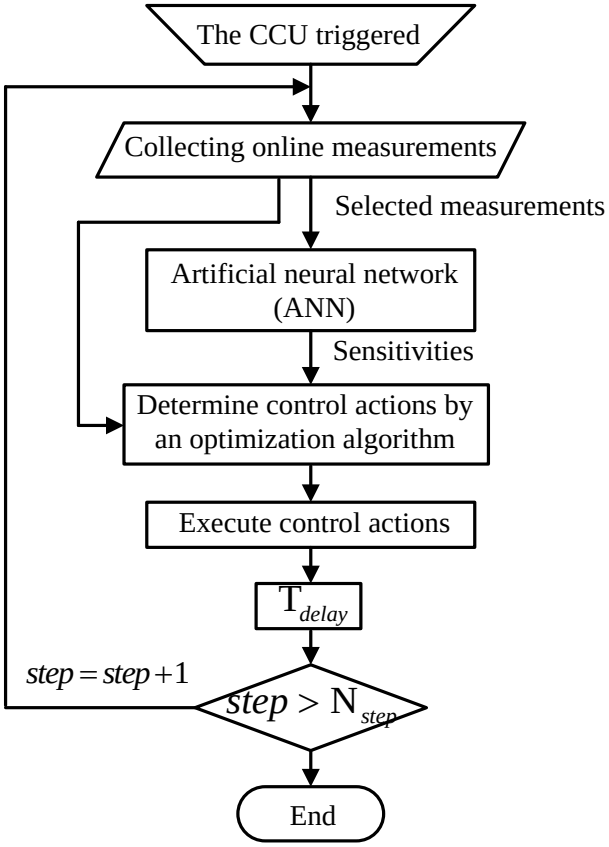

Fig. 4.3 Flowchart of the CCU operation principle

4.3.1 Conditions of triggering the CCU

To relieve the computation burden, the CCU is triggered, when necessary, in following conditions:

- *Voltage violation*
- *Considerable change of operation condition:* It is reasonable that when the networks significantly change their operation condition, optimal operation setting-points of the networks need to be adjusted as a response. Level of the change could be specified based all

available measurements, this is however out of scope of this study.

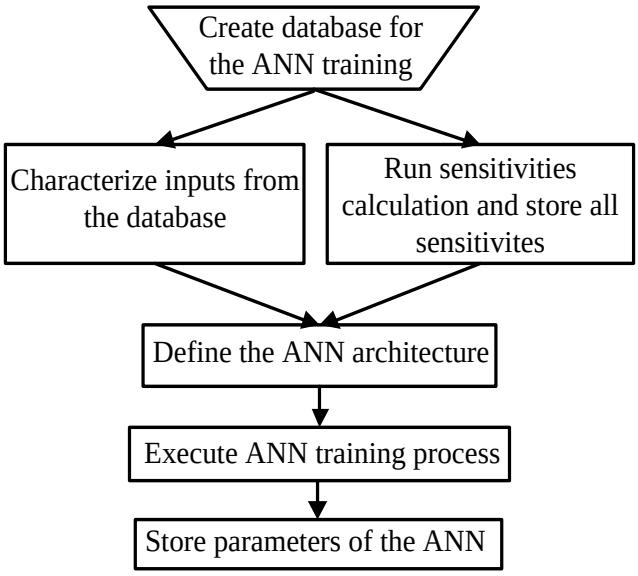

Fig. 4.4 Flowchart of building the ANN

4.3.2 Artificial neural network

As indicated earlier, the ANN is used to approximate sensitivities with several online measurements as its input. The procedure of creating the ANN involves several steps, as shown in Fig. 4.4, in which the ANN training process is offline performed. Firstly, a database is created by using historic or predicted or approximated load profiles. Characterizing input of the ANN as well as calculating sensitivities (considered as the output) from the created database is performed afterwards. Next, architecture of the ANN is characterized in connection with above set of input and output. Then process of training is carried out to specify parameters of the ANN which all are stored afterwards.

1) Sensitivities Calculation at an Operating Point:

Sensitivities calculation is generally categorized into two methods, analytical and numerical. The analytical one uses steady-state power equations in a LF calculation, for example, inverse of the Jacobian matrix providing the sensitivity of bus voltages with respect to power variations. In addition, Van Cutsem *et al.* [68] fully reported formulations to compute sensitivities between different variables in networks. The numerical is that sensitivities may be approximated by several LF calculations, each obtained by a small perturbation to one control variable. In this study, we use the latter to calculate sensitivities.

4.3.3 Determination of the control actions

The CCU based on MPC mechanism calculates the change of control variables $\Delta \boldsymbol{u}(k)$ at time instant k, shown in (4.2), not only to maintain the monitored voltages within permissible limits, but also to possibly minimize the losses.

$$\Delta \boldsymbol{u}(k) = \left[\Delta \boldsymbol{q}_g(k)^T, \Delta V_{tap}(k), \Delta \boldsymbol{p}_g(k)^T \right]^T \tag{4.2}$$

with $\Delta \boldsymbol{u}(k) = \boldsymbol{u}(k) - \boldsymbol{u}(k-1)$

4.3.3.1. Formulation of the overall objective function

The overall objective function of the CCU is a function of multi-objectives corresponding to following control variables:

- *Reactive Power of DGs:*

Different objective functions can be used by the system operators, besides the traditional transmission losses minimization, the others such as minimization of reactive power cost [69], [70], or minimization of deviations from contracted transactions [71], or minimization of the cost of adjusting reactive power control devices [59], [72]. In this study, losses minimization is selected, and the objective function (OF) at time instant *k* is therefore as follows:

$$OF_1(k) = \min \left(\left(\frac{\partial \boldsymbol{P}_{loss}}{\partial \boldsymbol{q}_g} \right)^T \Delta \boldsymbol{q}_g(k) \right) \tag{4.3}$$

where $\boldsymbol{P}_{loss}$ is a vector of the active power losses

- *Tap-changer of the Transformer:* The higher number of OLTC tap changer operations is proportional to higher cost in maintenance and shorter its lifetime; consequently, minimization of tap changer operations is often a favorite optimization target. On the other hand, tap changers will be activated by:

i) Changes in operation conditions push the controlled voltage at substation V_{ctr} out of the dead-band.

ii) Or a shift of the dead-band is caused by a change of V_{tap} so that the controlled voltage at substation V_{ctr} out of the dead-band. Therefore, minimization of change of V_{tap} could leads to the least number of OLTC movements.

$$OF_2(k) = \min\left(\left|\Delta V_{tap}(k)\right|\right) \tag{4.4}$$

➢ *Active Power Generation of DGs:* One of economic operation ways is maximization of active power production from DGs. This is permanently satisfied at local level because DGs always try to capture maximum power by tracking actual conditions such as wind speed, solar, etc. However, under certain operation conditions such as voltage violation, etc., some curtailments of active power of DGs are requested to save normal operation. Consequently, minimization of active power curtailment becomes necessary in the network operation control.

$$OF_3(k) = \min\left(\sum_{j=1}^{N_g}\left|\Delta p_{gj}(k)\right|\right) \tag{4.5}$$

where N_g is the number of DGs

As mentioned earlier, the CCU is essentially a MPC which finds a sequence of control actions in N_C steps. Therefore, overall objective of the CCU is formulated as follows with incorporation of these objective functions in (4.3), (4.4), (4.5) under a relation describing by a weighting matrix, $\boldsymbol{w}$, to penalize expensive control actions.

$$OF = \min\sum_{i=0}^{N_C-1}\left(\boldsymbol{w}^T\left[OF_{1,2,3}(k+i)\right]^T\right) \tag{4.6}$$

subject to:

● Constraints of control variables

$$\mathbf{u}^{\min} \le \boldsymbol{u}(k+i) \le \mathbf{u}^{\max} \tag{4.6a}$$

● Constraints of voltage

$$\mathbf{V}^{\min} \le \boldsymbol{V}(k+i) \le \mathbf{V}^{\max} \tag{4.6b}$$

● Constraint of reactive power exchange with external grid

$$\left|\mathrm{Q}_{\mathrm{PCC}}^{\mathrm{ref}} - Q_{PCC}^{meas}(k+i)\right| \le \varepsilon \tag{4.6c}$$

(4.6) indicates that control actions of the CCU do not cause any interaction with PI control unit. Therefore, it may be translated to (4.6):

$$\left|\frac{\partial Q_{PCC}}{\partial \boldsymbol{u}}\Delta\boldsymbol{u}(k+i)\right| \le \varepsilon \tag{4.6d}$$

4.3.3.2. The voltage constraint-Its problems and its adaptation into the optimization algorithm

The constraint (4.6) can be rewritten as follows:

$$\mathbf{V}^{\min} \le \boldsymbol{v}^{meas}(k \mid k) + \sum_{l=0}^{i} \Delta \boldsymbol{V}(k+l) \le \mathbf{V}^{\max} \tag{4.7}$$

, then can be transformed into:

$$\boldsymbol{LB}(k+i \mid k) \le \sum_{l=0}^{i} \Delta \boldsymbol{V}(k+l) \le \boldsymbol{UB}(k+i \mid k) \tag{4.8}$$

with $\begin{cases} \boldsymbol{LB}(k+i \mid k) = \mathbf{V}^{\min} - \boldsymbol{v}^{meas}(k \mid k) : \text{Lower bound} \\ \boldsymbol{UB}(k+i \mid k) = \mathbf{V}^{\max} - \boldsymbol{v}^{meas}(k \mid k) : \text{Upper bound} \end{cases}$

and $\Delta \boldsymbol{V}(k+l)$ is calculated based impacts of three following events:

$$\Delta \boldsymbol{V}(k+l) = \Delta \boldsymbol{V}_1(k+l) + \Delta \boldsymbol{V}_2(k+l) + \Delta \boldsymbol{V}_3(k+l) \tag{4.9}$$

- $\Delta \boldsymbol{V}_1$: Impacts of control actions on voltage changes.

$$\Delta \boldsymbol{V}_1(k+l) = \frac{\partial \boldsymbol{V}}{\partial \boldsymbol{u}} \Delta \boldsymbol{u}(k+l) \tag{4.10}$$

- $\Delta \boldsymbol{V}_2$: Especially due to slow response of tap position changes, it is treated as known disturbances.

$$\Delta \boldsymbol{V}_2(k+l) = \frac{\partial \boldsymbol{V}}{\partial V_{tap}} \Delta V_{ctr}^{tap} \gamma(k+l) \tag{4.11}$$

- $\Delta \boldsymbol{V}_3$: A case that could happens is that at the time when the CCU collects measurements, PI control unit still not yet fulfill reactive power exchange due to its slow response. Consequently, the CCU has to account for influence on voltages caused by further output evolution of PI control unit as follows.

$$\Delta \boldsymbol{V}_3(k+l) = \frac{\partial \boldsymbol{V}}{\partial \boldsymbol{q}_g} \Delta \boldsymbol{q}_g^{PI}(k+l) \tag{4.12}$$

$$\Delta \boldsymbol{q}_g^{PI}(k+l) = \left(\frac{Q_{PCC}^{ref}(k+l) - Q_{PCC}^{meas}(k+l)}{N_{DGs}} \right) \left(\frac{\partial Q_{PCC}}{\partial \boldsymbol{q}_g} \right)^{-1} \tag{4.13}$$

where $\Delta \boldsymbol{q}_g^{PI}$ is reactive power of DGs further required by PI controller, and $\partial \boldsymbol{V} / \partial \boldsymbol{q}_g$ is sub-matrix of the matrix $\partial \boldsymbol{V} / \partial \boldsymbol{u}$

On the other hand, to avoid excessive control actions caused by inaccurate sensitivities leading to voltage violation and to ensure voltages within their limits at the end of the

prediction horizon, range of voltage bounds need to be tuned narrower at beginning of the control horizon and progressively expanded to its actual value up to the end of control horizon. Consequently, the voltage bounds in (4.8) can be adaptively adjusted as follows:

$$\begin{cases} \boldsymbol{LB}(k+i\,|\,k) = \lambda(k+i)\boldsymbol{LB}(k+i\,|\,k) \\ \boldsymbol{UB}(k+i\,|\,k) = \lambda(k+i)\boldsymbol{UB}(k+i\,|\,k) \end{cases} \tag{4.14}$$

with $\lambda(k+i) \triangleq \beta\left(\frac{\mathrm{N_C}-(i+1)}{\mathrm{N_C}}\right)$ and β is tuning factor

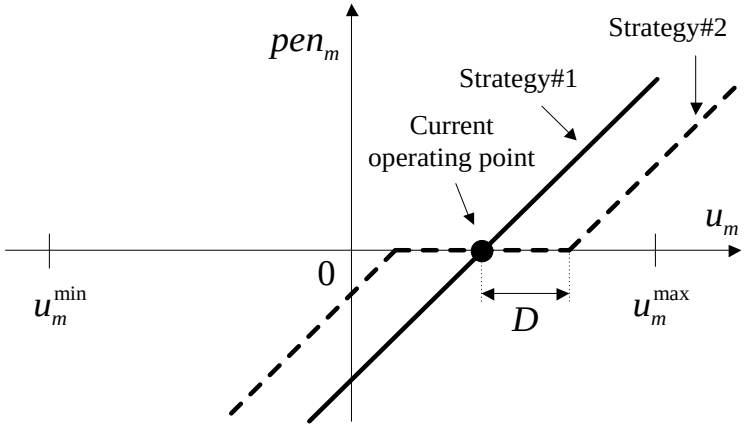

Fig. 4.5 Determination of penalty value of each control variable $\boldsymbol{u_m}$

4.3.3.3. Modification of the overall objective function to achieve better performance

In this chapter, sensitivities are calculated based on small perturbation of each control variables (e.g., smaller than 10% of its nominal value). Therefore, modification of the overall objective to attempt keeping change magnitude of control variables around their actual values is necessary to enhance accuracy of the sensitivities. To do so, an additional penalty term imposed on the change of control variables should be added in the objective function; therefore, (4.6) becomes as follows:

$$OF = \min \sum_{i=0}^{\mathrm{N_C}-1}\left(\boldsymbol{w}^T\left[OF_{1,2,3}(k+i)\right]^T + \sum_{m=1}^{\mathrm{N_g}} pen_m(k+i)\right) \tag{4.15}$$

with pen_m is calculated in base on two following strategies presented in Fig. 4.5:

► Strategy#1:

$$pen_m(k+i) = \alpha\Delta u_m(k+i) \tag{4.16}$$

where α is slope of characteristic lines

► Strategy#2: A dead-band to be used is to penalize only large change of control variables.

$$pen_m(k+i) = \begin{cases} 0 & \text{, if } |\Delta u_m(k+i)| \le D_m \\ \alpha \Delta u_m(\text{k+i}) & \text{, otherwise} \end{cases} \quad (4.17)$$

Introduction of D_m indicates that change of mth control variable only be encouraged in this range. And value of D_m should be selected equal to the value of perturbation of these variables in sensitivities calculation process, hence $D_m \leq 10\%$ of the nominal value.

4.3.4 Adaptive selection of the control horizon

Losses minimization at loss control mode of the controller would firstly be concerned during normal operation. To reach this target, the controller must be sure that voltages are always acceptable, even inaccurate sensitivities subjected. This can be achieved by setting $N_C \geq 2$, as explained in (4.14), which however leads to more computational expense.

On contrary, it would be reasonable that when voltage violation takes place somewhere over the network, voltage control mode should be activated, and it is expected that voltage should go into the limits as fast as possible, hence N_c should be minimum (hence, $N_C = 1$).

4.4 Test network and algorithm implementation

4.4.1 Test network and measurement deployment

The test network in Fig. 4.6 is taken from a U.K. generic distribution network (UKGDN), available in [73]. It comprises of 75 load buses (except bus#1000 and bus#1100) and 22 DG units (3MW in the nominal capacity of each), connects to transmission system through a cable (its Thévenin reactance of 0.1 p.u of 200 MVA short-circuit power used in this chapter) and a 33/11 kV transformer equipped with OLTC which is able to regulate voltage in range of ± 10% nominal voltage at distribution network side with 19 its tap positions. Reactive power capacity of each DG is limited in range ±2 MVAR.

Besides measurements at all DG buses, voltage of several additional buses is also measured as in Fig. 4.7, in order to expect that if voltages at these buses are admissible, those at the other busses are too.

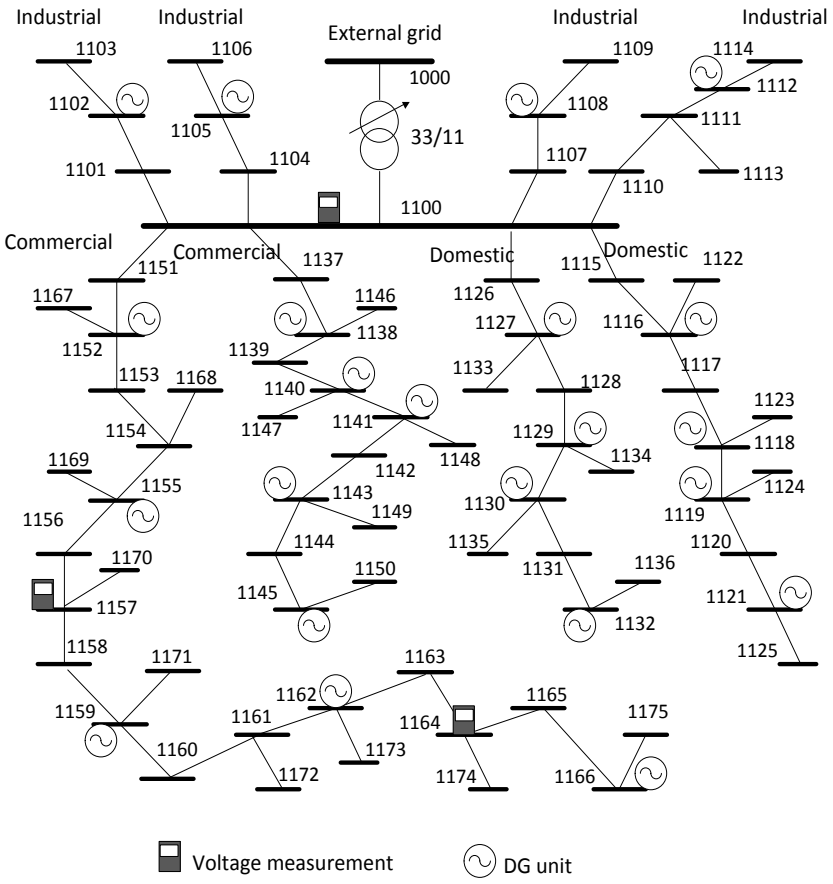

Fig. 4.6 Test network

4.4.2 Characteristic and parameters setup of the controller

4.4.2.1. The ANN

Half hourly normalized active power load and generation profiles over one year along are provided in the UKGDN. However, since the load profiles given in form of each consumer class among four ones (Domestic/Unrestricted (D/U), Domestic-Economy (D/E), Industrial (I), and Commercial (C)), the methodology, given in [74] and belongs to approximation methods, of mixing consumer classes at each bus to create load profile (used as the database of the ANN) is adopted in this chapter. Then the ANN training takes over a whole year with 17520 half-hour time steps of the database.

Finally, it is worth mentioning that the CCU requires the ANN to provide three kinds of sensitivities such as: $\partial \boldsymbol{P}_{loss}/\partial \boldsymbol{q}_g$, $\partial \boldsymbol{V}/\partial \boldsymbol{u}$ and $\partial Q_{PCC}/\partial \boldsymbol{u}$

4.4.2.2. Parameters setup and algorithm selection for the controller

Preserving the voltages in the distribution network within ±5% of their nominal values is aim of the controller. Table 4-1 describes necessary parameters that need to be set up for the controller operation.

Table 4-1 Parameters of the controller

PI control unit		Corrective control unit	
K_I	K_P	T_{delay}	N_{step}
0.01	0.1	10 s	4

As discussed before, N_{step} indicates trade-off between controller performance and computational expense since larger N_{step} could translate to higher performance and higher computational burden. In this fashion, $N_{step} = 4$ is intuitively selected in this study. In addition, it is also assumed that calculation time of controller to give control actions is 2 s.

The problem in (4.6) can be obviously solved by using various optimization methods; however, in this study, a sequential equality constrained quadratic programming method in IMSL library is adopted.

4.5 Results and discussion

4.5.1 Losses minimization performance of the controller

4.5.1.1. Impacts of the overall objective function modified

Fig. 4.7 shows response of the controller in fulfilling reactive power demand which is requested by TSOs.

As discussed in Part III-C-3, two strategies were proposed to improve performance of the controller. In each strategy, value of the slope, α=1.0, 0.1, 0.05 and 0.01, is simulated in turn. And they are compared with the original strategy (without penalty term in the objective function, α=0.0), namely Baseline. It can be seen from Fig. 4.8 that in case of Baseline, performance of losses minimization can be comparative with the cases of two strategies; however, much fluctuation of power unexpectedly appears. This is because control variables

requested by the controller move far from their actual values to attempt minimizing the losses. Unfortunately, such large change of control variables could aggravates inaccuracy of their sensitivities which are approximated by small perturbation around their actual values. In contrast, with introduction of two proposed strategies, the drawback of Baseline case can be solved.

In Strategy#1, the controller displays too different performances with various slopes α. On the other hand, introduction of a dead-band around actual value of each control variables in Strategy#2 can alleviate dependence between the controller performance and the slope α, hence selection of α becomes easier.

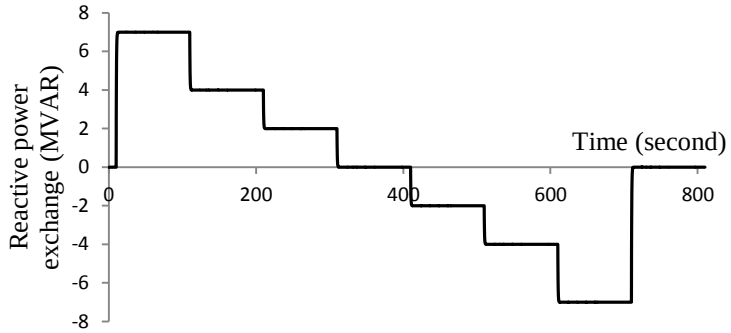

Fig. 4.7 Correction of reactive power exchange

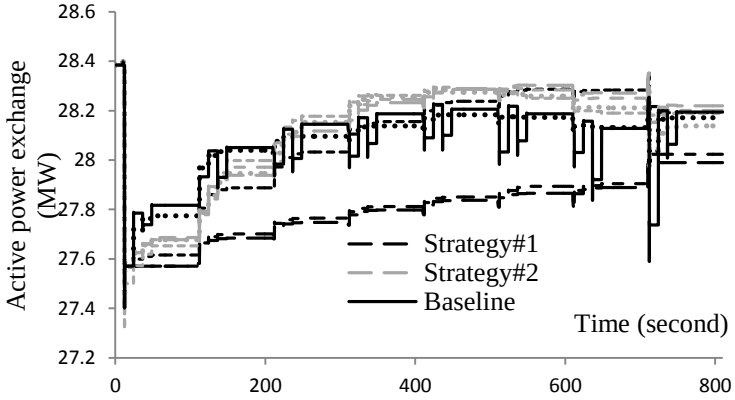

Fig. 4.8 Active power exchange inversely proportional to losses reduction: Largely to small dashed black lines describe Strategy#1 with α from bigger to smaller. The similarly featured lines but with light black color present Strategy#2, and solid black line is of Baseline

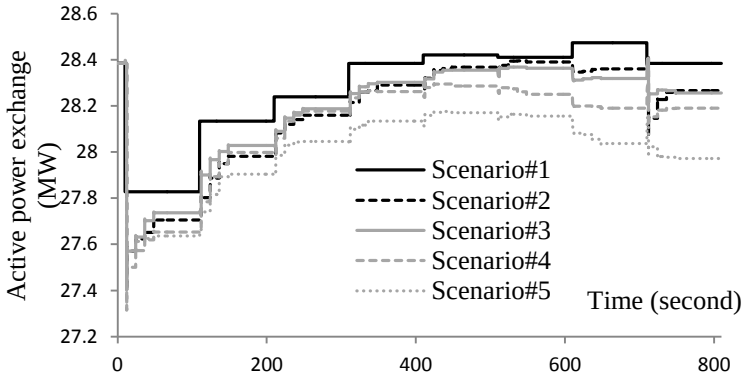

Fig. 4.9 Active power exchange inversely proportional to losses reduction

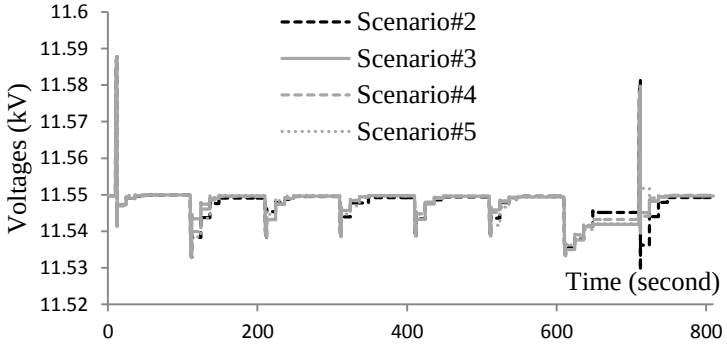

Fig. 4.10 Voltage at bus#1166 with highest probability of voltage violation

4.5.1.2. Impacts of sensitivities accuracy

To demonstrate, performance of the controller is strongly dependent on accuracy of sensitivities. Here we investigate the performance of the controller in following scenarios with the same operation conditions of the previous case. Accuracy of the sensitivities decreases to from Scenario#2 to #5.

- ✓ Scenario#1: At each new operating point, optimal LF calculated by a heuristic optimization algorithm, namely Mean Variance Mapping Optimization (MVMO), is adopted in order to minimize the losses. This scenario apparently provides the best performance and hence, considered as a base case for comparison.
- ✓ Scenario#2: Sensitivities are directly computed by using LF calculation (not using the ANN) at each calculation step.
- ✓ Scenario#3: The sensitivities are provided by the ANN with 66 input signals, ($\boldsymbol{v}_g^{meas}, \boldsymbol{p}_g^{meas}, \boldsymbol{q}_g^{meas}$) of all 22 DGs.

- ✓ Scenario#4: It is repetition of Scenario#3, however with only 33 input signals of 11 DGs.
- ✓ Scenario#5: Sensitivities are initially calculated by LF calculation, and remaining unchanged during simulation time.

Fig. 4.9 presents that performance of the controller in minimizing the losses is directly proportional to accuracy of sensitivities. Moreover, from Scenario#3 and #4 it is a further assertion that training performance of the ANN can be improved with increasing number of its input.

It is the fact that with nature of model-based, closed-loop and carefully but not conservatively reaching to targets (i.e., adaptive length of control horizon according to actual operation condition), the proposed controller, as shown in Fig. 4.10, displays ability of regulating voltage subjected to inaccuracy of sensitivities.

4.5.2 Voltage correction performance of the controller

4.5.2.1. Impacts of adaptive selection of the control horizon

In this scenario, it is assumed that the network operates at the condition with low load and high generation so that some buses are facing high voltage conditions.

To investigate performance of voltage regulation in terms of length of the control horizon in the proposed controller, three strategies such as adaptive length introduced in Part III-D, long one (e.g. $N_c = 2$) and short one ($N_c = 1$, preferred by the network operator) are compared. In this investigation we assume the CCU triggered at t=10s merely for creating clearer pictures as in Fig. 4.11. Then the voltage starts decreasing at t=12s when control actions apply. The short and the adaptive one have faster capacity in correcting the voltage than the long. As a result, at t=22s, while the short and the adaptive work for loss control, the long still continue correcting voltage. In other words, due to inaccurate model, the short produces excessive control actions, hence voltage breach at t=24 s. This is not repeated in the adaptive since in loss control mode the adaptive becomes a long one which carefully calculate sequences of control actions to reach targets within several time steps ahead.

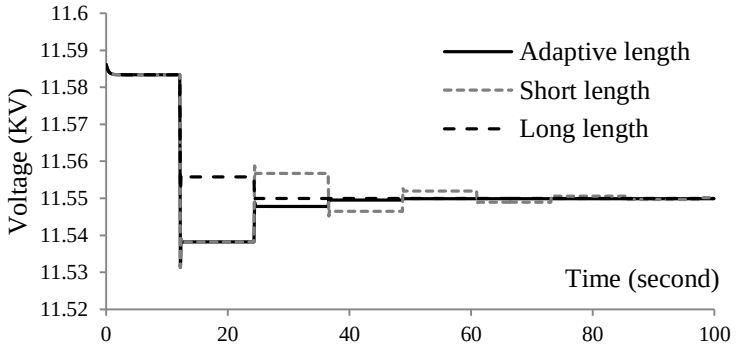

Fig. 4.11 Voltage at bus#1166 with highest probability of voltage violation

4.5.2.2. Voltage correction without OLTC of the transformer

Initially all DGs optimally operate to keep reactive power exchange zero. Afterwards at t=10 s and t=100 s, a large amount of 20 MVAR export and then down to 5 MVAR, respectively, is requested by TSOs, and Fig. 4.12 presents response of the controller to fulfill this demand.

It can be seen from Fig. 4.14 and Fig. 4.15 that during the time interval between t=10 s and t=100 s when the large amount of reactive power demanded, DGs closer to the substation try to fulfill reactive power exchange, meanwhile other DGs at the end of several feeders, where voltages reach to their limits (±5% nominal voltage), absorb reactive power to decrease voltage. But it can be seen that reactive power capacity of these DGs is insufficient to correct voltages. Drop of active power generation of DGs is needed, as shown in Fig. 4.13. As soon as the reactive power demand reducing to 5 MVAR at t=100 s, the CCU realizes that reactive power control is able to bring the voltages into their limits, so active power curtailment should be eliminated. However, to avoid excessive control actions caused by inaccurate model or measurement noises, the CCU carefully took some sequences to gradually eject expensive control actions, thereby always keeping the voltages in the limits over the simulation time, as shown in Fig. 4.15.

At each triggered at t=10 s and t=100 s, the CCU have four chances, which defined by N_{step} =4, to reach its target as well as improve its performance. Fig. 4.16 presents that with loss control mode the controller is able to improve its performance in minimizing the losses.

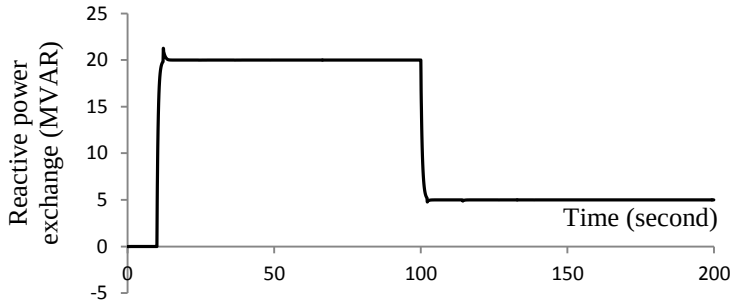

Fig. 4.12 Correction of reactive power exchange

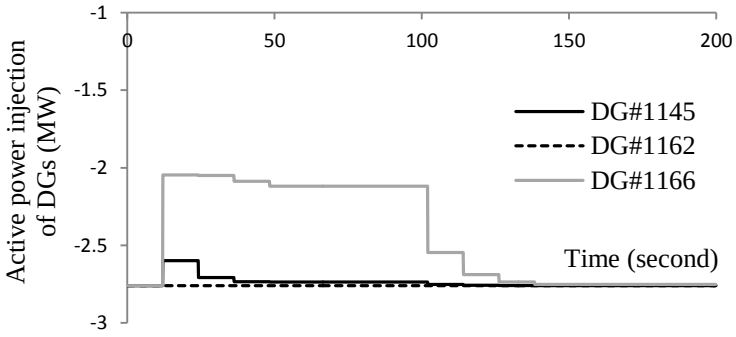

Fig. 4.13 Active power injection of DGs

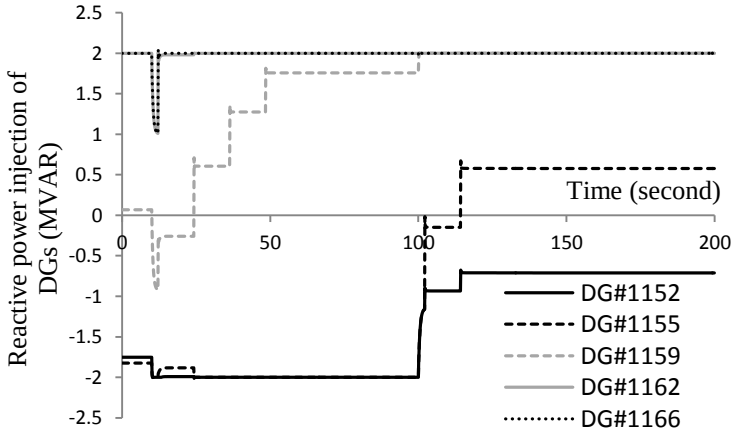

Fig. 4.14 Reactive power injection of DGs

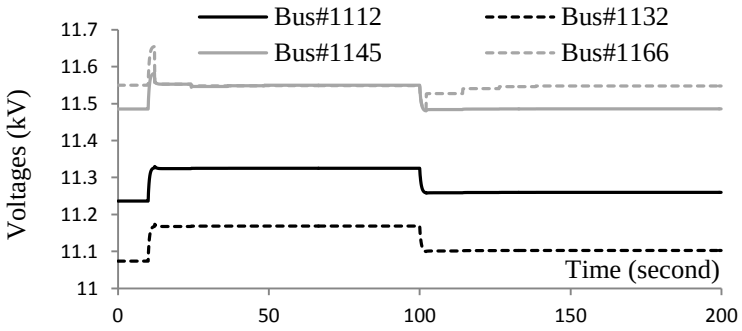

Fig. 4.15 Voltage at several buses

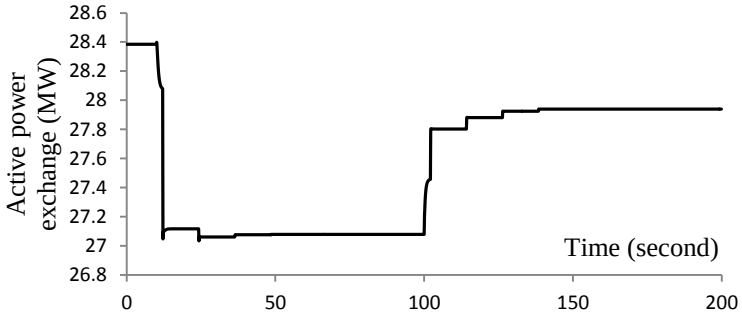

Fig. 4.16 Active power exchange inversely proportional to losses reduction

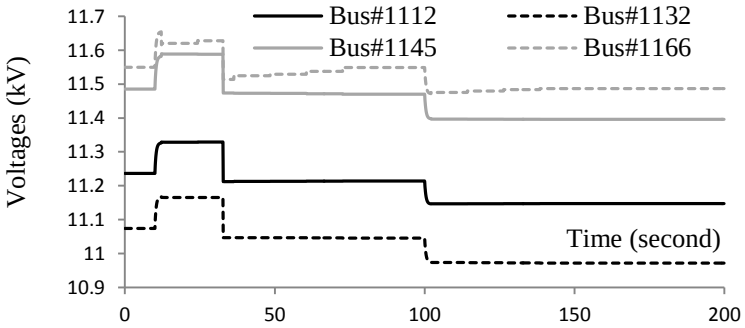

Fig. 4.17 Voltage of monitored buses

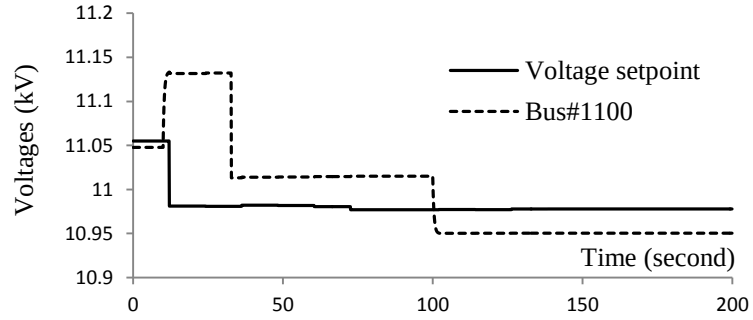

Fig. 4.18 Voltage at important points of OLTC transformer

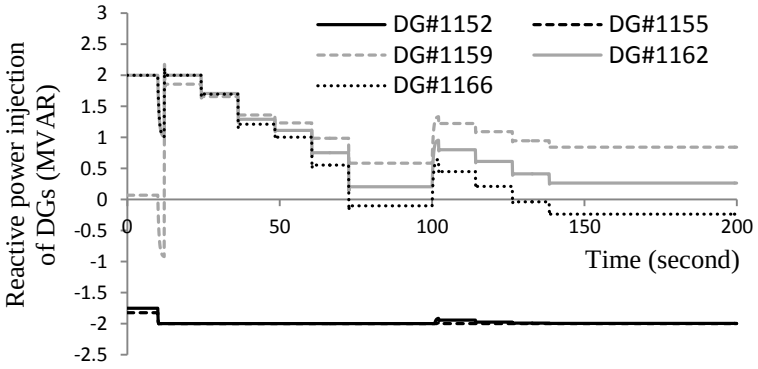

Fig. 4.19 Reactive power of DGs

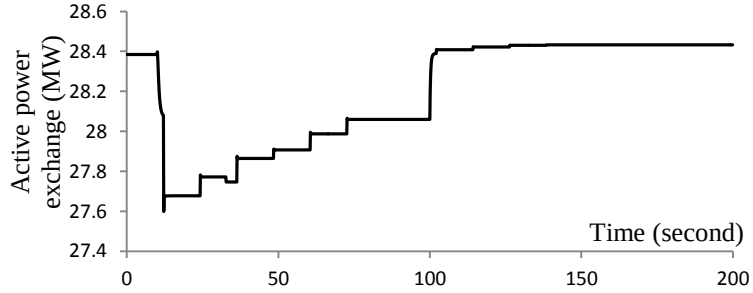

Fig. 4.20 Active power exchange as indication of loss reduction

4.5.2.3. Voltage correction with OLTC of the transformer

With this scenario we aim at investigating voltage correction performance of the controller by using either DGs or OLTC of the transformer. Reactive power demand of TSO is repetition of last scenario, as shown in Fig. 4.12. It is noted that OLTC tap changer serves as a cheaper control action than active power curtailment control action, and that the time delay for the first tap change as well as for subsequent tap changes is 20s.

Fig. 4.17 presents voltage corrections by optimum control actions. The transformer takes one movement of tap-changer at t=32 s to correct voltages.

It can be seen from Fig. 4.18 that the voltage set-point ordered by the controller firstly changes at t=12s, which pushes the OLTC monitored voltage at bus#1100 out of the acceptable dead-band. After the time delay 20s, the movement of tap-changer is performed at t=32s. It is worth to emphasize that at t=24 s, the CCU operates in the loss control mode with regulating reactive power of DGs only, as shown in Fig. 4.19, since it knows that in next 10 seconds voltage will be corrected by the OLTC transformer. Later, since decrease of reactive power exchange demand at t=100s does not cause voltage violation, the CCU is triggered just for the purpose of losses minimization.

It clearly appears from Fig. 4.15 and Fig. 4.20 that voltage correction by using cheap control variable as OLTC instead of active power curtailment able to provide much higher performance in minimizing the losses.

4.6 Conclusions

In this chapter a centralized control scheme based on MPC and PI control unit has been successfully developed for accommodating largely increasing integration of distributed generators into distribution networks and satisfying the conflicting objectives of the TSOs and DNOs.

The proposed controller using sensitivities approach to replace with full LF calculation was successfully demonstrated to be effective for both voltage correction and losses minimization

Essential computation unit of the proposed controller serves as a corrective control one, only activated in several predefined conditions, thus helps significantly relieving computation burden in comparison with this of other previous controllers. With adaptive length of control horizon, the controller is able to drive the network operation close to optimal operating point as fast as possible without violation on operation conditions, even model inaccuracies or delays of the control actions subjected.

Chapter 5
Online optimal control of reactive power sources using measurement-based approach

In chapter 4, the sensitivities based controller was introduced. Impacts of accuracy of sensitivities on the controller's performance were also analyzed, and the typical methods of calculating sensitivities were briefly summarized. It can be seen that along with online measurements, information on system model, such as system topology, cable parameters, etc., is strictly required by sensitivities calculation. However, there is a reality that since existing power systems were built many years ago, the system model is often not well-known and hence leading to inaccuracy of estimated sensitivities or state estimation. As a consequence, the controllers would provide an improper control decision making. In this context, this chapter aims at introducing a sensitivities estimation approach based on only measurements without knowledge on system model, namely measurement-based approach, and its application on solving the optimal reactive power dispatch (RPD) problem. The proposed approach requires synchronized measurements within a predefined timeslot at all busses in system, hence it could be applicable to transmission power systems in which phasor measurement units (PMUs) could be equipped at all busses in future.

5.1 Introduction

Voltage control and optimal RPD play an important role in guaranteeing not only secure power flow but also to optimize operational states of the system that achieve the largest possible benefit from an economic view point. This issue has become more important in recent years due to the increased number of market participants, the continuous growth of power demands as well as the large-scale integration of renewable resources [75].

There is a large number of publications dealing with the solution of the RPD problem by using *model-based* approach through power flow calculation [76]-[78]. Basically, the model-

based approach refers to the state estimation, that system states are estimated through both available measurements and the system model. The approach is often faced with the drawback of strong dependence on accuracy of the system model. In the 2011 San Diego blackout, for example, the fact that the system model was not up-to-date resulted in inaccurate state estimation, and operators were not aware that certain lines were overloaded or close to being overloaded [79].

To overcome the drawback, this chapter introduces a *measurement-based* approach in [80] which are able to be adaptive to changes in operating point (such as generation or load variations) and topology change (such as outage of a transmission line). The main difference of the controllers introduced in this chapter with the aforementioned others is its use of only measurements without knowledge on system model for control.

5.2 Formulation of the RPD problem

In this study, the target of RPD is to minimize the objective function, which is the minimization of active power losses over branches, while satisfying the inequality constraints. All objective functions and constraints are formulated as follows.

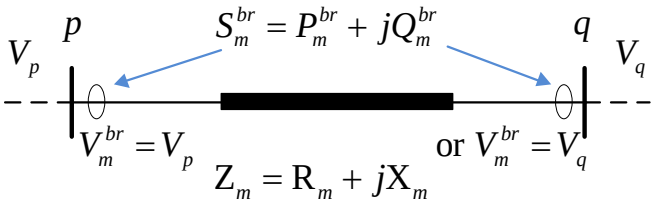

Fig. 5.1 Schematic diagram of a transmission branch *m*

5.2.1 Objective functions

Fig. 5.1 shows a schematic diagram of transmission branch *m* from bus *p* to bus *q*, in which active power losses can be expressed as a function of active and reactive power flow (P_m^{br}, Q_m^{br}) over the branch and corresponding voltage magnitude, V_m^{br}, as follows.

$$P_m^{loss} = R_m I_m^2 = R_m \frac{P_m^{br2} + Q_m^{br2}}{V_m^{br2}} \tag{5.1}$$

Note that $V_m^{br} = V_p$ or $V_m^{br} = V_q$ depend on the side of the power measurement, and the subscript *br* stands for *branch*.

State variables of the system are chosen as follows:

$$\boldsymbol{x} = \left[\left[\boldsymbol{x}_1\right]^T, \left[\boldsymbol{x}_2\right]^T \right]^T \tag{5.2}$$

where $\boldsymbol{x}_1 = [Q_1^{br}, \dots, Q_m^{br}, \dots, Q_{\mathrm{N}_{br}}^{br}]^T$ is branch reactive power flow and N_{br} is the number of branches, and $\boldsymbol{x}_2 = [V_1^{br}, \dots, V_m^{br}, \dots, V_{\mathrm{N}_{br}}^{br}]^T$ is bus voltages corresponding to those branches.

The overall objective of this optimization problem is minimization of total active power losses; hence

$$\min P^{loss} = \sum_{m=1}^{\mathrm{N}_{br}} P_m^{loss} = \mathbf{R}^T \boldsymbol{I}^2(\boldsymbol{x}_1, \boldsymbol{x}_2) \tag{5.3}$$

where $\mathbf{R} = [\mathrm{R}_1, \dots, \mathrm{R}_m, \dots, \mathrm{R}_{\mathrm{N}_{br}}]^T$ is a vector of branch resistances, $\boldsymbol{I}^2 = [I_1^2, \dots, I_m^2, \dots, I_{\mathrm{N}_{br}}^2]^T$ is a vector of branch currents squared.

Assuming the system is working at a chosen operating point with state variables defined by ($\boldsymbol{x}_1^0 = \boldsymbol{q}^{br,0}, \boldsymbol{x}_2^0 = \boldsymbol{v}^{br,0}$). From (5.3), optimal changes of the variables ($\Delta\boldsymbol{x}_1$, $\Delta\boldsymbol{x}_2$) to new operating point must satisfy:

$$\min P^{loss} = \mathbf{R}^T \boldsymbol{I}^2(\boldsymbol{x}_1^0 + \Delta\boldsymbol{x}_1, \boldsymbol{x}_2^0 + \Delta\boldsymbol{x}_2) \tag{5.4}$$

Set $\boldsymbol{I}_{\boldsymbol{D}}^{\boldsymbol{2}}$ is diagonal matrix of $\boldsymbol{I}^2$ and linearizing (5.4) for the chosen operating point $\boldsymbol{x}^0$, (5.4) is equivalent to (5.5):

$$\min \Delta P^{loss} \approx \mathbf{R}^T \left[\frac{\partial \boldsymbol{I}_D^2(\boldsymbol{x}_1^0)}{\partial \boldsymbol{x}_1^0} \Delta\boldsymbol{x}_1 + \frac{\partial \boldsymbol{I}_D^2(\boldsymbol{x}_2^0)}{\partial \boldsymbol{x}_2^0} \Delta\boldsymbol{x}_2 \right] \tag{5.5}$$

with ΔP^{loss} depicting the loss reductions.

For simplicity, (5.5) can be rewritten as:

$$\min \Delta P^{loss} \approx \boldsymbol{w}^T \Delta\boldsymbol{x} \tag{5.6}$$

with $\boldsymbol{w} = \left[\mathbf{R}^T \frac{\partial \boldsymbol{I}_D^2(\boldsymbol{x}_1^0)}{\partial \boldsymbol{x}_1^0}, \mathbf{R}^T \frac{\partial \boldsymbol{I}_D^2(\boldsymbol{x}_2^0)}{\partial \boldsymbol{x}_2^0} \right]^T$ is a weighting matrix.

Problem (5.6) can be solved using linear programming. However, in this study the LSE algorithm is selected for dealing with all optimization problems. In [81], it was pointed out that the estimation of parameter and the value of objective function of both methods is approximately equal, hence their performances are the same.

From the physical point of view the problem at hand is the minimization of the losses, and the solutions are twofold:

i) Reactive power flows $\boldsymbol{Q}^{br}$ in all branches should ideally be zero; hence optimal changes $\Delta\boldsymbol{Q}^{br,opt}$ corresponding to current operating point should be:

$$\Delta\boldsymbol{x}_1^{opt} = \left[-Q_1^0,...,-Q_m^0,...,-Q_{br}^0\right]^T \tag{5.7}$$

ii) The new voltages $\boldsymbol{x_2^0} + \Delta\boldsymbol{x_2}$ should reach their maximum values $\boldsymbol{V}^{br,max}$, hence:

$$\Delta\boldsymbol{x}_2^{opt} = \boldsymbol{V}^{br,\max} - \boldsymbol{x}_2^0 \tag{5.8}$$

These establish an optimal set of magnitude changes $\Delta\boldsymbol{x}^{opt} = \left[[\Delta\boldsymbol{x}_1^{opt}]^T, [\Delta\boldsymbol{x}_2^{opt}]^T\right]^T$ which state variables try to reach by minimizing the differences between them. Therefore, problem (5.6) can be reformulated in form of the least square algorithm as follows:

$$\boldsymbol{w}_D^T\Delta\boldsymbol{x}^{opt} = \boldsymbol{w}_D^T\Delta\boldsymbol{x} \tag{5.9}$$

with $\boldsymbol{\omega}_D^T$ is diagonal matric of $\boldsymbol{\omega}^T$

On the other hand, in this study reactive power injected into buses is considered as control variables $\boldsymbol{u} = [Q_1, \dots, Q_{\mathrm{N}_{bus}}]^T$ to achieve optimal state variables.

$$\Delta\boldsymbol{x}_1 \approx \boldsymbol{S}_{\boldsymbol{u}}^{\boldsymbol{x}_1}\Delta\boldsymbol{u} \tag{5.10}$$

with $\boldsymbol{S}_{\boldsymbol{u}}^{\boldsymbol{x}_1} = [\boldsymbol{s}_{\boldsymbol{u}}^{x_{1,1}}, \dots, \boldsymbol{s}_{\boldsymbol{u}}^{x_{1,m}}, \dots, \boldsymbol{s}_{\boldsymbol{u}}^{x_{1,\mathrm{N}br}}]^T$ is sensitivity matrix of $\boldsymbol{x}_1$with respect to control variables $\boldsymbol{u}$, whose elements $\boldsymbol{s}_{\boldsymbol{u}}^{x_{1,m}} = [\partial Q_m^{br}/\partial Q_1 \,,\dots, \partial Q_m^{br}/\partial Q_{\mathrm{N}_{bus}}]^T$are sensitivities of reactive power in branches with respect to reactive power injection at buses.

Similarly, relationship between state variables $\boldsymbol{x}_2$ and control variables $\boldsymbol{u}$ is formulated as follows:

$$\Delta\boldsymbol{x}_2 \approx \boldsymbol{S}_{\boldsymbol{u}}^{\boldsymbol{x}_2}\Delta\boldsymbol{u} \tag{5.11}$$

Therefore, (5.10) and (5.11) become

$$\Delta\boldsymbol{x} \approx \boldsymbol{S}_{\boldsymbol{u}}^{\boldsymbol{x}}\Delta\boldsymbol{u} \tag{5.12}$$

with $\boldsymbol{S}_{\boldsymbol{u}}^{\boldsymbol{x}} = \left[[\boldsymbol{S}_{\boldsymbol{u}}^{\boldsymbol{x_1}}]^T, [\boldsymbol{S}_{\boldsymbol{u}}^{\boldsymbol{x_2}}]^T\right]^T$ as sensitivity matrix of state variables with respect to control variables.

Substituting (5.12) into (5.9), the overall objective function becomes:

$$\boldsymbol{w}_D^T\Delta\boldsymbol{x}^{opt} = \boldsymbol{w}_D^T\boldsymbol{S}_{\boldsymbol{u}}^{\boldsymbol{x}}\Delta\boldsymbol{u} \tag{5.13}$$

The change of control variables $\Delta \boldsymbol{u}$ can be achieved by solving the following LSE problems

$$\min \boldsymbol{e}^T \boldsymbol{e} \tag{5.14}$$

with $\boldsymbol{e} = \boldsymbol{\omega}_D^T \Delta \boldsymbol{x}^{opt} - \boldsymbol{\omega}_D^T \boldsymbol{S}_{\boldsymbol{u}}^{\boldsymbol{x}} \Delta \boldsymbol{u}$

5.2.2 Constraints

$$\Delta \boldsymbol{u}^{\min} \le \Delta \boldsymbol{u} \le \Delta \boldsymbol{u}^{\max} \tag{5.15}$$

$$\boldsymbol{V}^{\min} \le \boldsymbol{V} \le \boldsymbol{V}^{\max} \tag{5.16}$$

with $= [V_1, \dots, V_j, \dots, V_{\mathrm{N}_{bus}}]^T$: bus voltage vector

$$\boldsymbol{V} = \boldsymbol{V}^0 + \Delta \boldsymbol{V} = \boldsymbol{V}^0 + \boldsymbol{S}_{\boldsymbol{u}}^{\boldsymbol{V}} \Delta \boldsymbol{u} \tag{5.17}$$

with $\boldsymbol{V}^0$is voltage profile at current operating point, $\boldsymbol{S}_{\boldsymbol{u}}^{\boldsymbol{V}} = [\boldsymbol{s}_{\boldsymbol{u}}^{V_1}, \dots, \boldsymbol{s}_{\boldsymbol{u}}^{V_j}, \dots, \boldsymbol{s}_{\boldsymbol{u}}^{V_{N_{bus}}}]^T$ is sensitivity matrix of bus voltages with respect to control variables $\boldsymbol{u}$, whose elements $\boldsymbol{s}_{\boldsymbol{u}}^{V_j} = [\partial V_j/\partial Q_1 \ ,\dots, \partial V_j/\partial Q_{\mathrm{N}_{bus}}]^T$is sensitivities of bus voltages with respect to reactive power injection at buses.

5.3 Sensitivities estimation approach based measurement

In (5.10), $\boldsymbol{S}_{\boldsymbol{u}}^{\boldsymbol{x}_1}$, sensitivities of reactive power in branches with respect to reactive power injection at buses have to be known. To achieve this, for example, regarding branch *m*, $\boldsymbol{s}_{\boldsymbol{u}}^{x_{1,m}} = [\partial Q_m^{br}/\partial Q_1 \ ,\dots, \partial Q_m^{br}/\partial Q_i \ ,\dots, \partial Q_m^{br}/\partial Q_{N_{bus}}]^T$ can be estimated as follows.

At time *t* with sufficiently small $\Delta t > 0$, $\mathrm{N}_{meas} + 1$ set of synchronized measurements are supplied from PMU and stored beforehand.

$$\begin{cases} \boldsymbol{x}_{meas}\left((k+1)\Delta t\right), \ k = 1,\dots,\mathrm{N}_{meas} \\ \boldsymbol{u}_{meas}\left((k+1)\Delta t\right), \ k = 1,\dots,\mathrm{N}_{meas} \\ \boldsymbol{V}_{meas}\left((k+1)\Delta t\right), \ k = 1,\dots,\mathrm{N}_{meas} \end{cases} \tag{5.18}$$

Assuming a high voltage system, i.e. large X/R ratio, the impact of active power injection on voltage as well as on reactive power flow is negligible. Consequently, (5.10) becomes

$$\Delta \boldsymbol{x}_{1,meas} = \boldsymbol{S}_{\boldsymbol{u}}^{\boldsymbol{x}_1} \Delta \boldsymbol{u}_{meas} \tag{5.19}$$

with $\Delta \boldsymbol{x}_{1,meas} = [\Delta \boldsymbol{x}_{1,meas}(1), \dots, \Delta \boldsymbol{x}_{1,meas}(k), \dots, \Delta \boldsymbol{x}_{1,meas}(\mathrm{N}_{meas})]$ in which $\Delta \boldsymbol{x}_{1,meas}(k)$=$\boldsymbol{x}_{1,meas}((k+1)\Delta t)$-$\boldsymbol{x}_{1,meas}(k\Delta t)$, and

$\Delta \boldsymbol{u}_{meas} = [\Delta \boldsymbol{u}_{meas}(1), \ldots, \Delta \boldsymbol{u}_{meas}(k), \ldots, \Delta \boldsymbol{u}_{meas}(\mathrm{N}_{meas})]$ in which $\Delta \boldsymbol{u}_{meas}(k)$=$\boldsymbol{u}_{meas}((k+1)\Delta t)$-$\boldsymbol{u}_{meas}(k\Delta t)$.

It is noted that $\boldsymbol{S}_{\boldsymbol{u}}^{\boldsymbol{x_2}}$ in (5.11) is sub-matrix of $\boldsymbol{S}_{\boldsymbol{u}}^{\boldsymbol{V}}$ which can be specified from (5.17) as follows:

$$\Delta \boldsymbol{V}_{meas} = \boldsymbol{S}_{\boldsymbol{u}}^{\boldsymbol{V}} \Delta \boldsymbol{u}_{meas} \tag{5.20}$$

with $\Delta \boldsymbol{V}_{meas} = [\Delta \boldsymbol{V}_{meas}(1), \ldots, \Delta \boldsymbol{V}_{meas}(k), \ldots, \Delta \boldsymbol{V}_{meas}(\mathrm{N}_{meas})]$ in which $\Delta \boldsymbol{V}_{meas}(k)$=$\boldsymbol{V}_{meas}((k+1)\Delta t)$-$\boldsymbol{V}_{meas}(k\Delta t)$

Finally $\boldsymbol{S}_{\boldsymbol{u}}^{\boldsymbol{x_1}}$ and $\boldsymbol{S}_{\boldsymbol{u}}^{\boldsymbol{V}}$ in (5.19) and (5.20) can in turn be achieved by solving the following LSE problems in (5.14) with $\boldsymbol{e} = \Delta \boldsymbol{x}_{1,meas} - \boldsymbol{S}_{\boldsymbol{u}}^{\boldsymbol{x_1}} \Delta \boldsymbol{u}_{meas}$ and $\boldsymbol{e} = \Delta \boldsymbol{V}_{meas} - \boldsymbol{S}_{\boldsymbol{u}}^{\boldsymbol{V}} \Delta \boldsymbol{u}_{meas}$, respectively.

5.4 Test system and simulation results

5.4.1 Test system

Fig. 5.2 shows the one-line diagram of the Western Electricity Coordinating Council (WECC) 3-machine 9-bus system with which the proposed method is tested. Bus#1 is considered as a slack bus, while bus#2 and bus#3 are connected to generators - thus PQ buses. The control variables are reactive power injection by these two these generators.

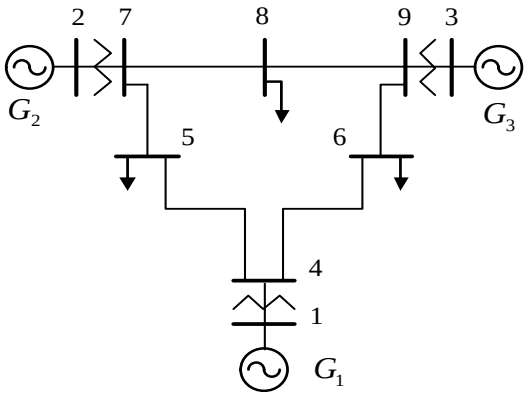

Fig. 5.2 Network topology for WECC 3-machine 9-bus system

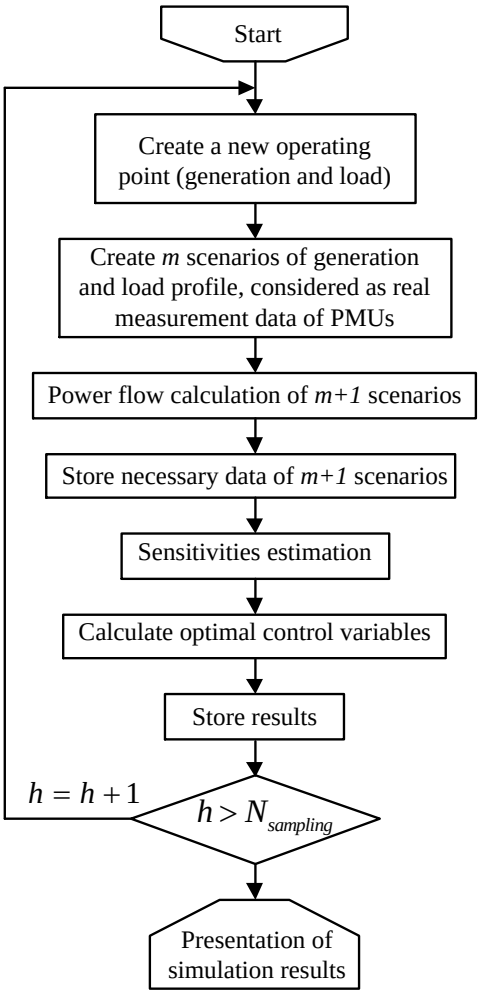

Fig. 5.3 Flowchart of testing the proposed approach

5.4.2 Experimental setup

The simulation study is performed as presented in **Error! Reference source not found.**. irst of all, a new operating point corresponding to a sampling step is created. Then, to simulate PMU measurements which are assumed to be available at this time instant, we create 800 time-series data for the active and reactive power injection at each bus, based on the above operating point. For example, the power injection (P_i, Q_i) at bus i is formed as follows

$$\begin{aligned} P_i(k) &= P_i^0(k) + \sigma_1^P P_i^0(k)\gamma_1^P + \sigma_2^P \gamma_2^P \\ Q_i(k) &= Q_i^0(k) + \sigma_1^Q Q_i^0(k)\gamma_1^Q + \sigma_2^Q \gamma_2^Q \end{aligned} \tag{5.21}$$

with $P_i^0(k)$ and $Q_i^0(k)$ as nominal active and reactive power injection at bus i at instant $k\Delta t$, respectively, and γ_1 and γ_2 as pseudorandom values drawn from standard normal distributions with 0-mean and standard deviations σ_1=0.02 and σ_2=0.02, respectively. The first component of variation, $\sigma_1^P P_i^0(k)\gamma_1^P$ and $\sigma_1^Q Q_i^0(k)\gamma_1^Q$ represents the inherent fluctuations in generation and load, while the second component, $\sigma_2\gamma_2$, represents random noise measurement.

Later, N_{meas} =801 sets of synchronized power flow, bus power injection and voltages are calculated and stored. They are then utilized in (5.19) and (5.20) to estimate the sensitivities which are necessary in order to solve the problem in (5.14) to provide optimal control variables. To demonstrate performance of the proposed approach, Monte Carlo simulation is adopted with the number of iterations equivalent to these sampling steps, $N_{sampling} = 100$ is selected in this study.

The proposed approach is then compared with the model- based approach which uses a heuristic optimization algorithm, mean-variance mapping optimization (MVMO) used in this study, in incorporation with power flow calculation to find optimal control variables for the purpose of losses minimization.

5.4.3 Simulation results

5.4.3.1. Performance of proposed approach versus this of model-based approach with accurate model

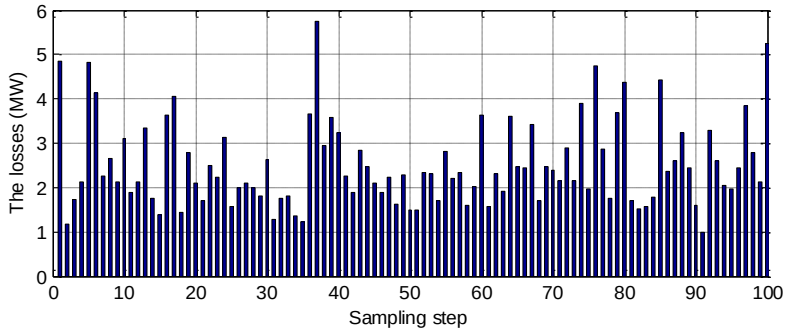

Fig. 5.4 The losses before optimization

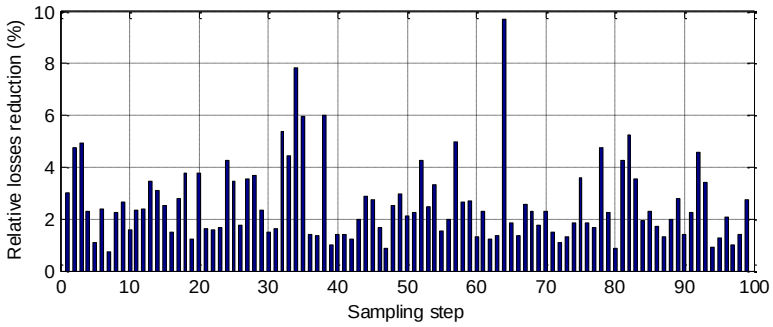

Fig. 5.5 After model-based optimization implementation

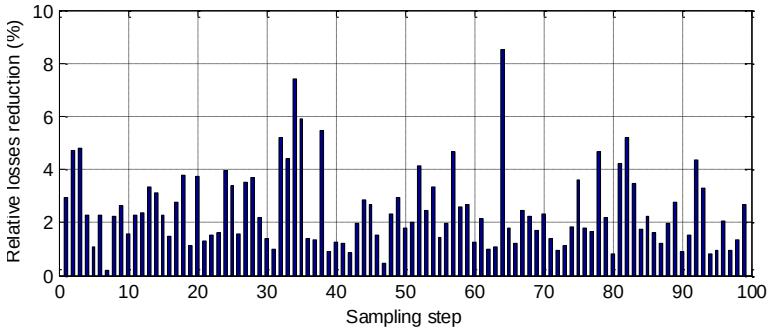

Fig. 5.6 After measurement-based optimization implementation

Fig. 5.4 presents the losses corresponding to the created operating points before applying optimization. While Fig. 5.5 shows relative loss reduction of model-based approach, Fig. 5.6 presents those of measurement-based approach.

In terms of statistical evaluation, the average relative reduction is used. The average relative loss reduction of the whole system is computed as follows:

$$e^{loss}(\%) = \frac{100}{\mathrm{N}_{sampling}} \sum_{h} \left| \frac{\hat{P}^{loss}(h) - P^{loss}(h)}{P^{loss}(h)} \right| \tag{5.22}$$

with $\mathrm{N}_{sampling}$ as the number of sampling steps, $\hat{P}^{loss}$ and P^{loss} the losses after and before optimization implementation, respectively.

Table 5-1 Average relative reductions of total losses

Model based optimization (%)	Measurement based optimization (%)
2.5671	2.4287

It can be concluded from Table 5-1 that the performance in terms of loss reduction using measurement-based approach is comparable to those of the model-based approach.

Fig. 5.7 demonstrates that the measurement-based approach is able to adapt to changes in operating points through satisfying the voltage constraint of (±5% nominal value).

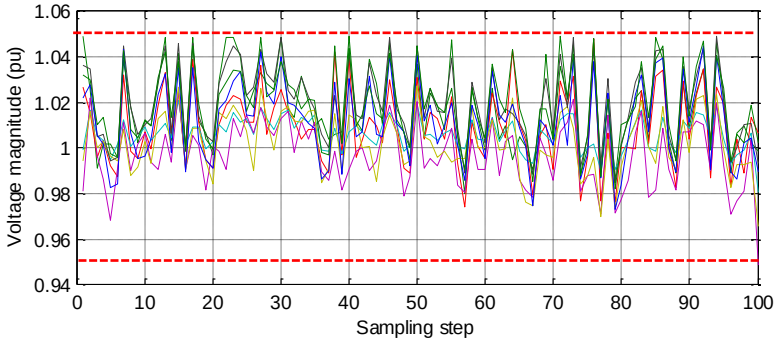

Fig. 5.7 Voltage magnitude at all buses (excepting the slack bus)

5.4.3.2. Performance of the proposed approach versus those of model-based approach with inaccurate model

In this section, the capability of the proposed approach to adapt to changes in topology of system is investigated. Here, it is assumed that the line which connects bus#6 and bus#9 is a double line and one of them experiences outage without being detected by system operators.

It can be seen from Fig. 5.8, the model-based approach leads to voltage violation in certain intervals which are indicated with blue circles. In contrast in Fig. 5.9, since the measurement-based approach can be adaptive to changes in the topology, voltages still remain within their limits.

5.4.3.3. Computation speed

Numerical experiments were performed on a Dell 3350 Laptop with an Intel® Core™ i7-2640 CPU, 2.8 GHz processing speed, and 8GB RAM. The simulation tool MATPOWER is used to perform power flow calculation.

Average CPU time for calculation of an operating point is 0.053 (s) for the test system. For more complex power systems, high performance computing could be required to enable this approach for real-time application.

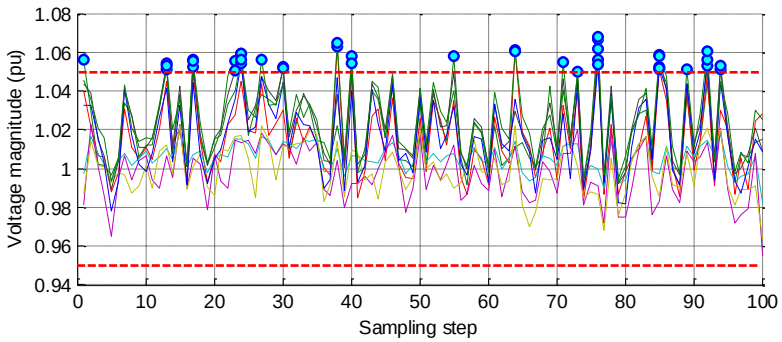

Fig. 5.8 Voltage magnitude at all buses (excepting the slack bus), after *model*-based optimization implementation

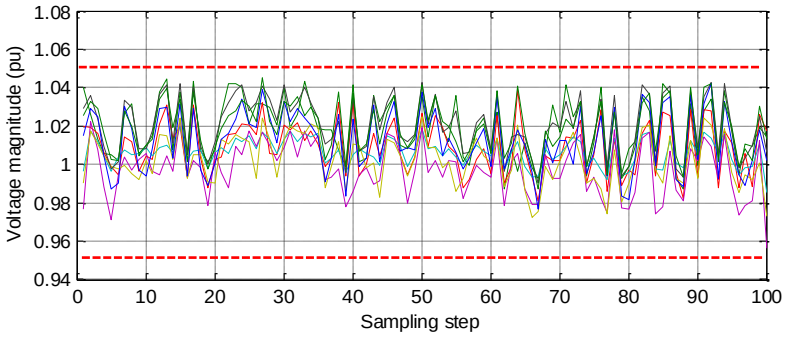

Fig. 5.9 Voltage magnitude at all buses (excepting the slack bus), after *measurement*-based optimization implementation

5.5 Discussions

The main focus of this chapter is the mathematical formulation of measurement-based approach and the theoretical and numerical demonstration of the approach's performance in comparison to the model-based one in the specific operation conditions. However, in real world other uncertainties (e.g. outage of generators or transmission lines, noise of measurement, etc.), which can unpredictably occur during system operation, negatively influence the proposed approach's performance.

Since the measurement-based approach acquires time-series data in an estimation window, it is possible that data varying over a wide margin (caused by collecting data from either pre- or post- disturbances) can be collated. This can lead to inaccurate sensitivity estimation due to inadequate tracking the operating points. Solutions to this problem could be the

implementation of weighted least squares (WLS) estimation which places more weight on recent measurements and less on past ones.

Besides it can happen that in large dataset there exists bad sub-dataset which is caused by measurement and communication devices. Detection and identification of bad data are commonly performed after an estimate has been computed by processing the measurement residuals, using schemes such as χ^2-test and hypothesis testing, respectively [82]. Furthermore, if LSE is replaced by recursive LSE governed by the forgetting factor, introduced in [83], bad data can be reduced or erased by setting suitable forgetting factor as proposed.

5.6 Conclusions

In this chapter, an approach to optimally control reactive power sources by using only measurements from PMUs, without any knowledge on system's topology has been proposed. Performance of the proposed approach was demonstrated to be comparable to those of the traditional model-based approaches, under ideal operating conditions of the system which indicates that the system model is accurately known. However, when the system's topology changes or the model is not up-to-date, the proposed approach showed a much better performance over the model-based approach.

Chapter 6

Multi-agent system based solution of the optimal reactive power dispatch problem

Cooperation of regional operators in solving optimal reactive power dispatch (ORPD) problems on large systems is beneficial despite of many challenges. One major challenge is the fact that each regional operator is typically not enthusiastic to expose the local system data. To deal with such systems, the chapter therefore proposes a control scheme in which a large area is partitioned into Multi-agent based system where each operator is considered as a control agent and uses a model of its local system and communication links with its neighboring control agents to come to agreement on the evolution of interconnections and to determine optimal local control actions and states. At each agent, a linearized objective function enforced with constraints has to be solved to determine control variables; which are tap positions of transformers and reactive power injections. Calculation procedure at each agent based on sensitivity coefficients, thus impact of change magnitudes of control variables on control performance would be significant and hence is fully analyzed. The proposed algorithm is applied to the modified IEEE 30-bus system and numerical results are presented.

6.1 Introduction

Voltage stability assessment is one of the major concerns in power system planning and secure operation as power grids span over several regions and sometimes even countries [84]. A direct link between the voltage and the reactive power makes it possible to control the voltage to desired values by the control of the reactive power. The operator of the power system is responsible to control the transmission system voltage which means enough reactive power available to handle voltage violation conditions [85]. In normal conditions, reactive power of the system dictates not just the voltage profile but also leads to more losses.

Loss minimization is an indispensable objective that must be considered in efficient power system operation [85]–[87]. Hence, to achieve certain global control objectives (e.g. N-1 secure operation, reactive power planning, minimization of losses etc.) it is necessary to coordinate control actions among the regional operators and avoid exposing local system data pertaining to regional infrastructure [88]. We consider loss minimization as our objective function and voltage profile is maintained within safe limits.

Optimization approaches based on power flow calculations often provide accurate results, but calculating nonlinear equations requires large computational time and resources, hence not preferred by real-time applications [89]. In this chapter we propose an optimization approach where the objective function is augmented for incorporating global optimization of linearized large scale multi-agent power system using Lagrangian decomposition algorithm [90]-[91]. The aim is to maintain centralized coordination among agents via Master agent, leaving loss minimization as the only distributed optimization which is analyzed while protecting the local sensitive data. The efficiency of the local objective function stems from the use of real power loss sensitivity with respect to the control variables of the system. Control variables are defined as reactive power injection of generators and tap-changers of transformers. The Power loss sensitivities with respect to all control variables in the system are used in the first stages which are calculated from a linearized model of the system achieved through various control schemes and stored over regular intervals (viz. state estimation, PMU measurements etc.) [92], [93]. Ultimately, we have a centralized convex optimization problem which is solved using aforementioned decomposition algorithm.

Lagrangian decomposition is a classical approach for solving constrained optimization problems. The augmented Lagrangian method adds an additional term to the unconstrained objective which mimics a Lagrange multiplier [94]. This method has been extensively used for solving numerous engineering problems especially in the power systems field [95]- [97]. The advantage of this algorithm is the fact that local grid data does not have to be made globally available, which is often of crucial concern in actual power system operation, albeit degrading the computational performance since it involves iterating many times to reach graceful optimization. The optimization is carried out until the agents negotiate with the neighboring areas on their inter-area variables (i.e. voltages at the interlinked buses).

The remainder of the chapter is sectioned as follows, In Section 6.2; we formulate the control scheme and the objective function exploiting power loss sensitivities. In Section 6.3, we propose the augmented Lagrange formulation and its implementation. In Section 6.4; a modified IEEE 30-bus system has been studied and the results and performance analysis of the control scheme for various scenarios have been depicted and finally conclude the chapter in Section V.

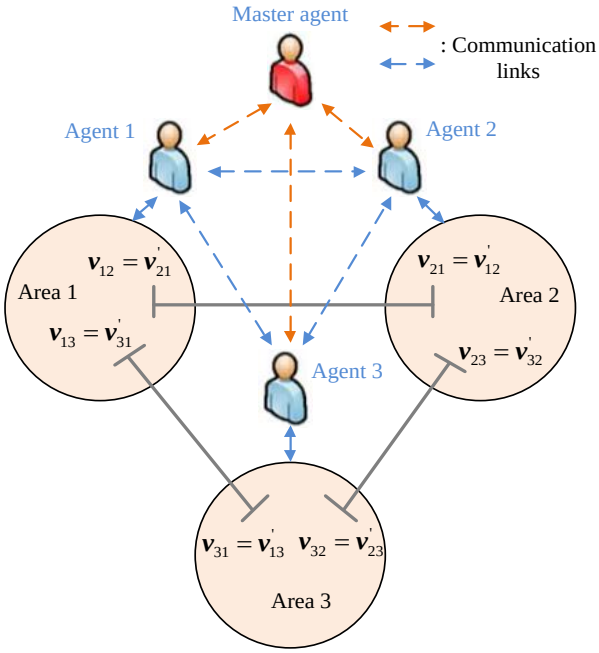

Fig. 6.1 Schematic diagram of a transmission branch *m*

6.2 Control scheme

6.2.1 Power system model

A power system in the steady state is modeled by the load flow equations:

$$f(\boldsymbol{x}, \mathbf{z}, \boldsymbol{u}) = 0 \tag{6.1a}$$

$$\boldsymbol{u}^{\min} \le \boldsymbol{u} \le \boldsymbol{u}_i^{\max} \tag{6.1b}$$

where $\boldsymbol{x}$ denotes state variables, $\mathbf{z}$ is vector of parameters, and $\boldsymbol{u}$ the control variables ($\boldsymbol{\alpha}$ tap-changer set-points and $\boldsymbol{q}$ reactive power injection of generators).

Consider the test system partitioned into N^a areas (e.g., $N^a = 3$ in Fig. 6.1), each controlled by a control agent that has only a model of its own area. The interconnections between areas

are modeled using so-called *inter-area variables*. These variables, eg., $\boldsymbol{v}'_{ij}$ is voltage magnitude at interconnection buses, connected to area *i*, of neighboring areas *j* which is expected by area *i*, and $\boldsymbol{v}_{ji}$ is voltage magnitude at these buses, but expected by its own area *j;* therefore, accordingly to physical base, $\boldsymbol{v}'_{ij} = \boldsymbol{v}_{ji}$ must be satisfied.

Thus, (6.1a) can be expressed in form of each area as follows

$$\mathrm{f}(\boldsymbol{x}_i, \boldsymbol{z}_i, \boldsymbol{u}_i, \boldsymbol{v}'_{ij}) = 0, \quad i = 1,..., \mathrm{N}^a,\ j \in \mathrm{N}_i \tag{6.2a}$$

$$\boldsymbol{u}_i^{\min} \le \boldsymbol{u}_i \le \boldsymbol{u}_i^{\max} \tag{6.2b}$$

$$\boldsymbol{v}'_{ij} = \boldsymbol{v}_{ji} \tag{6.2c}$$

where N_i is the set of neighboring areas connected to area *i*. And $\boldsymbol{x}_i$, $\boldsymbol{z}_i$, $\boldsymbol{u}_i$ denotes state variables, vector of parameters and control variables of area *i*, respectively.

6.2.2 Optimal control problem formulation

The purpose of an optimal reactive power dispatch is mainly to improve the voltage profile in the system and to minimize systems losses. In this study, losses minimization is considered as the objective function J, while voltage profile is kept at values between 0.9 p.u. and 1.1 p.u. The objective functions in (6.3a) are introduced in a linearized form through sensitivities that are yielded by linearization of the load flow equations around the nominal operating point as presented in Appendix. Changes of the control variables $\Delta \boldsymbol{w}_i(k)$ at time-instant *k* are achieved by minimizing the objective functions (6.3a)

$$\min \mathrm{J} = \sum_{i=1}^{N^a} \mathrm{J}_i \tag{6.3a}$$

$$\mathrm{J}_i = \left(\left(\frac{\partial P_i^{loss}}{\partial \boldsymbol{w}_i} \right) \Delta \boldsymbol{w}_i(k) \right) \tag{6.3b}$$

$$\boldsymbol{w}_i = \left[\left[\boldsymbol{u}_i \right]^T, \left[\boldsymbol{v}'_{ij} \right]^T \right]^T \text{ with } j \in \mathrm{N}_i \tag{6.3c}$$

Constraints

$$\boldsymbol{v}'_{ij} = \boldsymbol{v}_{ji} \tag{6.3d}$$

$$\Delta \boldsymbol{w}_i^{\min} \le \Delta \boldsymbol{w}_i(k) \le \Delta \boldsymbol{w}_i^{\max} \tag{6.3e}$$

$$\Delta \mathbf{v}_i^{\min} \le \Delta \boldsymbol{v}_i(k+1) \le \Delta \mathbf{v}_i^{\max} \tag{6.3f}$$

$$\mathbf{v}_i^{\min} \le \boldsymbol{v}_i(k+1) \le \mathbf{v}_i^{\max} \tag{6.3g}$$

$$\boldsymbol{v}_i(k+1) = \boldsymbol{v}_i(k) + \left(\frac{\partial \boldsymbol{v}_i}{\partial \boldsymbol{w}_i} \right)_D \Delta \boldsymbol{w}_i(k) \tag{6.3h}$$

where $\boldsymbol{\partial P_i^{loss} / \partial w_i}$ and $\boldsymbol{\partial v_i \ / \partial w_i}$ that is loss sensitivities and voltage sensitivities of area *i* with respect to control variables of area *i* and inter-area variables connected to area *i*, respectively, is calculated as in Appendix.. $\mathbf{v_i^{min}}$ and $\mathbf{v_i^{max}}$ is minimum and maximum of acceptable voltages in area *i*, respectively.

6.2.3 Proposed control algorithm

To reach an optimal state, the systems probably need a large change of control variables from a current operating point, in an association with a certain control objective as in (6.3a). The association referring to sensitivities in this chapter is typically estimated with small change of control variables around their actual values. Therefore, any large changes results in unanticipated outcomes, most of them being degeneration of performance. It is thus necessary to impose constraints of such changes onto the control formulation as in (6.3a) and (6.3a), hence requiring multiple control circles to approach optimal state. As a result, the numerical process of the optimal reactive power dispatch should require the discrete control circles described below:

- *Step 1*: Formulate (6.3a) with updated sensitivities
- *Step 2*: Solve problem (6.3a) and use the results as based values for the next control circle.
- *Step 3*: Check whether the real power loss in each area is significantly different from that of the previous control circle, equivalent to termination condition in (6.4) is satisfied. If so, repeat the process, otherwise stop.

$$\mathrm{J}_i(k+1) - \mathrm{J}_i(k) \ge \varepsilon_i^{loss} \text{ with } i = 1, ..., \mathrm{N}^a \tag{6.4}$$

Importantly, it can be seen that the overall control problem (6.3a) is not separable into sub-problems only using local variables of one agent *i* alone due to the interconnecting constraints (6.3a). Therefore, a distributed algorithm based multi-agent system is introduced and

presented in the next section in order to achieve global optimum of the whole system by separately solving sub-problems.

6.3 Multi-agent based approach

6.3.1 Augmented Lagrange formulation

In order to deal with the interconnecting constraints (6.3a), an augmented Lagrangian formulation of this problem can be formulated [89][90]. Using such an approach, the interconnecting constraints are removed from the constraint set and added to the objective function in the form of additional linear cost terms, based on Lagrange multipliers ($\boldsymbol{\Lambda} = \boldsymbol{\lambda}_{ij}$, with i=1,..,N^a and $j \in \mathrm{N}_i$), and additional quadratic terms. The augmented Lagrange function used to replace (6.3a) is defined as

$$\mathrm{L}(\boldsymbol{\Lambda}) = \sum_{i=1}^{\mathrm{N}^a} \left(\mathrm{J}_i + \sum_{j \in \mathrm{N}_i} \left((\boldsymbol{\lambda}_{ij})^{\mathrm{T}} (\boldsymbol{v}'_{ij} - \boldsymbol{v}_{ji}) + \frac{\mathrm{c}}{2} \left\| \boldsymbol{v}'_{ij} - \boldsymbol{v}_{ji} \right\|_2^2 \right) \right) \tag{6.5}$$

with constraints being the ones in (6.3a) without (6.3a), and coefficient c is a positive scalar penalizing interconnecting constraint violations.

Then (6.5) can be decomposed in the form of each sub-problem so that they can be tackled and solved independently with i=1,..,N^a as

$$\begin{aligned} \min_{\boldsymbol{w}_i, \boldsymbol{v}'_{ij}} \mathrm{J}_i + \sum_{j \in \mathrm{N}_i} \Bigg(& \begin{bmatrix} (\boldsymbol{\lambda}_{ij})^{\mathrm{T}} & (-\boldsymbol{\lambda}_{ji})^{\mathrm{T}} \end{bmatrix} \begin{bmatrix} \boldsymbol{v}'_{ij} \\ \boldsymbol{v}_{ij} \end{bmatrix} \\ & + \frac{\mathrm{c}}{2} \left\| \begin{bmatrix} \mathrm{I} & 0 \\ 0 & \mathrm{I} \end{bmatrix} \begin{bmatrix} \boldsymbol{v}'_{ji,prev} \\ \boldsymbol{v}_{ji,prev} \end{bmatrix} - \begin{bmatrix} 0 & \mathrm{I} \\ \mathrm{I} & 0 \end{bmatrix} \begin{bmatrix} \boldsymbol{v}'_{ij} \\ \boldsymbol{v}_{ij} \end{bmatrix} \right\|_2^2 \Bigg) \end{aligned} \tag{6.6}$$

where $\boldsymbol{v}'_{ji.prev}$ and $\boldsymbol{v}_{ji.prev}$ are $\boldsymbol{v}'_{ji}$ and $\boldsymbol{v}_{ji}$, respectively computed at the previous iteration for the other agents.

6.3.2 Implementation algorithm

The implementation algorithm proposed in [94] is described in Fig. 6.2. Firstly, each agent in turn updates its sensitivities and then minimizes its problem (6.6) to determine its optimal local and inter-area variables, while the variables of the other agents stay fixed. After last

agent complete its optimization sub-problem, the inter-area variables in transmitted to Master agent where termination conditions such as agreement on the inter-area variables in (6.9) or maximum allowable number of iterations in (6.10) are checked. If the conditions are satisfied, the determined actions are implemented. Otherwise, updating the Lagrangian multipliers is performed following the strategy described by (6.7) and (6.8), and the whole process is then repeated in one new iteration.

$$\boldsymbol{\lambda}_{ij,iter+1} = \boldsymbol{\lambda}_{ij,iter} + \mathrm{c}\left(\boldsymbol{v}'_{ij,iter+1} - \boldsymbol{v}_{ji,iter+1}\right) \tag{6.7}$$

$$\boldsymbol{\lambda}_{ji,iter+1} = \boldsymbol{\lambda}_{ji,iter} + \mathrm{c}\left(\boldsymbol{v}'_{ji,iter+1} - \boldsymbol{v}_{ij,iter+1}\right) \tag{6.8}$$

$$\boldsymbol{v}'_{ij,iter+1} - \boldsymbol{v}_{ji,iter+1} < \varepsilon^{v} \tag{6.9}$$

$$iter \le iter^{\max} \tag{6.10}$$

with $\forall i, j \in \mathrm{N}^{a}$

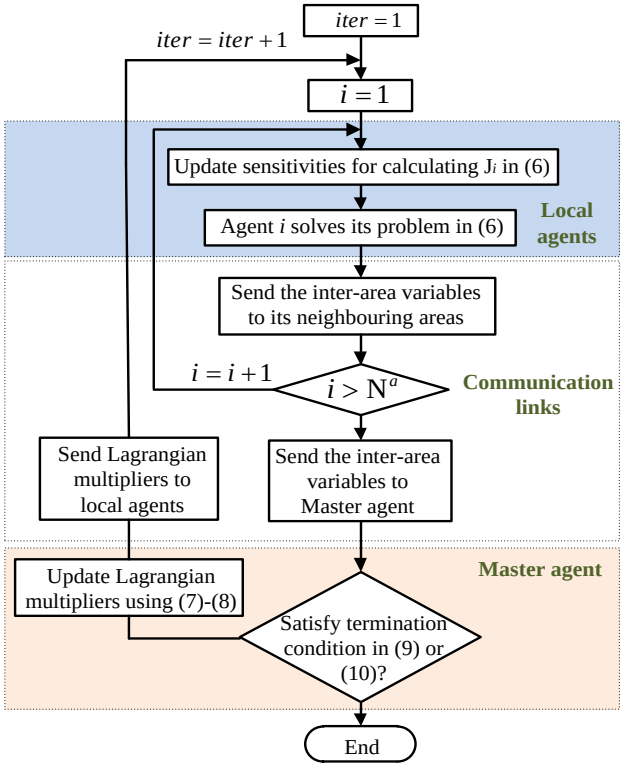

Fig. 6.2 Flow chart of implementation algorithm

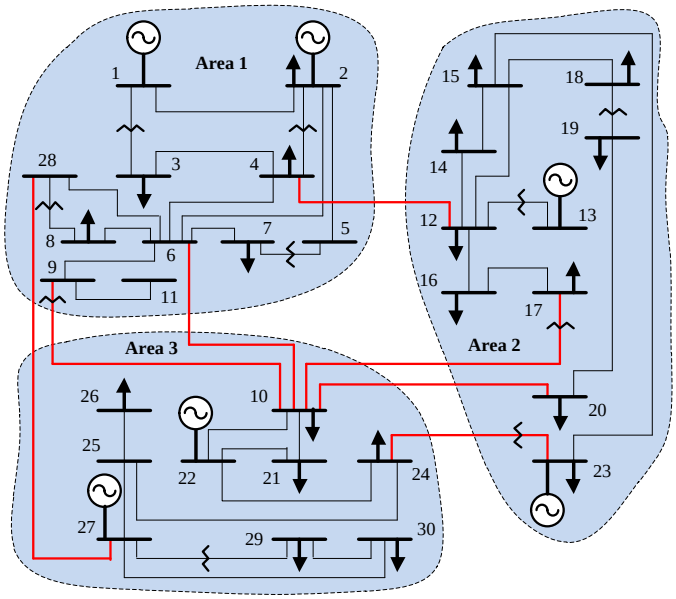

Fig. 6.3 Modified IEEE 30-bus system

6.4 Case studies and simulation results

6.4.1 Case studies

Firstly, it is worthy to mention that the proposed approach can be extended to any number of interconnected areas with an arbitrary number of interconnection-lines without conceptual modification to its structure.

The proposed method has been implemented on a modified IEEE 30-bus system taken from [98]. The test system is partitioned into three areas as shown in Fig. 6.3 totally comprising of ten transformers equipped with tap-changers, each having two generators and several loads. Total number of interconnection lines is seven corresponding to fourteen inter-area variables.

6.4.2 Simulation results

It is noted that simulation results below are given with setting-up initial control parameters as presented in Table 6-1. For purpose of studying on impacts of these parameters on the overall control performance, they are divided into two groups: The one of general parameters referring to the control algorithm presented in the part II-C (considered as an outer-loop of overall control algorithm in this chapter), and another (considered as inner-loop) being relevant with multi-agent based approach in the part III-B.

Table 6-1 Setup parameters

General parameters				Parameters of multi-agents system		
ε_i^{loss} (MW)	$\lvert\Delta\mathbf{v}_i^{max}\rvert$ &$\lvert\Delta\mathbf{v}_i^{min}\rvert$ (p.u.)	$\lvert\Delta\boldsymbol{q}_i^{max}\rvert$ &$\lvert\Delta\boldsymbol{q}_i^{min}\rvert$ (MVAR)	$\lvert\Delta\boldsymbol{\alpha}_i^{max}\rvert$ &$\lvert\Delta\boldsymbol{\alpha}_i^{min}\rvert$ (p.u.)	$\varepsilon^{\boldsymbol{v}}$ (p.u.)	c	$iter^{max}$
0.01	0.03	0.02	0.002	0.0005	9.5	300

6.4.2.1. Performance comparison between multi-agent based system versus single-agent based system

Table 6-2 Power loss convergence between the test system managed by multi-agents and single-agent

Control circle No.	Multi-agent				Single-agent
	Area 1 (MW)	Area 2 (MW)	Area 3 (MW)	Total (MW)	Total (MW)
1	4.6341	1.6414	1.1029	7.3784	7.3784
2	4.3574	1.6158	1.0899	7.0631	6.679
3	4.1376	1.6066	1.0886	6.8327	6.2077
4	3.7285	1.5814	1.0581	6.368	5.83
5	3.4451	1.554	1.043	6.0421	5.5356
6	3.2059	1.5366	1.0328	5.7754	5.3163
7	3.0039	1.5293	1.0269	5.5601	5.1591
8	2.8541	1.5345	1.0204	5.409	5.0318
9	2.7493	1.5516	1.0136	5.3144	4.9593
10	2.6798	1.5637	1.0101	5.2537	4.9148
11	2.6479	1.5123	1.003	5.1633	4.8647
12	2.6202	1.5035	1.0016	5.1253	4.8545
13	2.5958	1.4718	1.008	5.0756	4.8055
14	2.5787	1.441	1.0135	5.0332	4.7998
15	2.5565	1.4132	1.0256	4.9953	
16	2.5408	1.3877	1.0342	4.9628	

17	2.5308	1.3587	1.0492	4.9387
18	2.5283	1.3439	1.0705	4.9427
19	2.5126	1.3258	1.0853	4.9237

It can be seen from Table 6-2 that the single-agent provides a better convergence value of the losses than that of multi-agent. This can likely stems from the fact that higher values $\boldsymbol{\varepsilon^{\nu}}$ of the agreement on inter-area variables in (6.9) are, worse performance in the losses is. Moreover, convergence speed of the single-agent is faster as well.

In addition, the proposed control algorithm shows its capability in establishing cooperation between agents to achieve the global objective. This can be seen from Table 6-2 that from control circle 12, losses of area 3 present a trend in increase, in the meantime, those of other areas decrease and whole system decreases as a response.

6.4.2.2. Impacts of general parameters on the proposed control scheme's performance

In order to study impacts of control parameters on the performance, each simulation experiment below is carried out with varying only one of the parameters while keeping the others unchanged. The parameters are set up at values presented in Table 6-1.

Fig. 6.4 depicts loss convergence with different change limits selected of voltages. As can be seen following, the narrower limits provide a better convergence value but with slower convergence speed within initial control circles that is far from optimum operating state. The large limits often lead to fluctuation of convergence value, since the algorithm performance depends on sensitivities accuracy that is inversely proportional with the limits, thus higher risk of triggering the termination condition (6.9).

Again, algorithm performance is adversely influenced by larger change magnitude of control variables as presented in Fig. 6.5 and Fig. 6.6. This is clear because sensitivities calculated are used for small change of control variables.

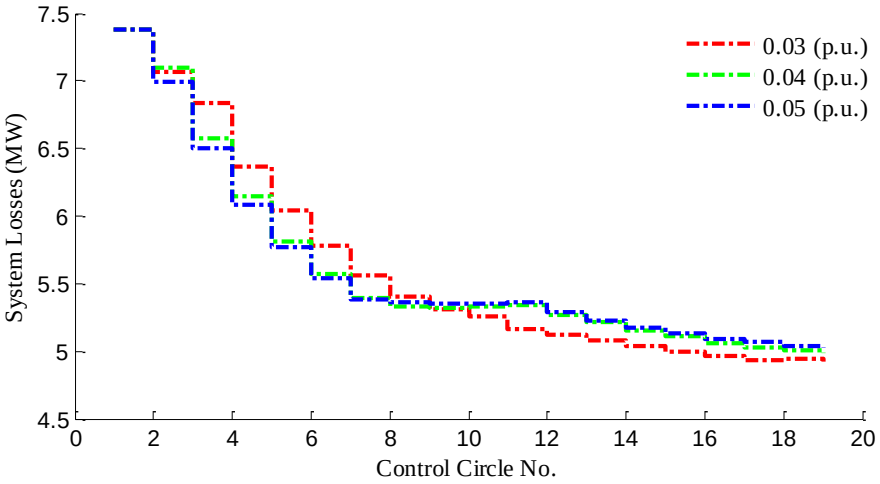

Fig. 6.4 Loss convergence with different change limits of voltages

$$|\Delta \mathbf{v}_i^{max}| = |\Delta \mathbf{v}_i^{min}|$$

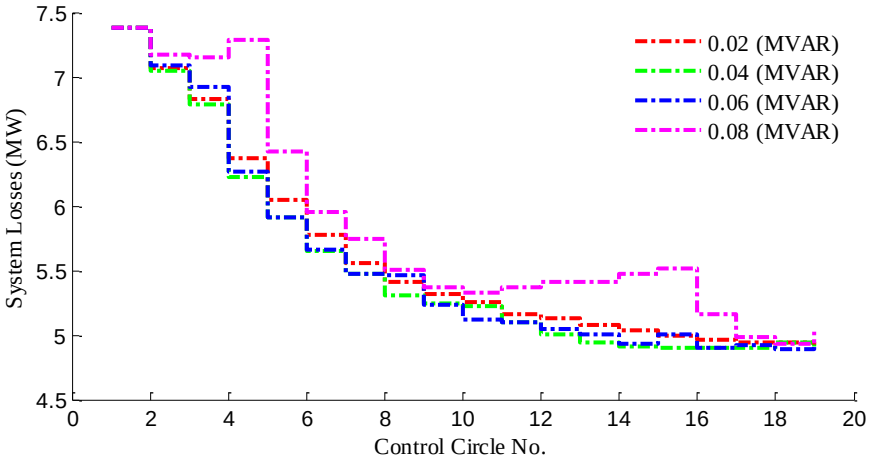

Fig. 6.5 Loss convergence with different change limits of reactive power injection from generators

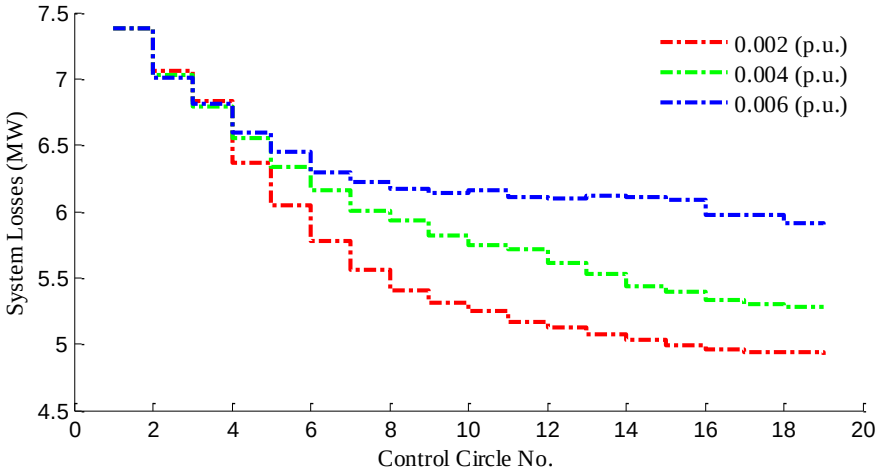

Fig. 6.6 Loss convergence with different change limits of tap movement

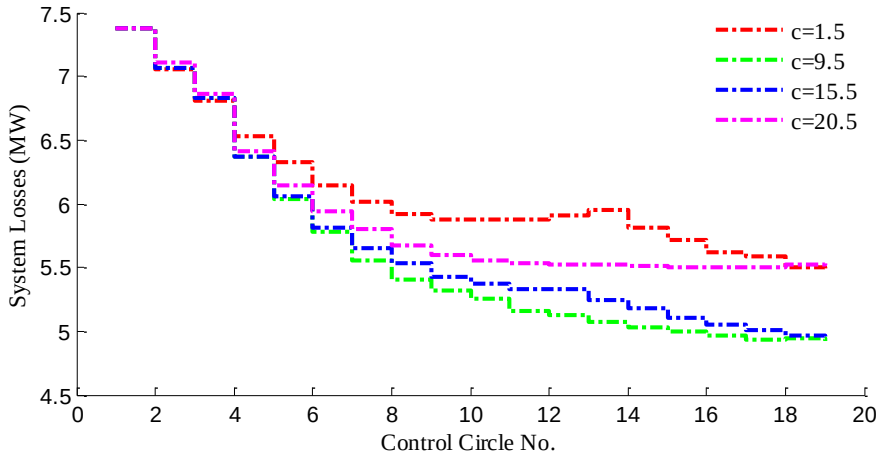

Fig. 6.7 Loss convergence with different coefficient c

6.4.2.3. Impacts of multi-agent parameters on the proposed control scheme's performance

From Fig. 6.7, it is likely that determining a correct value of the coefficient c in order to achieve the best of performance seems to be difficult. Moreover, it should be highlighted that the coefficient c has an intense association with the control algorithm's performance.

6.5 Conclusions

The need of coordination and protecting sensitive data in large interconnected grids for reliable operation of power system incepted the idea of a Multi-agent based system. An

effective augmented Lagrange decomposition algorithm was implemented and analyzed, while considering loss minimization as its objective function. This approach not just protects the local data but also gives a fair strike to the conventional Single-agent based system as seen in the simulation results.

On the other hand, improper selection of the general and multi-agents systems parameters degrades the performance as shown in control scheme's performance plots. Selection of these parameters for now was based on trial and error but for future work, proper estimation of these parameters plays a vital role in the reduction of computational time and will also enrich the performance of the algorithm. In addition, further investigation is required to develop faster and robust algorithms, and minimizing communications overhead should be included in the objective function.

Chapter 7
Conclusions

Voltage breach was identified as a major challenge in accommodating large-scale RES integration into current power systems. Besides an expensive resort of power curtailment this dissertation has demonstrated that reactive power control should be the first concern due to its low-cost feature and its availability. In fact, along with conventional reactive power sources such as transformer tap-changer, capacitive compensation devices, etc., reactive power injection of RES based generators could also be a favorite possibility because of its fast response capability enabled by advance power electronics interface, even additional cost for this ancillary service imposed in future electricity market or already available in some countries nowadays. And it is demonstrated in this dissertation to be effective in mitigating voltage violation over the power system at medium voltage levels where reactive power is in a strong conjunction with voltage due to high ratio of X/R of connection lines.

Intermittent nature of RES integrated into power systems results in voltage fluctuation and various power flows. Tracking optimal or near-to-optimal operating points in real-time was demonstrated in this thesis to be possible with assumption that measurements at all buses or several properly selected buses are available and accurate enough. Especially, if tap-changers or shunt reactors, etc., belonging to group of integer or binary variables, are considered as one of the control variables, intensively their movements negatively affecting their lifetime have to be taken into account in system operation and control. Predictive control that determines control variables at current time instant based on available measurements and prediction of generation and load demand at succeeding time steps was referred as the most effective approach to avoid unnecessary movements.

Grid codes in several countries pointed that wind farms connected into grids must share duty in stabilizing power systems, and this rule is also on the way to be imposed on distribution systems where high ratio of RES penetration is embedded. In domain of voltage and reactive power control, PI controller installed at connection point of distribution systems to regulate voltage value requested by operators of external power systems could provide

many benefits such as continuous and smooth regulation behavior, no need of additional computation units, ease for optimization algorithm adaption. However, interaction of the PI controllers with the other controllers in power systems has to be studied to ensure that power systems are stable during faults or severe disturbances.

Voltage and reactive power control may be categorized into three groups of architectures, local, distributed/decentralized, and hierarchical/centralized. Each can be translated into different benefits in either operation or economic viewpoint. The local is a kind of architecture in which each control unit uses only local information to achieve its own objectives without cooperation with the other units in system, hence requiring no communication, whereby global objectives of entire system are hardly achieved. This is why the local is architecture of low-efficient that refers to poor-capability of achieving global objectives and ensuring proper operation of the systems. In contrary to the local, the hierarchical/centralized is a high-efficient architecture that is able to overcome most challenges in operation, especially achieving global control objectives while operation constraints satisfied. Nevertheless, this architecture confronts a lot of challenges due to its strong dependence on information systems and nature of data concentration such cyber-attacks, processing massive data, time delay caused transferring control signals and data, etc. Furthermore, this architecture is vulnerable to single-point failure. Communication links between grid devices and hosted software are vulnerable to disruption. Centralized controllers can also malfunction and prevent proper operation of a critical grid application. On the other hand, to mitigate large amount of data transmitted to central controllers while maintaining observability of the controllers, pseudo-measurements that augment the available real-time measurements are calculated using short-term forecasts or historical data are also often adopted. Since pseudo-measurements are much less accurate than the real-time measurements, performance of the centralized controller decreases as a response. In this context, a question is raised, whether operation constraints are satisfied by using such measurements. This thesis introduced a centralized controller inspired from model predictive control approach using pseudo-measurements to determine control actions which is capable of driving the system operation close to optimal operating point as fast as possible without violation on operation conditions, irrespective of model inaccuracies or subjected to the delays of control actions. With a group of distributed/decentralized control units or a set of

control units, often named *agents*, installed in the power system use embedded controls to monitor local conditions. They also communicate with other agents to get data on system conditions at other nearby agents. These local controls analyze all this data in real time and can quickly make decisions. Another prominent feature of this architecture is its ability of preventing sensitive data exposition of each control area while interacting with the other areas.

It is likely that computational intelligence and artificial intelligence play a very important role in solving new challenges posed by wide-range integration of renewable energy sources. In fact, the power systems nowadays are often equipped with a lot of control devices with continuous and discrete behavior in order to stabilize the systems and to satisfy ambition of maximizing operation benefits. However, to do so, it is required that these control devices must be properly coordinated, which is very hard to achieve due to its nature of falling into problems of mixed integer nonlinear optimization. To deal with such problems, heuristic optimization algorithms have been demonstrated to be effective, although several drawbacks exist. To alleviate the drawbacks, the MVMO, a mature heuristic optimization tool, is enhanced in the thesis with new features to exploit the asymmetrical properties of the algorithm's mapping function so that it can find the optimum more quickly with minimum risk of premature convergence. With possessing similar importance as of computation intelligence, artificial intelligence has been utilized in various applications in power systems, particularly in this thesis it presented its learning ability to augment observability of the controllers in which available measurements are restricted.

The measurement based approach's capability of adapting to changes in system operating point and topology without any knowledge on system parameters has been demonstrated. The approach acquires time series data in an estimation window that is then processed to form sufficient number of equations so that solutions, being sensitivity coefficients in this dissertation, of these equations are viable. Since control actions are calculated from the sensitivity coefficients that are computed based on only measurements, any topology changes do not affect performance of the controllers. However, the approach requires all buses in power systems to have PMUs installed and measurements of all PMUs have to be transmitted to a centralized controller where sensitivity coefficients are estimated. Consequently, besides

relying on quality of PMUs the approach is also subjected to cohesive drawbacks of centralized controllers as aforementioned.

References

[1] S. Engelhardt, I. Erlich, C. Feltes, J. Kretschmann, and F. Shewarega, "Reactive Power Capability of Wind Turbines Based on Doubly Fed Induction Generators," *IEEE Trans. on Energy Conversion*, vol. 26, no. 1, pp. 364 - 372, March 2011.

[2] I. Erlich, W. Winter, and A. Dittrich, "Advanced grid requirements for the integration of wind turbines into the German transmission system," in *Proc. 2006 IEEE Power Engineering Society General Meeting.*

[3] V. S. Pappala, W. Nakawiro, and I. Erlich, "Predictive optimal control of wind farm reactive sources," in *Proc. 2010 IEEE PES Transmission and Distribution Conference and Exposition*, pp. 1-7, Apr. 2010.

[4] S. Foster, L. Xu, B. Fox, " Coordinated reactive power control for facilitating fault ride through of doubly fed induction generator- and fixed speed induction generator-based wind farms," *IET Renewable Power Generation*, vol. 4, no. 2, pp. 128-138, March 2010.

[5] W. Nakawiro, I. Erlich, and J.L. Rueda, "A novel optimization algorithm for optimal reactive power dispatch: A comparative study," in *Proc. 4th International Conference on Electric Utility Deregulation and Restructuring and Power Technologies, Weihai, Shandong, China, July 2011*.

[6] I. J. Fang, G. Li, X. Liang, and M. Zhou;, "An optimal control strategy for reactive power in wind farms consisting of VSCF DFIG wind turbine generator systems," in *Proc. 2011 4th International Conference on Electric Utility Deregulation and Restructuring and Power Technologies*, pp. 1709-1715, July 2011.

[7] I. Erlich, W. Nakawiro, and M. Martinez, "Optimal dispatch of reactive sources in wind farms," in *Proc. 2011 IEEE Power and Energy Society General Meeting*, pp. 1-7, July 2011.

[8] M. Varadarajan and K. S. Swarup, "Network loss minimization with voltage security using differential evolution," *Electric Power Systems Research*, vol. 78, no. 5, pp. 815-823, May 2008.

[9] Q. H. Wu and J. T. Ma, "Power system optimal reactive power dispatch using evolutionary programming," *IEEE Transactions on Power Systems*, vol. 10, no. 3, pp. 1243-1249, Aug 1995.

[10] A. Abbasy and S.H. Hosseini, "Ant Colony Optimization-Based Approach to Optimal Reactive Power Dispatch: A Comparison of Various Ant Systems," in *Proc. 2007 IEEE Power Engineering Society Conference and Exposition in Africa*, pp. 1 – 8, July 2007.

[11] M. Tripathy and S. Mishra,, "Bacteria Foraging-Based Solution to Optimize Both Real Power Loss and Voltage Stability Limit," *IEEE Transactions on Power Systems*, vol. 22, no. 1, pp. 240-248, Feb. 2007.

[12] J. Lampinen and I. Zelinka, "On stagnation of the differential evolution algorithms," in *Proc. 6th Int. Conf. Soft Computing.*, pp. 76-83, 2000.

[13] W. Nakawiro and I. Erlich, "A new adaptive differential evolution algorithm for voltage stability constrained optimal power flow," in *Proc. 2011 Power Systems Computation Conference*, pp. 1 – 7, Aug.2011.

[14] I. Erlich, G. K. Venayagamoorthy, and W. Nakawiro, " A mean-variance optimization algorithm," in *Proc. 2010 IEEE World Congress on Computational Intelligence, Barcelona, Spain.*

[15] E.ON Netz GmbH, "Grid Code High and Extra High Voltage," April 2006.

[16] V.S. Pappala, S.N. Singh, M. Wilch, and I. Erlich, "Reactive Power Management in Offshore Wind Farms by Adaptive PSO," in *Proc. 2007 International Conference on Intelligent Systems Applications to Power Systems*, pp. 1-8, Nov. 2007.

[17] E.ON Netz GmbH. (2008, Apr.). Requirements for offshore grid connections in the E.O.N. Netz Network. Bayreuth, Germany [Online]. Available: http://www.eon-netz.com.

[18] I. Erlich, F. Shewarega, C. Feltes, F. Koch and J. Fortmann, "Determination of Dynamic Wind Farm Equivalents using Heuristic Optimization," Paper accepted for publication the 2nd 2012 IEEE Power & Energy Society General Meeting, San Diego, USA.

[19] International Confederation of Energy Regulators, "Renewable Energy and Distributed Generation: International Case Studies on Technical and Economic Considerations," Ref: I12-CC-17-03, Feb. 2012.

[20] G. K. Viswanadha Raju and P. R. Bijwe, “Reactive power/voltage control in distribution systems under uncertain environment,” *IET Gener. Transm. Distrib.*, vol. 2, no. 5, p. 752, 2008.

[21] T. Niknam, M. Zare, and J. Aghaei, “Scenario-Based Multiobjective Volt/Var Control in Distribution Networks Including Renewable Energy Sources,” *IEEE Trans. Power Deliv.*, vol. 27, no. 4, pp. 2004–2019, Oct. 2012.

[22] H. Hatta and H. Kobayashi, “Demonstration study on centralized voltage control system for distribution line with sudden voltage fluctuations,” in *SmartGrids for Distribution, 2008. IET-CIRED. CIRED Seminar*, 2008, pp. 1–4.

[23] K. T. Tan, X. Y. Peng, P. L. So, Y. C. Chu, and M. Z. Q. Chen, “Centralized Control for Parallel Operation of Distributed Generation Inverters in Microgrids,” *IEEE Trans. Smart Grid*, vol. 3, no. 4, pp. 1977–1987, Dec. 2012.

[24] T. Senjyu, Y. Miyazato, A. Yona, N. Urasaki, and T. Funabashi, “Optimal Distribution Voltage Control and Coordination With Distributed Generation,” *IEEE Trans. Power Deliv.*, vol. 23, no. 2, pp. 1236–1242, Apr. 2008.

[25] M. E. Baran and I. M. El-Markabi, “A Multiagent-Based Dispatching Scheme for Distributed Generators for Voltage Support on Distribution Feeders,” *IEEE Trans. Power Syst.*, vol. 22, no. 1, pp. 52–59, Feb. 2007.

[26] Z. Bie, G. Li, H. Liu, X. Wang, and X. Wang, “Studies on voltage fluctuation in the integration of wind power plants using probabilistic load flow,” in *Power Engineering Society General Meeting, 2008. IEEE*, Pittsburgh, PA, 2008, pp. 1–7.

[27] B. Q. Khanh, “Assessment of voltage sag in distribution system regarding the uncertainty of wind based distributed generation,” in *Energytech, 2011 IEEE*, 2011, pp. 1–6.

[28] C.-L. Su, “Stochastic Evaluation of Voltages in Distribution Networks With Distributed Generation Using Detailed Distribution Operation Models,” *IEEE Trans. Power Syst.*, vol. 25, no. 2, pp. 786–795, May 2010.

[29] S. Zhang, K. J. Tseng, and S. S. Choi, “Statistical voltage quality assessment method for grids with wind power generation,” *IET Renew. Power Gener.*, vol. 4, no. 1, p. 43, 2010.

[30] D. Villanueva, J. L. Pazos, and A. Feijoo, “Probabilistic Load Flow Including Wind Power Generation,” *IEEE Trans. Power Syst.*, vol. 26, no. 3, pp. 1659–1667, Aug. 2011.

[31] J. Usaola, “Probabilistic load flow in systems with wind generation,” *IET Gener. Transm. Distrib.*, vol. 3, no. 12, p. 1031, 2009.

[32] A. Soroudi, “Possibilistic-Scenario Model for DG Impact Assessment on Distribution Networks in an Uncertain Environment,” *IEEE Trans. Power Syst.*, vol. 27, no. 3, pp. 1283–1293, Aug. 2012.

[33] United States of America, Federal Energy Regulatory Commission, “Interconnection for wind energy,” 18 CFR Part 35, Dec. 2005.

[34] P., Dispersed Generation, and Energy Storage. IEEE Standards Coordinating Committee 21 on Fuel Cells, Institute of Electrical and Electronics Engineers., IEEE-SA Standards Board., and IEEE Xplore (Online service), *IEEE standard conformance test procedures for equipment interconnecting distributed resources with electric power systems*. New York, N.Y.: Institute of Electrical and Electronics Engineers, 2005.

[35] Converter Applications in Future European Electricity Network UNIFLEX PM, 2007 [online]Available:http://www.eee.nottingham.ac.uk/uniflex/Documents/W2_AU_DV_2001_B.pdf

[36] National Grid Electricity Transmission, “The grid code,” London, Issue 4 Revision 2, Mar. 2010.

[37] BDEW, “Technische Richtlinie Erzeugungsanlagen am Mittelspannungsnetz, ” Juni 2008.

[38] T. W. Eberly and R. C. Schaefer, “Voltage versus VAr/power-factor regulation on synchronous generators,” *IEEE Trans. Ind. Appl.*, vol. 38, no. 6, pp. 1682–1687, Nov. 2002.

[39] S. Engelhardt, I. Erlich, C. Feltes, J. Kretschmann, and F. Shewarega, “Reactive Power Capability of Wind Turbines Based on Doubly Fed Induction Generators,” *IEEE Trans. Energy Convers.*, vol. 26, no. 1, pp. 364–372, Mar. 2011.

[40] H. V. Pham, J. L. Rueda, and I. Erlich, “Online Optimal Control of Reactive Sources in Wind Power Plants,” *IEEE Trans. Sustain. Energy*, vol. 5, no. 2, pp. 608–616, Apr. 2014.

[41] I. Erlich, G. K. Venayagamoorthy, and N. Worawat, "A Mean-Variance Optimization Algorithm," presented at the IEEE Congress on Evolutionary Computation, Barcelona, 2010.

[42] Ning Lu, T. Taylor, Wei Jiang, Chunlian Jin, J. Correia, L. R. Leung, and Pak Chung Wong, "Climate Change Impacts on Residential and Commercial Loads in the Western U.S. Grid," *IEEE Trans. Power Syst.*, vol. 25, no. 1, pp. 480–488, Feb. 2010.

[43] United Kingdom Generic Distribution Network (UKGDS). Available: http://monaco.eee.strath.ac.uk/ukgds/

[44] R. Singh, B. C. Pal, and R. A. Jabr, "Statistical Representation of Distribution System Loads Using Gaussian Mixture Model," *IEEE Trans. Power Syst.*, vol. 25, no. 1, pp. 29–37, Feb. 2010.

[45] G. Valverde, A. T. Saric, and V. Terzija, "Probabilistic load flow with non-Gaussian correlated random variables using Gaussian mixture models," *IET Gener. Transm. Distrib.*, vol. 6, no. 7, p. 701, 2012.

[46] J. L. Rueda, D. G. Colome, and I. Erlich, "Assessment and Enhancement of Small Signal Stability Considering Uncertainties," *IEEE Trans. Power Syst.*, vol. 24, no. 1, pp. 198–207, Feb. 2009.

[47] I. Erlich, "Analysis and simulation of dynamic behavior of power system, " Department of Electrical Engineering, Dresden University, Germany, 1995.

[48] German Ministry for the Environment, Nature Conservation and Nuclear Safety, "Windenergie Report 2008," Kassel, Germany, 0327584, 2008.

[49] COM(2007) 1 final, "Communication from the Commission to the European council and the European Parliament," *An energy policy for Europe*, 10 January 2007.

[50] A. L'Abbate, G. Fulli, F. Starr and S.D. Peteves, "Distributed power generation in Europe: Technical issues for further integration," *JRC Scientific and Technical Reports*, 2007.

[51] A.G. Madureira and J.A. Pecas Lopes, "Coordinated voltage support in distribution networks with distributed generation and microgrids," *Renewable Power Generation, IET*, vol. 3, no. 4, pp. 439-454, Dec. 2009.

[52] H.V. Pham, J.L. Rueda and I. Erlich, "Online optimal control of reactive sources in wind power plants," *IEEE Trans. Sustainable Energy*, vol. PP, no. 99, pp. 1-9, Aug. 2013.

[53] A. Vargas and M.E. Samper, "Real-time monitoring and economic dispatch of smart distribution grids: High performance algorithms for DMS applications," *IEEE Trans. Smart Grid*, vol. 3, no. 2, pp. 866-877, Jun. 2012.

[54] S. Liew and G. Strbac, "Maximising penetration of wind generation on existing distribution networks," *Pro. Inst. Elect. Eng., Gen., Transm., Distrib.*, vol 149, no. 3, pp. 256-262, May 2003.

[55] T.Senjyu, Y. Miyazato, A. Yona, N. Urasaki and T. Funabashi, "Optimal distribution voltage control and coordination with distributed generation," *IEEE Trans. Power Delivery*, vol. 23, no. 2, pp. 1236-1242, April 2008.

[56] Aouss Gabash and Pu Li, "Active-reactive optimal power flow in distribution networks with embedded generation and battery storage," *IEEE Trans. Power Sytem*, vol. 27, no. 4, pp. 2026-2035, Nov. 2012.

[57] Q. Zhou and J.W. Bialek, "Generation curtailment to manage voltage constraints in distribution networks," *IET Gen. Trans. & Dist*. vol. 1, no.3, pp. 492-498, May 2007.

[58] G. Valverde and T. Van Cutsem, "Model predictive control of voltages in active distribution networks," *IEEE Trans. Smart Grid*, vol. PP, no. 99, pp.1-10, Feb. 2013.

[59] M. Brenna, E.D. Berardinis, L.D. Carpini, F. Foiadelli, P. Paulon, P. Petroni, G. Sapienza, G. Scrosati and D. Zaninelli, "Automatic distributed voltage control algorithm in smart grids applications," *IEEE Trans Smart Grid*, vol. 4, no. 2, pp. 877-885, Jun. 2013.

[60] M.A. Kashem, G. Ledwich, "Multiple distributed generators for distribution feeder voltage support," *IEEE Trans. Energy Conversion*, vol. 20, no. 3, pp. 676-684, Sep. 2005.

[61] T. Sansawatt, L.F. Ochoa and G.P. Harrison, "Smart decentralized control of DG for voltage and thermal constraint management," IEEE Trans. Power Sytem, vol. 27, no. 3, pp. 1637-1645, Aug. 2012.

[62] D.A. Roberts, “Network management systems for active distribution networks – A feasibility study,” *DTI Technology Programme*, report number: K/EL/00310/REP, 2007.

[63] I. Erlich, W. Winter, and A. Dittrich, "Advanced grid requirements for the integration of wind turbines into the German transmission system," in *Proc. 2006 IEEE Power Engineering Society General Meeting.*

[64] ENTSO-E, “Network Code on Demand Connection,” pp.1-63, Dec. 2012. [Online]. Available: https://entsoe.eu.

[65] A. Keane, L.F. Ochoa, E. Vittal, C.J. Dent and G.P. Harrison, “Enhanced utilization of voltage control resources with distributed generation,” *IEEE Trans. Power Syst.*, vol. 26, no. 1, pp. 252–260, Feb. 2011.

[66] L.F. Ochoa, A. Keane and G.P. Harrison, “Minimizing the reactive support for distributed generation: enhanced passive operation and smart distribution networks,” *IEEE Trans. Power Syst.*, vol. 26, no. 4, pp. 2134–2142, Nov. 2011.

[67] G. Valverde and T. Van Cutsem, “Control of dispersed generation to regulate distribution and support transmission voltages,” *Proc. IEEE PES PowerTech Conference*, Jun. 2013.

[68] T. Van Cutsem and C. Vournas, Voltage Stability of Electric Power Systems. Norwell, MA. USA: Kluwer, 1998.

[69] V.L. Paucar and M.J. Rider, “Reactive power pricing in deregulated electrical markets using a methodology based on the theory of marginal costs,” *Proc. IEEE Large Engineering Systems Conference on Power Engineering*, pp. 7-11, 2001.

[70] I. El-Samahy, C.A. Canizares, K. Bhattacharya and J. Pan, “An optimal reactive power dispatch model for deregulated electricity markets,” *Proc. Power Engineering Society General Meeting*, pp. 1-7, Jun. 2007.

[71] J. Zhong and K. Bhattacharya, “Toward a competitive market for reactive power,” *IEEE Trans. Power Syst.*, vol. 17, pp. 1206-1215, .Nov. 2002.

[72] Y. Zhang and Z. Ren, “Optimal reactive power dispatch considering costs of adjusting the control devices,” *IEEE Trans. Power Syst.*, Vol. 20, pp. 1349-1356, Aug. 2005.

[73] United Kingdom Generic Distribution Network (UKGDS). [Online]. Available: http://sedg.ac.uk.

[74] R. Singh, B.C. Pal, and R.A. Jabr, “Statistical representation of distribution system loads using Gaussian mixture model,” *IEEE Trans. Power Syst.*, vol. 25, no. 1, pp. 29–37, Feb. 2010.

[75] K. Abdul-Rahman, W. Jun, E. Haq and P. Restanovic, "Considerations of reactive power/voltage control in CAISO market operations," *IEEE/PES General Meeting*, pp. 1-6, July 2011.

[76] H.V. Pham, J.L. Rueda and I. Erlich, "Online optimal control of reactive sources in wind power plants," *IEEE Trans. Sustainable Energy*, vol. 5, pp. 608-616, Apr. 2014.

[77] S. Duman, Y. Sönmez, U. Güvenc and N. Yörükeren, "Optimal reactive power dispatch using a gravitational search algorithm," *IET Gener., Transm. & Distrib.*, vol. 6, pp. 563-576, 2012.

[78] Yinliang Xu, Wei Zhang, Wenxin Liu and Frank Ferrese, "Multiagent-based reinforcement learning for optimal reactive power dispatch," *IEEE Trans. Systems, Man, and Cybernetics-Part C*, vol. 42, pp. 1742-1751, Nov. 2012.

[79] FERC and NERC. (2012, Apr.) Arizona-southern California outages on September 8, 2011: Causes and recommendations. [Online]. Available: http://www.ferc.gov/legal/staff-reports/04-27-2012-ferc-nerc-report.pdf

[80] Y. C. Chen, P. Sauer and A. D. Domínguez-García, “Online Computation of Power System Linear Sensitivity Distribution Factors,” in Proc. of the IREP Bulk Power System Dynamics and Control Symposium,” Crete, Greece, August 2013.

[81] J.A. Shamkhi, “The relationship between least square and linear programming,” Research Journal of Mathematical and Statistical Sciences, ISSN 2320-6047, vol. 1(2), March 2013.

[82] A. Abur and A. G. Exposito, *Power System State Estimation: Theory and Implementation*. New York: Marcel Dekker, 2004.

[83] C. Paleologu, J. Benesty, and S. Ciochina, “A robust variable forgetting factor recursive least-squares algorithm for system identification,” *IEEE Signal Process. Lett.*, vol. 15, pp. 597-600, 2008.

[84] M. Larsson and D. Karlsson, “Coordinated system protection scheme against voltage collapse using heuristic search and predictive control,” *IEEE Trans. Power Syst.*, vol. 18, no. 3, pp. 1001–1006, Aug. 2003.

[85] O. A. Mousavi and R. Cherkaoui, “Literature survey on fundamental issues of voltage and reactive power control,” *Ecole Polytech. Fédérale Lausanne Lausanne Switz.*, 2011.

[86] A. M. Ramly, N. Aminudin, I. Musirin, D. Johari, and N. Hashim, “Reactive Power Planning for transmission loss minimization,” in *Power Engineering and Optimization Conference (PEOCO), 2011 5th International*, 2011, pp. 116–120.

[87] Jizhong Zhu, Kwok Cheung, D. Hwang, and A. Sadjadpour, “Operation Strategy for Improving Voltage Profile and Reducing System Loss,” *IEEE Trans. Power Deliv.*, vol. 25, no. 1, pp. 390–397, Jan. 2010.

[88] G. Glanzmann and G. Andersson, “Incorporation of n-1 security into optimal power flow for facts control,” in *Power Systems Conference and Exposition, 2006. PSCE’06. 2006 IEEE PES*, 2006, pp. 683–688.

[89] S. Boyd and L. Vandenberghe, *Convex Optimization*, Cambridge University Press, Cambridge, United Kingdom, 2004.

[90] D. P. Bertsekas, *Constrained Optimization and Lagrange Multiplier Methods*, Academic Press, London, UK, 1982.

[91] A. G. Beccuti, T. H. Demiray, G. Andersson, and M. Morari, “A Lagrangian Decomposition Algorithm for Optimal Emergency Voltage Control,” *IEEE Trans. Power Syst.*, vol. 25, no. 4, pp. 1769–1779, Nov. 2010.

[92] Y. C. Chen, A. D. Dominguez-Garcia, and P. W. Sauer, “Online computation of power system linear sensitivity distribution factors,” in *Bulk Power System Dynamics and Control-IX Optimization, Security and Control of the Emerging Power Grid (IREP), 2013 IREP Symposium*, 2013, pp. 1–4.

[93] J. Peschon, D. S. Piercy, W. F. Tinney, and O. J. Tveit, “Sensitivity in power systems,” *Power Appar. Syst. IEEE Trans. On*, no. 8, pp. 1687–1696, 1968.

[94] R. R. Negenborn, B. De Schutter and J. Hellendoorn, “Multi-agent model predictive control for transportation networks: Series versus parallel schemes,” *in Proc. Of the 12th IFAC Symposium on Information Control Problems in Manufacturing*, Saint-Etienne, France, 2006.

[95] F. Zhuang and F. D. Galiana, “Towards a more rigorous and practical unit commitment by Lagrangian relaxation,” *Power Syst. IEEE Trans. On*, vol. 3, no. 2, pp. 763–773, 1988.

[96] B. Kim and R. Baldick, “A comparison of distributed optimal power flow algorithms,” *IEEE Trans. Power Syst.*, vol. 15, no. 2, pp. 599–604, May 2000.

[97] A. J. Conejo and J. A. Aguado, “Multi-area coordinated decentralized DC optimal power flow,” *Power Syst. IEEE Trans. On*, vol. 13, no. 4, pp. 1272–1278, 1998.

[98] N. I. Deeb and S. M. Shahidehpour, “An efficient technique for reactive power dispatch using a revised linear programming approach,” *Electr. Power Syst. Res.*, vol. 15, no. 2, pp. 121–134, 1988.

Appendix A

A.1 PDF of the input variables

A.1.1 PDF of nodal load demand

The nodal load demand is modeled by using a GMM with three mixture components. The mixture weights, parameters of 1st, 2rd and 3th mixture components are given in Table A-1, Table A-2, Table A-3 and Table A-4, respectively.

Table A-1 Mixture weights of nodal demand GMM

	Component 1	Component 2	Component 3
Mixture weights	0.193	0.57	0.237

Table A-2 Parameters of 1st mixture component

Mean (MW)										
Bus		1	2	3	4	5	6	7	8	9
Active power		0.7341	0.7301	0.7261	0.7222	0.7182	0.7142	0.7103	0.7063	0.7023
Reactive power		0.2891	0.2816	0.274	0.2664	0.2588	0.2513	0.2437	0.2361	0.2286
Covariance matrix										
		Active power								
	Bus	1	2	3	4	5	6	7	8	9
Active power	1	0.017	0.0168	0.0167	0.0165	0.0163	0.0162	0.016	0.0158	0.0157
	2	0.0168	0.0168	0.0167	0.0166	0.0165	0.0165	0.0164	0.0163	0.0163
	3	0.0167	0.0167	0.0167	0.0167	0.0168	0.0168	0.0168	0.0168	0.0169
	4	0.0165	0.0166	0.0167	0.0169	0.017	0.0171	0.0172	0.0173	0.0175
	5	0.0163	0.0165	0.0168	0.017	0.0172	0.0174	0.0176	0.0178	0.0181
	6	0.0162	0.0165	0.0168	0.0171	0.0174	0.0177	0.018	0.0183	0.0186
	7	0.016	0.0164	0.0168	0.0172	0.0176	0.018	0.0184	0.0188	0.0192
	8	0.0158	0.0163	0.0168	0.0173	0.0178	0.0183	0.0188	0.0194	0.0198
	9	0.0157	0.0163	0.0169	0.0175	0.0181	0.0186	0.0192	0.0198	0.0204
Reactive power	1	0.0072	0.007	0.0069	0.0068	0.0066	0.0065	0.0064	0.0062	0.0061
	2	0.007	0.0069	0.0068	0.0067	0.0066	0.0065	0.0064	0.0063	0.0062
	3	0.0067	0.0067	0.0066	0.0066	0.0065	0.0064	0.0064	0.0063	0.0063
	4	0.0065	0.0065	0.0065	0.0065	0.0064	0.0064	0.0064	0.0064	0.0063
	5	0.0063	0.0063	0.0063	0.0063	0.0064	0.0064	0.0064	0.0064	0.0064
	6	0.0061	0.0061	0.0062	0.0062	0.0063	0.0063	0.0064	0.0064	0.0065
	7	0.0059	0.006	0.006	0.0061	0.0062	0.0063	0.0064	0.0065	0.0066
	8	0.0056	0.0058	0.0059	0.006	0.0062	0.0063	0.0064	0.0065	0.0067
	9	0.0054	0.0056	0.0058	0.0059	0.0061	0.0062	0.0064	0.0066	0.0067
		Reactive power								
	Bus	1	2	3	4	5	6	7	8	9
Active power	1	0.0072	0.007	0.0067	0.0065	0.0063	0.0061	0.0059	0.0056	0.0054
	2	0.007	0.0069	0.0067	0.0065	0.0063	0.0061	0.006	0.0058	0.0056
	3	0.0069	0.0068	0.0066	0.0065	0.0063	0.0062	0.006	0.0059	0.0058
	4	0.0068	0.0067	0.0066	0.0065	0.0063	0.0062	0.0061	0.006	0.0059
	5	0.0066	0.0066	0.0065	0.0064	0.0064	0.0063	0.0062	0.0062	0.0061
	6	0.0065	0.0065	0.0064	0.0064	0.0064	0.0063	0.0063	0.0063	0.0062
	7	0.0064	0.0064	0.0064	0.0064	0.0064	0.0064	0.0064	0.0064	0.0064
	8	0.0062	0.0063	0.0063	0.0064	0.0064	0.0064	0.0065	0.0065	0.0066
	9	0.0061	0.0062	0.0063	0.0063	0.0064	0.0065	0.0066	0.0067	0.0067
Reactive power	1	0.0031	0.003	0.0029	0.0028	0.0026	0.0025	0.0024	0.0023	0.0022
	2	0.003	0.0029	0.0028	0.0027	0.0026	0.0025	0.0024	0.0023	0.0022
	3	0.0029	0.0028	0.0027	0.0026	0.0025	0.0024	0.0024	0.0023	0.0022
	4	0.0028	0.0027	0.0026	0.0026	0.0025	0.0024	0.0023	0.0023	0.0022
	5	0.0026	0.0026	0.0025	0.0025	0.0024	0.0024	0.0023	0.0023	0.0022
	6	0.0025	0.0025	0.0024	0.0024	0.0024	0.0023	0.0023	0.0023	0.0022
	7	0.0024	0.0024	0.0024	0.0023	0.0023	0.0023	0.0023	0.0023	0.0022
	8	0.0023	0.0023	0.0023	0.0023	0.0023	0.0023	0.0023	0.0023	0.0022
	9	0.0022	0.0022	0.0022	0.0022	0.0022	0.0022	0.0022	0.0022	0.0023

Table A-3 Parameters of 2rd mixture component

Mean (MW)										
Bus		1	2	3	4	5	6	7	8	9
Active power		0.4506	0.4374	0.4243	0.4111	0.3979	0.3848	0.3716	0.3584	0.3453
Reactive power		0.1794	0.171	0.1625	0.154	0.1456	0.1371	0.1287	0.1202	0.1118
Covariance matrix										
		Active power								
	Bus	1	2	3	4	5	6	7	8	9
Active power	1	0.024	0.0216	0.0193	0.0169	0.0146	0.0123	0.0099	0.0076	0.0052
	2	0.0216	0.0195	0.0174	0.0154	0.0133	0.0112	0.0091	0.007	0.0049
	3	0.0193	0.0174	0.0156	0.0138	0.012	0.0101	0.0083	0.0065	0.0047
	4	0.0169	0.0154	0.0138	0.0122	0.0107	0.0091	0.0075	0.0059	0.0044
	5	0.0146	0.0133	0.012	0.0107	0.0094	0.008	0.0067	0.0054	0.0041
	6	0.0123	0.0112	0.0101	0.0091	0.008	0.007	0.0059	0.0049	0.0038
	7	0.0099	0.0091	0.0083	0.0075	0.0067	0.0059	0.0051	0.0043	0.0035
	8	0.0076	0.007	0.0065	0.0059	0.0054	0.0049	0.0043	0.0038	0.0032
	9	0.0052	0.0049	0.0047	0.0044	0.0041	0.0038	0.0035	0.0032	0.003
Reactive power	1	0.0122	0.0109	0.0097	0.0085	0.0073	0.0061	0.0048	0.0036	0.0024
	2	0.011	0.0099	0.0088	0.0077	0.0066	0.0055	0.0044	0.0033	0.0022
	3	0.0099	0.0089	0.008	0.007	0.006	0.005	0.004	0.0031	0.0021
	4	0.0088	0.0079	0.0071	0.0062	0.0054	0.0045	0.0036	0.0028	0.0019
	5	0.0077	0.0069	0.0062	0.0055	0.0047	0.004	0.0032	0.0025	0.0018
	6	0.0065	0.0059	0.0053	0.0047	0.0041	0.0035	0.0028	0.0022	0.0016
	7	0.0054	0.0049	0.0044	0.0039	0.0034	0.0029	0.0024	0.002	0.0015
	8	0.0043	0.0039	0.0035	0.0032	0.0028	0.0024	0.002	0.0017	0.0013
	9	0.0032	0.0029	0.0027	0.0024	0.0022	0.0019	0.0016	0.0014	0.0011
		Reactive power								
	Bus	1	2	3	4	5	6	7	8	9
Active power	1	0.0122	0.011	0.0099	0.0088	0.0077	0.0065	0.0054	0.0043	0.0032
	2	0.0109	0.0099	0.0089	0.0079	0.0069	0.0059	0.0049	0.0039	0.0029
	3	0.0097	0.0088	0.008	0.0071	0.0062	0.0053	0.0044	0.0035	0.0027
	4	0.0085	0.0077	0.007	0.0062	0.0055	0.0047	0.0039	0.0032	0.0024
	5	0.0073	0.0066	0.006	0.0054	0.0047	0.0041	0.0034	0.0028	0.0022
	6	0.0061	0.0055	0.005	0.0045	0.004	0.0035	0.0029	0.0024	0.0019
	7	0.0048	0.0044	0.004	0.0036	0.0032	0.0028	0.0024	0.002	0.0016
	8	0.0036	0.0033	0.0031	0.0028	0.0025	0.0022	0.002	0.0017	0.0014
	9	0.0024	0.0022	0.0021	0.0019	0.0018	0.0016	0.0015	0.0013	0.0011
Reactive power	1	0.0063	0.0057	0.0051	0.0045	0.0039	0.0033	0.0027	0.0022	0.0016
	2	0.0057	0.0052	0.0046	0.0041	0.0036	0.003	0.0025	0.002	0.0014
	3	0.0051	0.0046	0.0042	0.0037	0.0032	0.0027	0.0023	0.0018	0.0013
	4	0.0045	0.0041	0.0037	0.0033	0.0028	0.0024	0.002	0.0016	0.0012
	5	0.0039	0.0036	0.0032	0.0028	0.0025	0.0021	0.0018	0.0014	0.0011
	6	0.0033	0.003	0.0027	0.0024	0.0021	0.0018	0.0015	0.0012	0.0009
	7	0.0027	0.0025	0.0023	0.002	0.0018	0.0015	0.0013	0.001	0.0008
	8	0.0022	0.002	0.0018	0.0016	0.0014	0.0012	0.001	0.0009	0.0007
	9	0.0016	0.0014	0.0013	0.0012	0.0011	0.0009	0.0008	0.0007	0.0006

Table A-4 Parameters of 3th mixture component

Mean (MW)										
Bus		1	2	3	4	5	6	7	8	9
Active power		0.492	0.49	0.4879	0.4859	0.4838	0.4818	0.4798	0.4777	0.4757
Reactive power		0.1981	0.1931	0.188	0.183	0.1779	0.1728	0.1678	0.1627	0.1576
Covariance matrix										
		Active power								
	Bus	1	2	3	4	5	6	7	8	9
Active power	1	0.0286	0.027	0.0255	0.024	0.0224	0.0209	0.0194	0.0178	0.0163
	2	0.027	0.0257	0.0245	0.0232	0.0219	0.0206	0.0193	0.018	0.0167
	3	0.0255	0.0245	0.0234	0.0224	0.0213	0.0203	0.0193	0.0182	0.0172
	4	0.024	0.0232	0.0224	0.0216	0.0208	0.02	0.0192	0.0184	0.0176
	5	0.0224	0.0219	0.0213	0.0208	0.0203	0.0197	0.0192	0.0186	0.0181
	6	0.0209	0.0206	0.0203	0.02	0.0197	0.0194	0.0191	0.0188	0.0185
	7	0.0194	0.0193	0.0193	0.0192	0.0192	0.0191	0.0191	0.019	0.019
	8	0.0178	0.018	0.0182	0.0184	0.0186	0.0188	0.019	0.0193	0.0195
	9	0.0163	0.0167	0.0172	0.0176	0.0181	0.0185	0.019	0.0195	0.0199
Reactive power	1	0.0126	0.0118	0.011	0.0102	0.0095	0.0087	0.0079	0.0071	0.0064
	2	0.0118	0.0111	0.0104	0.0097	0.0091	0.0084	0.0077	0.007	0.0064
	3	0.0109	0.0104	0.0098	0.0092	0.0087	0.0081	0.0075	0.007	0.0064
	4	0.0101	0.0096	0.0092	0.0087	0.0083	0.0078	0.0073	0.0069	0.0064
	5	0.0093	0.0089	0.0086	0.0082	0.0079	0.0075	0.0072	0.0068	0.0064
	6	0.0085	0.0082	0.008	0.0077	0.0075	0.0072	0.007	0.0067	0.0065
	7	0.0076	0.0075	0.0073	0.0072	0.0071	0.0069	0.0068	0.0066	0.0065
	8	0.0068	0.0068	0.0067	0.0067	0.0067	0.0066	0.0066	0.0065	0.0065
	9	0.006	0.006	0.0061	0.0062	0.0063	0.0063	0.0064	0.0065	0.0065
		Reactive power								
	Bus	1	2	3	4	5	6	7	8	9
Active power	1	0.0126	0.0118	0.0109	0.0101	0.0093	0.0085	0.0076	0.0068	0.006
	2	0.0118	0.0111	0.0104	0.0096	0.0089	0.0082	0.0075	0.0068	0.006
	3	0.011	0.0104	0.0098	0.0092	0.0086	0.008	0.0073	0.0067	0.0061
	4	0.0102	0.0097	0.0092	0.0087	0.0082	0.0077	0.0072	0.0067	0.0062
	5	0.0095	0.0091	0.0087	0.0083	0.0079	0.0075	0.0071	0.0067	0.0063
	6	0.0087	0.0084	0.0081	0.0078	0.0075	0.0072	0.0069	0.0066	0.0063
	7	0.0079	0.0077	0.0075	0.0073	0.0072	0.007	0.0068	0.0066	0.0064
	8	0.0071	0.007	0.007	0.0069	0.0068	0.0067	0.0066	0.0065	0.0065
	9	0.0064	0.0064	0.0064	0.0064	0.0064	0.0065	0.0065	0.0065	0.0065
Reactive power	1	0.0057	0.0052	0.0048	0.0044	0.004	0.0036	0.0032	0.0028	0.0024
	2	0.0052	0.0049	0.0045	0.0042	0.0038	0.0035	0.0031	0.0027	0.0024
	3	0.0048	0.0045	0.0042	0.0039	0.0036	0.0033	0.003	0.0027	0.0024
	4	0.0044	0.0042	0.0039	0.0037	0.0034	0.0031	0.0029	0.0026	0.0023
	5	0.004	0.0038	0.0036	0.0034	0.0032	0.0029	0.0027	0.0025	0.0023
	6	0.0036	0.0035	0.0033	0.0031	0.0029	0.0028	0.0026	0.0024	0.0023
	7	0.0032	0.0031	0.003	0.0029	0.0027	0.0026	0.0025	0.0024	0.0022
	8	0.0028	0.0027	0.0027	0.0026	0.0025	0.0024	0.0024	0.0023	0.0022
	9	0.0024	0.0024	0.0024	0.0023	0.0023	0.0023	0.0022	0.0022	0.0022

A.1.2 PDF of variation of WG production

Wind speed variation is modeled by using the GMM with parameters given in Table A-5.

Table A-5 Parameters of the wind speed variation GMM components

	GMM Components		
	Component 1	Component 2	Component 3
Weight	0.3858	0.5472	0.0670
Mean (m/s)	4.1237	8.7288	12.7835
Variance	1.7153	2.8351	3.7741

The operation status of WGs is expressed mathematically in (3.8). To compute P_F and P_O, the reference values of WG component failure rates, obtained from [48], and summarized in Table A-6, are used. Firstly, E_{TF} is the sum of last column in Table A-6. Then, E_{TO} is result of total hours per year (8760 hours) minus the expected time in failure state E_{TF}. Finally, probabilities for WG operation status are presented in Table A-7.

Table A-6 Outage time period of the sub-assemblies per WG

Component	The number of failures	Typical downtime per failure (hour)	Total hours out per year
Electrical	0.551	36	19.84
Control unit	0.371	43.2	16.03
Sensors	0.28	38.4	10.75
Hydraulics	0.27	31.2	8.42
Yaw system	0.25	60	15
Brakes	0.2	72	14.4
Gearbox	0.13	151.2	19.66
Generator	0.13	139.2	18.10
Structure	0.12	96	11.52
Drive train	0.1	144	14.4

Table A-7 WG outage data

E_{TO} (h)	E_{TF} (h)	P_O	P_F
8611.88	148.12	0.983	0.017

A.2 Necessary data for control methods

A.2.1 Constant PF control method

Table A-8 PF angles for test cases

	Capacitive PF	Unity PF	Inductive PF
φ_{ref}	arcos(0.95)	arcos(1.0)	-1x arcos(0.95)

A.2.2 Voltage droop control method

A pre-specified voltage tolerance characteristic (e.g. around the rated voltage, 20 kV) has been set in this chapter within ±5% considering a WG reactive power rating of ±0.33 p.u. Recalling that the distribution network has four identical feeders, so Q_{max}, Q_{min} in Table A-9 constitute the reactive power capacity of WGs of all four feeders at each corresponding bus (e.g. bus 5 or bus 9). For load flow calculation, the buses with WGs, are considered as PQ buses. However, unlike typical treatment of PQ buses in load flow calculation, reactive power injection at these buses is managed by droop control, which depends on the voltage magnitude at these buses and peforms based on a predefined QV characteristic. In view of this, the voltage of PQ buses is updated at each iteration of the load flow calculation by accounting the QV characteristic.

Table A-9 Limits of voltage droop control method and direct control method

Scenario	V_{max} (kV)	V_{min} (kV)	Q_{max} (MVar)	Q_{min} (MVar)
A	21	19	2.64	-2.64
B			5.28	-5.28

A.2.3 Direct voltage control method

The voltage reference input V_{ref_WG} is set at 1.0 p.u in this study. Buses with direct voltage control are modeled as PV buses in the load flow analysis. As long as the WG is able to supply the required reactive power the voltage deviation is zero at these points. However, when the reactive power demand exceeds the limits, as presented in Table A-9, the load flow algorithm changes to PQ node, resulting in non-zero voltage difference. The PI control shown in Fig. 3.4 has the function of preventing interference of slow control in fast control scheme

of the WG. Thus, for design purposes, the proportional gain of the PI control can be considered relatively small and the integral time constant can be set within 10–20s.

A.2.4 Coordinated control method

Table A-10 Limits of the coordinated control method

Scenario	V_{max} (kV)	V_{min} (kV)	Q_{max} (MVar)	Q_{min} (MVar)	tap_{OLTC}^{max}	tap_{OLTC}^{min}
A	21	19	2.64	-2.64	13	-13
B			5.28	-5.28	13	-13

Table A-11 Parameters settings of MVMO technique

Number of iterations	200
N best populations	5
Factor f_s	1.0
d_i	1
Δd	1.5

Appendix B

In this Appendix, calculation of necessary sensitivities is introduced. As aforementioned, the sensitivities of the losses with respects to control variables are the main task to be estimated. They are decomposed into two layers of other sensitivities in this chapter as shown in (B-1). The first is sensitivities of the losses with respects to voltages whose sensitivities with respect to control variables are the second layer. Note that formulations below are used to calculate sensitivities for an area based on only its system data. The other areas are the same.

$$\frac{\partial P_i^{loss}}{\partial \boldsymbol{w}_i} = \frac{\partial P_i^{loss}}{\partial \boldsymbol{v}_i} \frac{\partial \boldsymbol{v}_i}{\partial \boldsymbol{w}_i} \tag{B-1}$$

► Calculation of the first layer $\partial P_i^{loss} / \partial \boldsymbol{v}_i$:

The objective is to minimize real power losses during the operation and control of a network. The real power loss P_i^{loss} of area *i* is presented by

$$P_i^{loss} = \sum_{k=1}^{\mathrm{N_{br}}} \mathrm{G}_k [v_h^2 + v_l^2 - 2v_h v_l \cos(\delta_h - \delta_l)] \tag{B-2}$$

where G_k is the conductance of line *k* which is connected between buses *h* and *l* in area *i*, and N_{br} is the number of branches of area *i*. In (B-2) the losses are represented by a nonlinear function of the bus voltages phase angles.

Then, the losses function is linearized as follows:

$$\frac{\partial P^{loss}}{\partial v_h} = \mathrm{G}_k [2v_h - 2v_l \cos(\delta_h - \delta_l)] \tag{B-3}$$

$$\frac{\partial P^{loss}}{\partial v_l} = \mathrm{G}_k [2v_l - 2v_h \cos(\delta_h - \delta_l)] \tag{B-4}$$

For every transmission line, the partial derivatives of P_i^{loss} with respect to the voltages at buses *h* and *l* are calculated. Partial derivatives pertaining to a certain bus are summed to form the power loss sensitivities with respect to all bus voltages in the system.

► Calculation of the second layer $\partial \boldsymbol{v}_i / \partial \boldsymbol{w}_i$: Vector of the control variables $\boldsymbol{w}_i$ is combination of three different vectors of following variables: the inter-area variable $\boldsymbol{v}'_{ij}$, reactive power injection of generators $\boldsymbol{q}_{g,i}$ and tap ratio $\boldsymbol{\alpha}_{tap,i}$. Therefore, sensitivities of the

second layer were calculated by computing three sensitivities such as $\partial \boldsymbol{v}_i / \partial \boldsymbol{v}'_{ij}$, $\partial \boldsymbol{v}_i / \partial \boldsymbol{q}_{g,i}$ and $\partial \boldsymbol{v}_i / \partial \boldsymbol{\alpha}_{tap,i}$.

+ It is clear that $\partial \boldsymbol{v}_i / \partial \boldsymbol{v}'_{ij}$ is an unity vector and $\partial \boldsymbol{v}_i / \partial \boldsymbol{q}_{g,i}$ is inversion of Jacobian matrix calculate below:

Reactive power injection at bus *k*

$$q_k = v_k \sum_{m=1}^{N_{bus}} (G_{km} v_m \sin\theta_{km} - B_{km} v_m \cos\theta_{km}) \tag{B-5}$$

Jacobian matrix is partly structured from partial derivatives of the reactive power injections as:

$$J_{km} = \frac{\partial q_k}{\partial v_m} = v_k (G_{km} \sin\theta_{km} - B_{km} \cos\theta_{km}) \tag{B-6}$$

$$\begin{aligned} J_{kk} = \frac{\partial q_k}{\partial v_k} &= 2v_k (G_{kk} \sin\theta_{kk} - B_{kk} \cos\theta_{kk}) \\ &+ \sum_{m=1, m\neq k}^{N_{bus}} v_m (G_{km} \sin\theta_{km} - B_{km} \cos\theta_{km}) \end{aligned} \tag{B-7}$$

+ In this chapter, changing the tap ratio of the transformer is equivalent to the injection of two reactive power increments into buses which are connected to the transformer terminals. Thus the sensitivities $\boldsymbol{v}_i / \partial \boldsymbol{\alpha}_{tap,i}$ are equivalent to two layers of sensitivities below:

$$\frac{\partial \boldsymbol{v}_i}{\partial \boldsymbol{\alpha}_{tap,i}} = \frac{\partial \boldsymbol{v}_i}{\partial \boldsymbol{q}_{tap,i}} \frac{\partial \boldsymbol{q}_{tap,i}}{\partial \boldsymbol{\alpha}_{tap,i}} \tag{B-8}$$

The sensitivities $\partial \boldsymbol{v}_i / \partial \boldsymbol{q}_{tap,i}$ is essentially a sub-matrix of the known $\boldsymbol{v}_i / \partial \boldsymbol{q}_{g,i}$. While $\partial \boldsymbol{v}_i / \partial \boldsymbol{\alpha}_{tap,i}$ is calculated as follows:

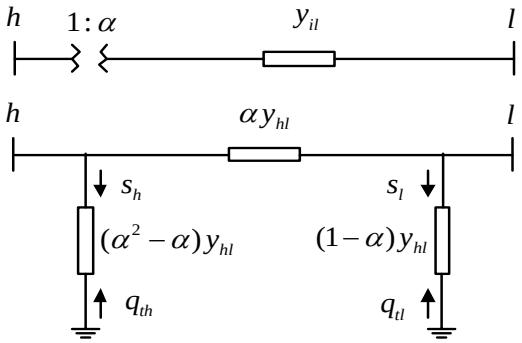

Fig. B-1 Model of tap changing transformer and its equivalent π circuit for the branch

Transformer tap changing is more difficult to model since two buses are directly involved in the tap changing process. Let us consider a transformer connecting buses *h* and *l* with tap α, as shown in Fig. B-1. This branch can be represented by an equivalent π circuit.

The admittance of the branch is:

$$y_{hl} = g_{hl} + jb_{hl} \tag{B-9}$$

From Fig. B-1, the complex power injection to bus *h* is

$$s_h = p_h + jq_h = v_h i_h^* = v_h \left[v_h(\alpha^2 - \alpha) y_{hl} \right]^* \tag{B-10}$$

where * indicates the complex conjugate of the variable. So,

$$s_h = v_h^2(\alpha^2 - \alpha) g_{hl} - jv_h^2(\alpha^2 - \alpha) b_{hl} \tag{B-11}$$

Similarly, the complex power injection to bus *l* is represented as

$$s_l = v_l^2(1-\alpha) g_{hl} - jv_l^2(1-\alpha) b_{hl} \tag{B-12}$$

From (B-11) and (B-12), the equations for q_h and q_l are

$$q_h = -v_h^2(\alpha^2 - \alpha) b_{hl} \tag{B-13}$$

$$q_l = -v_l^2(1-\alpha) b_{hl} \tag{B-14}$$

If Δq_h is the increment of q_h with respect to voltage and tap position changes, then

$$\Delta q_h = \frac{\partial q_h}{\partial v_h} \Delta v_h + \frac{\partial q_h}{\partial \alpha} \Delta \alpha \tag{B-15}$$

However, for the power flow in Fig. B-1, we have

$$\Delta q_{th} = -\Delta q_h \tag{B-16}$$

So, differentiating (B-13) with respect to v_h and α, we have

$$\Delta q_{th} = 2b_{hl} v_h (\alpha^2 - \alpha) \Delta v_h + b_{hl} v_h^2 (2\alpha - 1) \Delta \alpha \tag{B-17}$$

Similarly, differentiating (B-14) with respect to V_l and α, we have

$$\Delta q_{tl} = 2b_{hl} v_l (1-\alpha) \Delta v_l - b_{hl} v_l^2 \Delta \alpha \tag{B-18}$$

Moreover, equation (B-17) can be rewritten as follows

$$\Delta q_{th} = 2b_{hl} v_h \alpha(\alpha - 1) \Delta v_h + b_{hl} v_h^2 (\alpha - 1) \Delta \alpha + b_{hl} v_h^2 \alpha \Delta \alpha \tag{B-19}$$

Since the value of α is close to unity, and Δv_h and $\Delta \alpha$ are small, therefore

$$\frac{\Delta q_{th}}{\Delta \alpha} = b_{hl} v_h^2 \alpha \tag{B-20}$$

Similarly, from equation (B-18),

$$\frac{\Delta q_{tl}}{\Delta \alpha} = -b_{hl} v_l^2 \tag{B-21}$$